

INFORMATION TO USERS

This manuscript has been reproduced from the microfilm master. UMI films the text directly from the original or copy submitted. Thus, some thesis and dissertation copies are in typewriter face, while others may be from any type of computer printer.

The quality of this reproduction is dependent upon the quality of the copy submitted. Broken or indistinct print, colored or poor quality illustrations and photographs, print bleedthrough, substandard margins, and improper alignment can adversely affect reproduction.

In the unlikely event that the author did not send UMI a complete manuscript and there are missing pages, these will be noted. Also, if unauthorized copyright material had to be removed, a note will indicate the deletion.

Oversize materials (e.g., maps, drawings, charts) are reproduced by sectioning the original, beginning at the upper left-hand corner and continuing from left to right in equal sections with small overlaps.

Photographs included in the original manuscript have been reproduced xerographically in this copy. Higher quality 6" x 9" black and white photographic prints are available for any photographs or illustrations appearing in this copy for an additional charge. Contact UMI directly to order.

ProQuest Information and Learning
300 North Zeeb Road, Ann Arbor, MI 48106-1346 USA
800-521-0600

UMI[®]

NOTE TO USERS

This reproduction is the best copy available.

UMI[®]

University of Alberta

Chemistry of Deposition of Fine Particles in Catalytic Hydrotreaters

by

Sanyi Wang



A thesis submitted to the Faculty of Graduate Studies and Research in partial
fulfillment of the requirements for the degree of **Doctor of Philosophy**

in

Chemical Engineering

Department of Chemical & Materials Engineering

Edmonton, Alberta

Spring 2000



National Library
of Canada

Acquisitions and
Bibliographic Services

395 Wellington Street
Ottawa ON K1A 0N4
Canada

Bibliothèque nationale
du Canada

Acquisitions et
services bibliographiques

395, rue Wellington
Ottawa ON K1A 0N4
Canada

Your file Votre référence

Our file Notre référence

The author has granted a non-exclusive licence allowing the National Library of Canada to reproduce, loan, distribute or sell copies of this thesis in microform, paper or electronic formats.

The author retains ownership of the copyright in this thesis. Neither the thesis nor substantial extracts from it may be printed or otherwise reproduced without the author's permission.

L'auteur a accordé une licence non exclusive permettant à la Bibliothèque nationale du Canada de reproduire, prêter, distribuer ou vendre des copies de cette thèse sous la forme de microfiche/film, de reproduction sur papier ou sur format électronique.

L'auteur conserve la propriété du droit d'auteur qui protège cette thèse. Ni la thèse ni des extraits substantiels de celle-ci ne doivent être imprimés ou autrement reproduits sans son autorisation.

0-612-60037-8

Canada

University of Alberta

Library Release Form

Name of Author: Sanyi Wang

Title of Thesis: Chemistry of Deposition of Fine Particles in Catalytic Hydrotreaters

Degree: Doctor of Philosophy

Year this Degree Granted: Spring 2000

Permission is hereby granted to the University of Alberta Library to reproduce single copies of this thesis and to lend or sell such copies for private, scholarly, or scientific research purposes only.

The author reserves all other publication and other rights in association with the copyright in the thesis, and except as herein before provided, neither the thesis nor any substantial portion thereof may be printed or otherwise reproduced in any material form whatever without the author's prior written permission.

Sanyu WANG

404 RH, Michener Park

Edmonton, AB

Canada T6H 4M5

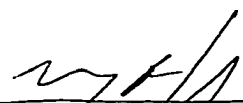
December 23, 1999

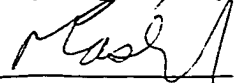
Date

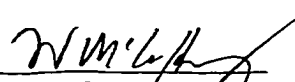
University of Alberta

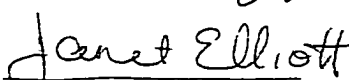
Faculty of Graduate Studies and Research

The undersigned certify that they have read, and recommend to the Faculty of Graduate Studies and Research for acceptance, a thesis entitled Chemistry of Deposition of Fine Particles in Catalytic Hydrotreaters submitted by SANYI WANG in partial fulfillment of the requirements for the degree of DOCTOR OF PHILOSOPHY in CHEMICAL ENGINEERING.

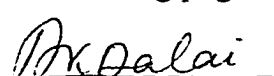

Murray R. Gray


Jacob H. Masliyah


William C. McCaffrey


Janet A. W. Elliott


Dongqing Li


Ajay K. Dalai

December 22, 1999
Date

To my parents, Joan, and Jasmine

Abstract

Fine particles in the gas oils derived from Athabasca bitumen tend to deposit in the catalyst beds of hydrotreating reactors, causing a continual increase in pressure drop across the reactor. The hydrodynamics of gas and liquid flow in hydrotreaters is quite complex, and the composition of the reaction system changes during hydrotreating. This thesis, consisting of three related sections, focuses on the role of chemistry in particle deposition under controlled hydrodynamic conditions.

- (1) Toluene-insoluble (TI) organic matter was deposited along with inorganic solids in hydrotreating reactors. Development of organic TI and its interaction with inorganic particles were studied by heating coker gas oil in an autoclave at 300-420 °C for a period ranging from 1 to 2 h. The product TI solid was collected and analyzed by scanning electronic microscopy (SEM) and energy dispersive x-ray analysis (EDX). At elevated temperatures, an emulsion of carbon-rich TI fraction in oil was formed, based on the observation of distinct carbon-rich spheres of ca. 2 μm under SEM. This TI fraction wetted the surfaces of non-polar solids such as asphaltene-treated kaolin and carbon black, giving convincing evidence of liquid coke formation at elevated temperatures and suggesting that surface properties have great influence on coke formation behavior.
- (2) The effect of surface properties of depositing particles, such as kaolin and iron sulfide, on their deposition was studied in packed beds of either glass beads or catalyst pellets in an autoclave at 375-380 °C. When kaolin was used, cake filtration prevailed due to rapid flocculation. Deep-bed filtration dominated when

asphaltene-treated kaolin was employed. Fine particles were fractionated between the collectors and the liquid phase, according to the specific coverage of asphaltene on the kaolin surface. Kaolin particle size (0.68 - 5 μm) was less significant than its specific coverage with asphaltenes in determining its deposition. The treatment with asphaltenes had no effect on the deposition of iron sulfide because its catalytic activity likely converted the asphaltenes, giving a clean mineral surface.

(3) The role of polar compounds, such as water, ammonia, quinoline, on the deposition of asphaltene-treated kaolin was studied by adding them into the reactor at reaction temperatures. It was proposed that water could displace some asphaltenes from the kaolin surface at hydrotreating conditions, making it more hydrophilic. This kaolin, with reduced specific coverage of asphaltenes on its surface, tended to deposit more easily on the collectors. Water also enhanced the removal of the adsorbed organic layer from authentic TI solids from Athabasca vacuum residue (525 °C+). Representative bases (ammonia and quinoline), on the other hand, showed no effect on deposition of kaolin.

Overall, these studies showed that the deposition behavior of fine particles depended on their surface chemistry at hydrotreating conditions, governing interactions with coke (1), and agglomeration and deposition on collector surfaces (2 & 3). These results were in agreement with industrial observations that more deposition occurred at the lower section of the hydrotreaters. In the presence of an active catalyst, the asphaltene layer would be gradually desorbed from fine particles due to the conversion of asphaltenes in the liquid phase. The gradual increase in reaction temperature along the hydrotreater

would enhance desorption of asphaltenes. Water would be generated by hydrodeoxygenation of gas oils, which would in turn promote removal of this asphaltene layer. Consequently, the reaction conditions would give the lowest concentration of asphaltenes on the mineral surface in the most active zone of the reactor, which would lead to the highest rate of particle deposition on the catalyst.

Acknowledgments

I would like to express my sincere thanks to all those who assisted me in achieving my goal today, although many of their names may be absent here. In particular, I am extremely grateful to my two mentors, Dr. M. R. Gray and Dr. J. H. Masliyah.

Without their thoughtful guidance, consistent encouragement, timely inspiration and unbelievable patience, it is nearly impossible for me to bring my Ph.D. program to fruition. I am deeply indebted to my co-worker, Dr. K. H. Chung, in Syncrude Research Center for his unreserved suggestions and incisive comments from time to time. It is they who taught me how to conduct fine research with scientific integrity. It is they who revised my paper manuscripts meticulously and tirelessly. They were not only my supervisors but also my friends.

A number of colleagues have been instrumental for me to develop positively in course of my program. These may include Dr. Y. Zhao, Dr. D. Banerjee, Ms. P. Stelmack, and Mr. L. Liu. Many thanks are due to Mr. P. Abel in Syncrude Research Center, Mr. R. Cooper, Mr. W. Boddez, Mr. R. Van de Heuvel, Mr. B. Scott and Ms. A. Koenig in our department for their invaluable and substantial assistance in my research over the years.

I would like to salute to my dear wife, Ms. Joan Z. Yang. I thank her for her unselfish sacrifice and consideration, and for all the experiences we shared, good or bad, during the ups and downs of my research. The demands of my work definitely resulted in added burden for her. I cannot forget to say sorry to my adorable daughter, Jasmine, for the time I should have been around her. This appreciation should

undoubtedly be extended to my parents for their love and generous spiritual support of their only son in the past few years.

I also want to extend a sincere thank you to all the members of my examination committee, particularly to Dr. A. K. Dalai and Dr. J. A. W. Elliott, for their careful reading of the thesis manuscript and suggestions for its further improvement. Finally, I take this unique opportunity to greatly acknowledge the funding provided by Syncrude Canada Limited for this project, with which I enjoyed spending the prime part of my lifetime in Alberta Oil Sands related research and obtained the excellent education at the University of Alberta.

Table of Contents

Contents	Page
Chapter 1: Introduction	1
1.1 Oil Sands of Alberta	1
1.2 Commercial Upgrading of Bitumen	3
1.3 Hydrotreating of Distillate Oils	5
1.3.1 Hydrotreating Processes	5
1.3.2 Deactivation of Hydrotreating Catalyst	6
1.3.3 Pressure Drop Buildup Problem in Hydrotreaters	8
1.4 Research Objective and Methodology	9
1.4.1 Major Objectives	9
1.4.2 Simulation of Commercial Hydrotreaters	10
1.4.3 Variables Studied in Particle Deposition in a Batch Reactor	11
1.5 Structure of Thesis	12
References	14
Chapter 2: Literature Review: Kinetics and Mechanism of	15
Toluene-Insolubles Formation During Processing of	
Heavy Oils	
2.1 Introduction	15
2.2 Definitions of Coking, Sediment Formation and Fouling	15
2.2.1 Coke Production	15
2.2.2 Sedimentation and Fouling	17

2.3 Fractionation of Petroleum	18
2.4 Structure of Asphaltenes	20
2.4.1 Steric-Stabilization Models	20
2.4.2 Thermodynamic Models for Asphaltene Solubility and Separation	23
2.4.3 Multiphase Behavior of Hydrocarbon Mixtures at Elevated Pressures and Temperatures	24
2.5 Kinetics and Mechanisms of TI Solids Formation	28
2.5.1 Wiehe's Phase-Separation Kinetic Model	28
2.5.2 Free Radical Reaction Mechanism	30
2.6 Factors Influencing the Formation of TI Solids	34
2.6.1 Hydrogen, Solvents, and Asphaltenes Content	36
2.6.2 Fine Solid Particles	39
2.7 Concluding Remarks	43
References	45
Chapter 3: Literature Review: Particle Deposition in Porous Media	50
3.1 Background	50
3.2 Difference between Aqueous and Non-Aqueous Systems	52
3.3 Stabilization of Colloids	52
3.4 Dielectric Filtration	57
3.5 Filtration Mechanisms	60
3.6 Process of Particle Deposition	62
3.7 Transient Behavior of Filtration	66

3.8 Particle Deposition on Coated Collector Surfaces	67
3.9 Particle Deposition in Non-Aqueous Systems	68
3.10 Hydrodynamics of Packed-Bed Reactors	70
References	72
Chapter 4: Toluene-Insoluble Fraction from Thermal Cracking	77
of Athabasca Gas Oil: Formation of an Emulsified	
Liquid that Wets Hydrophobic Dispersed Solids	
4.1 Introduction	77
4.2 Experimental	80
4.3 Results	86
4.3.1 Formation of a TI Emulsion from Coker Gas Oil	86
4.3.2 Photographs of Filter Cakes	92
4.3.3 Interactions of TI with Added Solids	92
4.3.4 Effects of Added Solids on TI Yield	98
4.3.5 TI Spheres versus Mesophase	99
4.4 Discussion	101
4.5 Conclusions	103
References	105
Chapter 5: Filtration of Fine Clays by Packed Beds at	107
Hydrotreating Conditions: Role of Surface Treatment	
with Asphaltenes	
5.1 Introduction	107

5.2 Materials and Methods	109
5.2.1 Feed and Packing Materials	109
5.2.2 Authentic Solids Derived from Athabasca Oil Sands	112
5.2.3 Treatment of Kaolin with Asphaltenes	114
5.2.4 Analysis of Samples	114
5.2.5 Amount of Asphaltene Coating on Kaolin	115
5.2.6 Reactor Apparatus	115
5.2.7 Height of Liquid Phase inside Reactor	118
5.2.8 Observation of Fluid Circulation Pattern	119
5.2.9 Reaction Procedure	121
5.2.10 Measurement of Particle Deposition	122
5.3 Results and Discussion	124
5.3.1 Liquid Phase Circulation at Room Temperature	124
5.3.2 Adsorption of Asphaltene on Kaolin	125
5.3.3 Deposition of Kaolin in Packed Beds	125
5.3.3.1 <i>Material Balance</i>	125
5.3.3.2 <i>Repeatability of Particle Deposition Measurements</i>	128
5.3.3.3 <i>Time Course of Particle Deposition</i>	128
5.3.4 Role of Asphaltene Coating and Free Asphaltenes in Particle Trapping	133
5.3.4.1 <i>Flocculation of Untreated Kaolin in TLGO</i>	136
5.3.4.2 <i>Effects of Asphaltene Treatment on the Kinetics of Kaolin Deposition</i>	137

5.3.5 Thermal Stability of Asphaltenes on Kaolin	142
5.3.6 Tests on Authentic TI Solids	147
5.3.7 Mechanism of Deposition and Industrial Implications	149
5.4 Conclusions	152
References	153
Chapter 6: Effects of Hydrotreating Reactions on Deposition of Fine Particles in Reactors	155
6.1 Introduction	155
6.2 Materials and Methods	158
6.2.1 Feed and Packing Materials	158
6.2.2 Asphaltene Treatment of Kaolin and Iron Sulfide	161
6.2.3 Reactor Apparatus and Liquid Addition System	162
6.2.4 Reaction Procedure	162
6.2.5 Measurement of Particle Deposition	164
6.3 Results and Discussion	165
6.3.1 Repeatability of Particle Deposition Measurements	165
6.3.2 Effect of Asphaltene Treatment on Particle Deposition	165
6.3.3 Effect of Hydrodeoxygenation (HDO) on Kaolin Deposition	167
<i>6.3.3.1 Pressure Increase and Deposition Behavior</i>	167
<i>6.3.3.2 Effect of Reactor Temperature</i>	169
<i>6.3.3.3 Effect of Reactor Pressure</i>	172
<i>6.3.3.4 Role of Condensing Water after Reaction</i>	172
<i>6.3.3.5 Mechanism of Water-Clay Interactions</i>	174

6.3.4 Effect of Hydrodenitrogenation (HDN) on Kaolin Deposition	178
6.4 Conclusions	180
References	182
Chapter 7: Synthesis	185
Formation of TI Coke: an Emulsion Process	185
Particle Deposition at Hydrotreating Conditions: Effect of Adsorbed Asphaltenes and Supercritical Water	186
Advances in Knowledge	186
Future Research	188
References	189
Appendices	190
Appendix 1: Use and Maintenance of the 500 mL Autoclave	190
Appendix 2: Porosity of a Clean Bed	197
Appendix 3: Correction for the Mass of Asphaltene-Treated Kaolin on a Hydrocarbon-Free Basis	198
Appendix 4: Calculation of Specific Deposit and Surface Coverage	203
Appendix 5: Repeatability of Particle Deposition Experiments	203
Appendix 6: Settling Experiments for Kaolin Suspension in Gas Oils	207

List of Tables

Table		Page
1-1	Properties of Athabasca bitumen (Chung et al., 1997)	2
4-1	Composition and properties of Athabasca coker gas oil	81
4-2	Composition and properties of kaolin	84
4-3	TI fraction formed from thermal reactions of gas oil (Reactions at 375 °C for 1 h; Solid concentration of 4 g/kg)	96
5-1	Composition and properties of Athabasca hydrocarbons	110
5-2	Characteristics of collector materials	113
5-3	Distribution of kaolin inside the reactor as the percentage of the total kaolin on a hydrocarbon-free basis (375 °C, 60 min of reaction time, 700 rpm, 20 g of glass beads, 0.98 g kaolin and 240 g TLGO; asphaltene-treated kaolin initially had 75 mg asphaltenes/g kaolin)	127
5-4	Carbon content of kaolin remaining in liquid product and trapped in the bed of glass beads (375 °C, 700 rpm, 60 min of reaction time, 20 g of glass beads, 240 g TLGO, 0.98 g asphaltene-treated kaolin with 75 mg asphaltenes/g kaolin)	145
5-5	Residual carbon content in kaolin from liquid product, specific deposit and coverage of kaolin on collectors under hydrogen and nitrogen atmosphere with fresh catalyst (375 °C, 700 rpm, 240 g TLGO, initial 6.2 MPa gas and 60 min of reaction time).	148
6-1	Physical properties of additives (Weast et al., 1983)	160
6-2	Properties of asphaltene-treated kaolin, iron sulfide, asphaltene-treated iron sulfide	163
6-3	Role of polar compounds on particle deposition (375 °C, 700 rpm, 20 g glass beads, 1 h of reaction time, 0.98 g of asphaltene-treated kaolin had a carbon content of 5.9%)	177

Appendices

A1-1	Specifications of the 500-mL autoclave and dimensions of its internals	191
A5-1	Distribution of kaolin in various parts in the autoclave after particle deposition experiments	204
A5-2	Repeatability of particle deposition experiments	206
A6-1	Settling Data for 40,000 ppm TGO/Clay Suspension	210

List of Figures

Figure		Page
1-1	The flow chart to obtain Syncrude sweet blend	4
1-2	Typical trickle-bed hydrotreating process (Gray, 1994)	7
2-1	Hypothetical mechanism of asphaltene aggregation from crude oils (Pfeiffer and Saal, 1940)	22
2-2	Phase diagram of asphaltene molecules from liquid media (Schabron and Speight, 1998)	25
2-3	Partial phase diagram for the pyrene-tetralin solvent system showing the two phase liquid region at 427 °C (Shaw, 1988)	27
2-4	Schematic diagram of chemical reactions and phase behavior in Wiehe's phase-separation kinetic Model (1993)	29
2-5	Temporal variation in the four product classes from thermolysis of the full residuum. Curves were calculated from the phase-separation kinetic model (Wiehe, 1993).	31
2-6	Thermal polymerization of styrene at 100 °C where benzoquinone was used as retarder (Billmeyer, 1962)	35
2-7	Schematic diagram of clays at interfaces of thermoplastic coke dispersed in oil (Tanabe and Gray, 1997)	40
2-8	Yield of coke from thermal cracking of Athabasca vacuum residue and solids-free Athabasca vacuum residue at 430 °C under a nitrogen atmosphere (Tanabe and Gray, 1997)	42
3-1	Variation of the total potential energy at different electrolyte molarity for charge-stabilized particles (Masliyah, 1994)	54
3-2	Highly sterically stabilized colloidal particles: (a) compression of adsorbed layer; (b) interaction of adsorbed layers (Sato and Ruch, 1980)	56
3-3	The schematic diagram of a dielectric filter (Barker et al., 1991)	59

3-4	Variation of filtration mechanism with particle size and difference in deposit morphology in each filtration mechanism (McDowell-Boyer et al., 1986)	61
3-5	Three dominant mechanisms for capturing suspended particles to a collector surface (Yao et al., 1971)	63
4-1	Boiling point distribution curve of Athabasca coker gas oil	82
4-2	Micrographs of filtered solids SEM sample setup, blank filter paper and coker gas oil feed. The scale at the bottom of each micrograph indicates a length of 1.36 mm, 15 μm , and 15 μm , respectively.	87
4-3	SEM micrographs of the filtered TI solids from thermally treated coker gas oil without solids added (375 $^{\circ}\text{C}$, 1 h reaction time). (a) Solid particles showing spheres with both rough and smooth surfaces. The scale at the bottom indicates a length of 10 μm ; (b) Coalescing spheres. The scale at the bottom indicates a length of 1 μm .	89
4-4	Effects of impeller speed and reaction time on the growth of TI spheres when coker gas oil was heated at 375 $^{\circ}\text{C}$ under H_2 atmosphere	90
4-5	EDX spectrum from the spherical particles of TI in products from runs without solids added (375 $^{\circ}\text{C}$, 1 h reaction time).	91
4-6	Variation of filter cake color with reaction temperature when 0.004 kg untreated kaolin/kg was present in the coker gas oil feed	93
4-7	Development of TI spheres in the liquid product as a function of reaction temperature when 4 g untreated kaolin/kg was present in the coker gas oil feed.	94
4-8	SEM micrographs of solids from liquid products from experiments with different solids added. All were reacted at 375 $^{\circ}\text{C}$ for 1 hr.: (a) 5 μm kaolin; (b) 0.2 μm kaolin; (c) 0.2 μm carbon black; (d) 5 μm asphaltene-coated kaolin.	95
4-9	EDX spectra for spherical and granular particles in liquid products from runs with 5 μm kaolin added to coker gas oil, reacted for 375 $^{\circ}\text{C}$, 1 h: (a) spherical particles; (b) granular particles	97
4-10	Effect of solvent etching on morphology of TI microspheres. Microspheres in sample (a), (b) and (c) were produced from coker gas oil after 2 h reaction at 420 $^{\circ}\text{C}$ and under H_2 atmosphere. Sample (d) was quinoline extracted.	100

5-1	Boiling point distribution of treated light gas oil	111
5-2	Schematic diagram of batch reactor, its internals and liquid addition system (All internals are shown to scale with respect to the dimensions of the batch reactor)	117
5-3	Schematic diagram of plexiglass model of reactor	119
5-4	Adsorption of asphaltenes on kaolin from 1:1 heptane/toluene mixture at 22 °C	126
5-5	Schematic representation of batch reactor as a recycle reactor	130
5-6	Variations of concentration of kaolin in liquid product with quantity of glass beads at 375 °C and 700 rpm when asphaltene-treated kaolin (75 mg asphaltenes/g kaolin) was used. The data points were fitted to a curve from <i>Equation 5-6</i> .	132
5-7	Photographs of the structure of kaolin deposit on top of the packed bed when untreated kaolin was used: (a) 20 g of glass beads; (b) 16.8 g of spent catalyst	134
5-8	Variations of concentration of kaolin in liquid phase with asphaltene treatment (375 °C, 700 rpm and 20 g glass beads): (a) asphaltene-coated kaolin with 75 mg asphaltenes/g kaolin; (a) asphaltene-coated kaolin with 37 mg asphaltenes/g kaolin; (c) untreated kaolin. The data were fitted to a curve from <i>Equation 5-6</i> .	139
5-9	Variations of specific deposit and residual carbon content in kaolin from liquid product with the initial ratio of asphaltenes to kaolin (375 °C, 700 rpm, 240 g TLGO, initial 6.2 MPa H ₂ and 60 min of reaction time). Asphaltenes were added to TLGO feed in the experiments on the right hand side of the dashed line.	140
5-10	Thermal stability of asphaltene coating on kaolin (375 °C, 700 rpm and initial hydrogen pressure of 6.2 MPa). The error bar shows the 95% confidence interval for packing of 20 g glass beads at reaction time of 60 min, based on five repeated runs.	143
5-11	Schematic illustration of mechanism for deposition of clays. The adsorbed organic components may be asphaltenes, humic material or other polar species.	151
6-1	Temporal variation of temperature and pressure when 2 mL water was added at 375 °C (1 g asphaltene-treated kaolin, 240 g TLGO, and 20 g of glass beads)	168

6-2	Cake formation on top of the packed bed of glass beads (375 °C, 1 h, 2 g of water, 700 rpm and 20 of glass beads)	170
6-3	Temporal variation of temperature and pressure when 2 mL water was added at 375 °C after reaction (1 g asphaltene-treated kaolin, 240 g glass beads, 240 g TLGO, and 20 of glass beads)	173
6-4	A schematic diagram for the settling of kaolin particles after the impeller was turned off	175
6-5	Mechanism for asphaltene displacement by supercritical water at hydrotreating conditions	176
6-6	Variations of specific deposit on a packed bed of glass beads with residual carbon content of kaolin from liquid product (375 °C, 700 rpm, 60 min of reaction time)	179

Appendices

A1-1	A schematic diagram of the 500 mL autoclave	192
A3-1	A schematic diagram of asphaltene-treated kaolin	199

Nomenclature

A	Stoichiometric coefficient	
a_a	Activity of solute asphaltene	
A^+	Fraction of reactant asphaltenes	wt %
A^*	Fraction of asphaltene cores	wt %
A_{ex}^*	Excess asphaltene cores beyond what can be held in solution	wt %
A_{max}^*	Maximum asphaltene cores that can be held in solution	wt %
C_0	Initial concentration of kaolin in liquid phase	kg/m^3
$C(t)$	Concentration of kaolin in liquid phase at time t	kg/m^3
C_{asp}	Carbon content of asphaltenes	wt %
C^*	Equilibrium concentration of kaolin in liquid phase	kg/m^3
C_{tk}	Carbon content of asphaltene-treated kaolin	wt %
d_m	Diameter of packing material	m
d_p	Diameter of depositing particles	m
f	Friction coefficient of the particle	kg/s
H^*	Fraction of product, nonvolatile heptane solubles	wt %
k	Deposition rate constant	min^{-1}
k_A	First-order reaction rate constant for reactant asphaltene thermolysis	min^{-1}
k_H	First-order reaction rate constant for reactant heptane solubles	min^{-1}
k_i	First-order reaction rate constant ($i = 1,2,3$)	min^{-1}
L_0	Interparticle separation	m

L_i	Length of each lobe of the i -th catalyst pellet	m
M_k	Mass of kaolin	kg
m	Mass of packing material loaded in the draft tube or Stoichiometric coefficient	kg
m_0	Initial mass of kaolin in the feed	kg
m^*	Mass of kaolin in the liquid product at the end of each run	kg
M_a	Molecular weight of solute asphaltene	g/mole
m_p	Mass of product	kg
m_f	Mass of feed	kg
$m_{s,p}$	Mass fraction of solids in the product	wt %
$m_{s,f}$	Mass fraction of solids in the feed	wt %
$m_{i,p}$	Mass fraction of the tie element in the solids filtered from the products	wt %
$m_{i,f}$	Mass fraction of the tie element in the solids filtered from the feed	wt %
m_{ik}	Mass of asphaltene-treated kaolin	kg
M_{asp}	Mass of asphaltene adsorbed	kg
n	Stoichiometric coefficient	
r	Radius of each lobe of a catalyst pellet	m
r_{gb}	Average radius of glass beads	m
S_L	Solubility limit	kg/kg
T	Absolute temperature	K
U_0	Stokes velocity	m/s
U_h	Hindered settling velocity	m/s

V	Concentration of volatiles	wt %
VR'	Fraction of vacuum residue not converted at time t	wt %
V_b	Volume of empty packed-bed in the draft tube	m^3
V_L	Volume of liquid phase	m^3
V_t	Volume of the packed bed	m^3
V_{gb}	Occupied volume of glass beads	m^3
V_p	Particle volume	m^3
x_a	Mole fraction solubility of solute asphaltene	mole/mole

Greek Symbols

ρ_{tk}	Density of asphaltene-treated kaolin	kg/m^3
ρ_k	Density of kaolin	kg/m^3
ρ_{asp}	Density of dry asphaltene	kg/m^3
ρ_a	Density of solute asphaltene	kg/m^3
ρ_p	Particle density	kg/m^3
ρ_0	Solvent density	kg/m^3
ρ_{kaolin}	Density of kaolin	kg/m^3
ρ_{gb}	Density of glass beads	kg/m^3
ρ	Density of packing	kg/m^3
μ_0	Viscosity of solvent medium	$Pa \times s$
σ^*	Equilibrium specific deposit of kaolin	kg/m^3
$\sigma(t)$	Specific deposit of kaolin on the bed of packing at time t	kg/m^3
γ_{sl}	Solid-liquid interfacial tension	N/m
γ_{sv}	Solid-vapor interfacial tension	N/m

γ_{lv}	Liquid-vapor interfacial tension	N/m
ϕ_s	Volume fraction of solvent	m ³ /m ³
δ_s	Solubility parameter of solvent	cal ^{0.5} /cm ^{1.5}
δ_s	Solubility parameter of solute asphaltene	cal ^{0.5} /cm ^{1.5}
ΔG	Gibbs free energy change	J/kg
ΔH	Change of enthalpy	J/kg
ΔS	Change of entropy	J/(kg×K)
ε	Porosity of the bed packing	m ³ /m ³

Abbreviations

R^\bullet	Free radical
C	Coke
CGO	Coker gas oil
D	Distillate (< 530 °C)
EDX	Energy dispersive X-ray analysis
H/C	Hydrogen/carbon atomic ratio
HDN	Hydrodenitrogenation
HDO	Hydrodeoxygenation
HDS	Hydrodesulfurization
I	Initiator or reaction intermediate
LGO	Light gas oil
M	Parent compound
MCR	Microcarbon residue

SCFE	Supercritical fluid extraction
SEM	Scanning electron microscopy
SSP	Side Stream Product
TGO	Treated gas oil
THF	Tetrahydrofuran
TI	Toluene-insoluble(s)
TLGO	Treated light gas oil
UNITAR	United Nations Institute for Training and Research
VR	Vacuum residue (530 °C +)

Chapter 1: Introduction

1.1 Oil Sands of Alberta

Oil sands are deposits of sand saturated with bitumen and water, which are commonly found at or near the earth's surface. About 98% of all oil sands are found in seven large deposits (Matar and Hatch, 1994). The Athabasca deposit in Western Canada is the largest, covering an area of 46,800 square kilometers and containing an estimated 137 billion cubic meters (862 billion barrels) of oil (Liu and Gunning, 1991). The oil-bearing formation has a thickness of up to 45 meters, covered with overburden and muskeg, a wet mass of partially decayed vegetation varying from 0 to 75 meters in thickness.

The Athabasca deposits are strip-mined if they are near the surface. In situ recovery processes are under development for deposits deeper than 75 m. The bitumen can be separated from oil sand in the form of froth by using hot water with a small amount of alkali, because the sand is water wet (Clark and Pasternak, 1932). Froth treatment minimizes the water and solids in the bitumen by diluting with naphtha and by processing through multi-staged centrifuges. The produced bitumen is a very viscous material having a density of approximately 1,050 kg/m³. It is then subjected to a cracking process to produce distillate fuels and coke. *Table 1-1* is a typical assay of Athabasca bitumen. It is noted that the total mass balance in this table is more than 100%, but the magnitude of each elemental concentration is still suggestive.

About one tenth of the Athabasca formation lies within 50 m of the surface, allowing economic recovery of bitumen by conventional strip-mining techniques (Berkowitz and Speight, 1975; Hocking, 1977). The Syncrude and Suncor mines are both located in an

Table 1-1. Properties of Athabasca bitumen (Chung et al., 1997)

Gravity, °API at 15.6 °C	7.8
Carbon, wt %	85.5
Hydrogen, wt %	11.0
Sulfur, wt %	4.7
Nitrogen, wt %	0.4
MCR, wt %	14
Nickel, wppm	80
Vanadium, wppm	220
Ash, wt %	0.75

area with relatively shallow overburden, so the oil sand can be mined by open-pit mining. Currently, the combined production of the two fully integrated plants, operated by Syncrude and Suncor respectively, exceeds 18% of the total Canadian crude oil production. A schematic flow chart of the Syncrude plant is shown in *Figure 1-1*, where CGO is the coker gas oil, SSP is the side stream product, LGO is the light gas oil, and TGO is the treated gas oil.

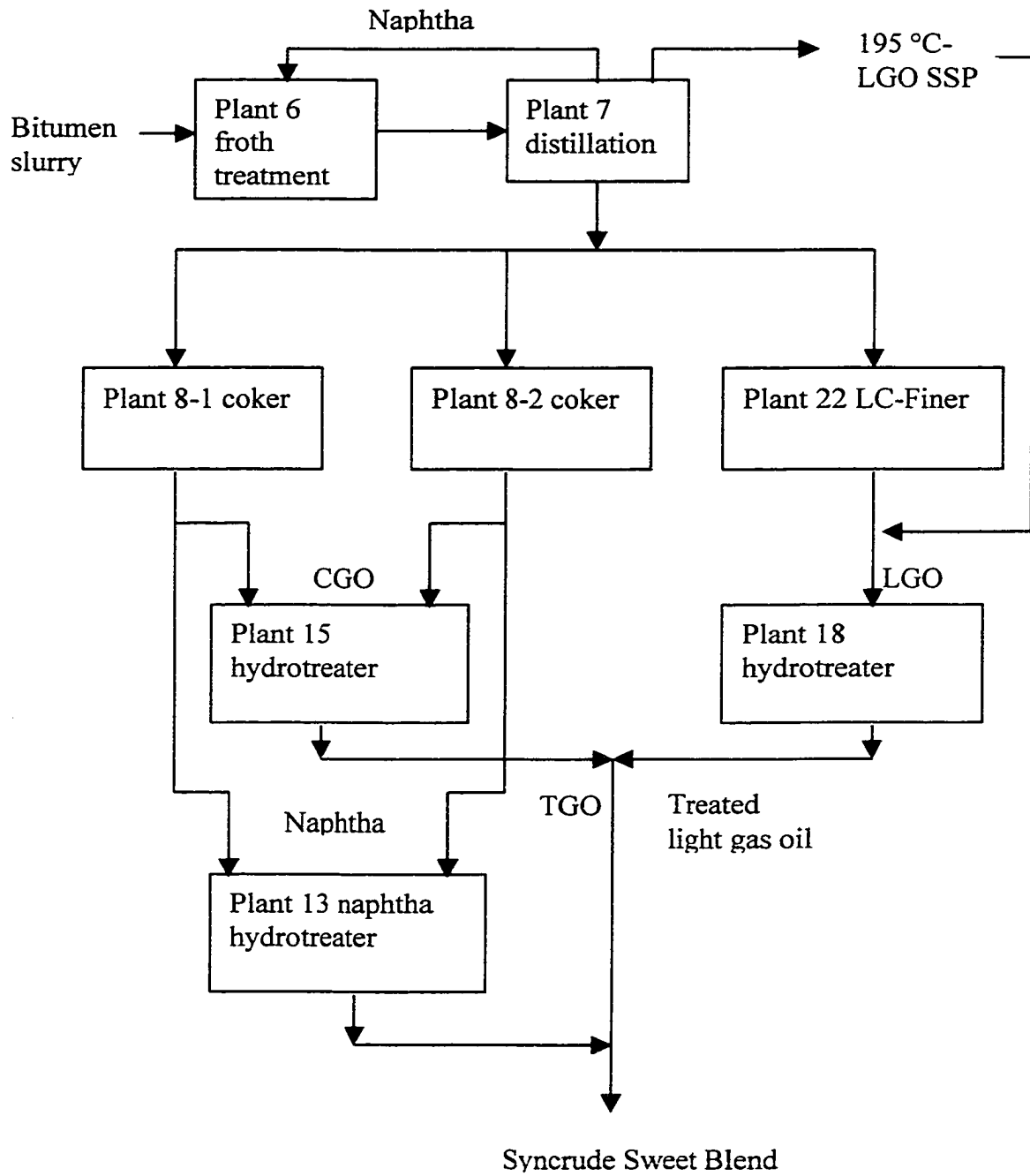
For deeper oil sand formations, where overburden stripping is no longer economical, in situ recovery techniques are being developed and tested by several operators.

Commercial application of steam processes has been underway at heavy oil deposits since the early 1960s (Speight, 1991). These methods usually use steam injection or underground combustion by burning part of the crude oil. This reduces the oil viscosity and partially vaporizes the oil in place, and the oil is driven out of the reservoir by a combination of steam, hot water, and gas drive (Speight, 1991). In addition to adding heat, these processes provide a driving force, i.e. pressure difference, to move oil to production wells. In situ combustion has been field tested under a wide variety of reservoir conditions, but few projects have proven economical and advanced to commercial scale, and results with Athabasca oil sand have been poor.

1.2 Commercial Upgrading of Bitumen

Bitumen has a number of properties that set it apart from conventional crude oils. However, the distinction is made primarily on the basis of viscosity and density according to the UNITAR definition (Gray, 1994). At original reservoir temperatures, heavy crude oils have a gas-free viscosity from 100 to 10,000 mPa-s, and bitumens have a

Figure 1-1. The flow chart to obtain Syncrude sweet blend



gas-free viscosity from 10,000 to several million mPa-s. Additionally, the hydrogen/carbon atomic ratio of bitumens is lower than that of most crude oils. Athabasca bitumen contains approximately 17% asphaltenes, and roughly one half of the bitumen has an atmospheric equivalent boiling point exceeding 524 °C. Most of these bitumens have high sulfur and nitrogen contents (*Table 1-1*), which require extensive further processing before use in commercial refineries. Due to the decreased availability of light sweet crude oils, and an increasing fraction of heavy and sour crude oils, upgrading bitumens into consumer products becomes more and more attractive.

Typically, the upgrading process is carried out in two steps. Primary upgrading (e.g. coking with delayed coker and hydroconversion with LC-Finer) focuses on the conversion of bitumen into lighter materials, and on the removal of impurities and contaminants, such as metals and mineral matter. Nitrogen and sulfur are only partly removed. Overall, the product after primary upgrading is improved over the raw material, but still falls short of the requirements of a conventional refinery due to its high contents of sulfur, nitrogen, metals, and unsaturates. The product is split into naphtha, light and heavy gas oil streams, which are processed further in the presence of a hydrotreating catalyst in the hydrotreater units at high partial pressures of hydrogen and elevated temperatures. The secondary upgrading, or hydrotreating, gives selective removal of the heteroatoms from the feed with little attendant conversion of the hydrocarbons. The reaction temperature ranges from 350 to 410 °C.

1.3 Hydrotreating of Distillate Oils

1.3.1 Hydrotreating Processes

Hydrotreating of distillates is often accomplished in a reactor packed with catalyst pellets. The hydrotreating catalyst is held in a fixed bed while the liquid and hydrogen gas normally flow downward co-currently. The boiling range of the feed, and the operating temperature and pressure in the hydrotreater will determine the fraction of the feed in the vapor phase and the fraction in liquid. Gas oil hydrotreaters normally operate in the trickling or pulse-flow regime, with liquid present inside the reactor column at all times. An example flow diagram for this process is illustrated in *Figure 1-2*.

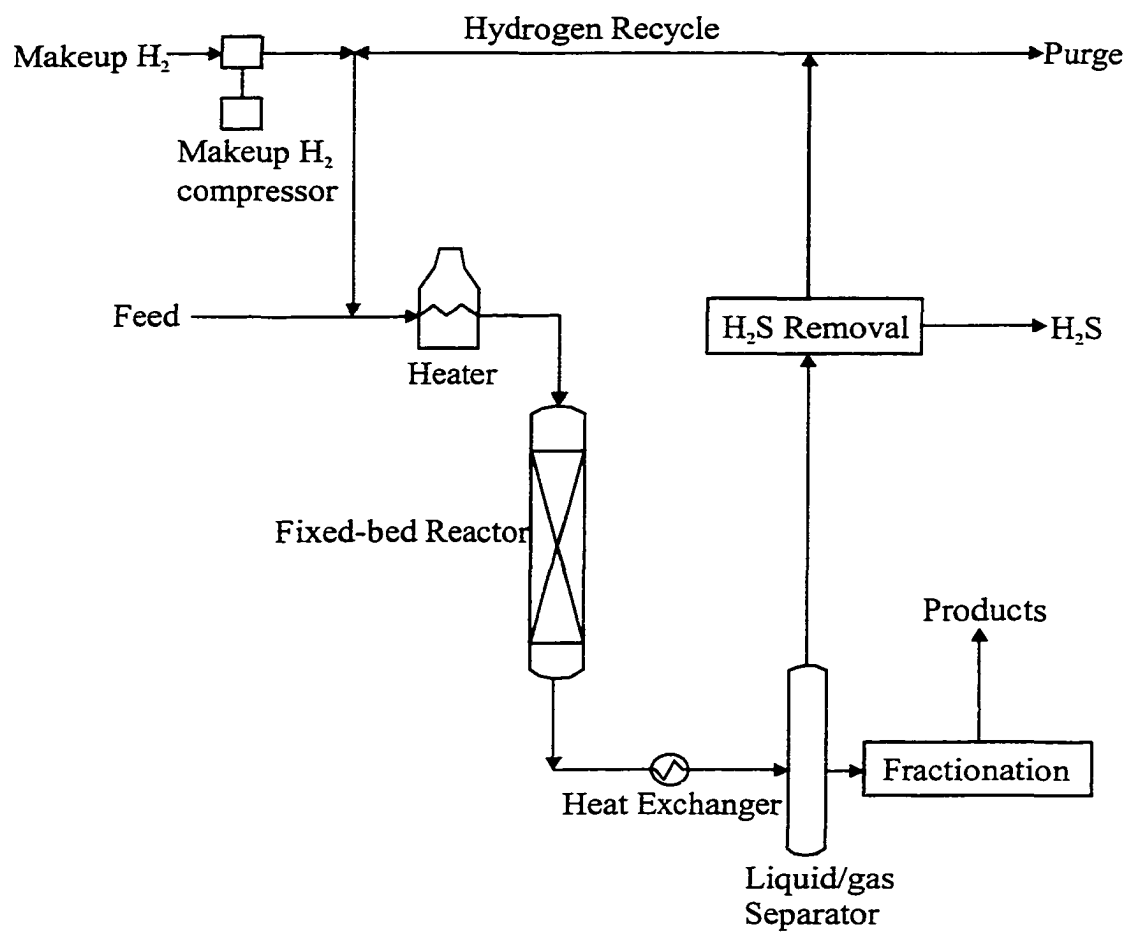
The feed is heated to the desired inlet temperature and then passes through the reactor with an excess hydrogen supply. Downstream of the reactor, hydrogen sulfide is removed by alkanolamine absorption, and the hydrogen is recompressed and reused. The light gases that form due to cracking are circulated with the hydrogen, which necessitates a purge. Fresh hydrogen is added to balance the loss in the purge stream and the consumption of hydrogen in reactions in the reactor.

Hydrotreating a cracked distillate involves a formidable combination of reactions that occur simultaneously: hydrodesulfurization (HDS), hydrodenitrogenation (HDN), hydrodeoxygenation (HDO), hydrogenation of aromatics, and thermal cracking. The hydrotreating reaction is exothermic, so that the exit temperature is higher than that at the inlet.

1.3.2 Deactivation of Hydrotreating Catalyst

The catalyst in the reactor is packed in beds with a depth of 3-6 m. Liquid is redistributed between each bed. This amount of catalyst in each bed is the practical limit

Figure 1-2. Typical trickle-bed hydrotreating process (Gray, 1994)



due to the physical strength of the catalyst and the need to ensure good liquid distribution. The catalyst in the packed bed deactivates with time, so the reactors are operated on a rising temperature profile to maintain a constant conversion level. The initial activity of the catalyst is important, along with the equilibrium catalytic activity and regenerability of the catalyst over an extended service life.

Coke formation is one of the causes for catalyst deactivation. The first step for coke deposition is the surface adsorption of coke precursors, followed by oligomerization and aromatization reactions (Gray, 1994). Increased hydrogen pressure reduces coke accumulation by suppressing the oligomerization and hydrogenating the adsorbed species.

1.3.3 Pressure Drop Buildup Problem in Hydrotreaters

Fine particles that may appear in Athabasca oil sands derived streams include corrosion products, coke and mineral solids. Corrosion products form from the surfaces of processing units and pipelines, usually by chemical reaction. Iron sulfide is a typical example of corrosion products in oil streams. It may form due to the reaction between iron salts or iron oxides, and hydrogen sulfide.

Coke is the carbonaceous material produced from petroleum during thermal processing. It has a high carbon content, of over 95% in weight on an ash free basis. The color varies from gray to black, and the material is insoluble in organic solvents. In processes such as delayed coking and fluid coking, fine coke particles can be entrained into coker distillates.

Athabasca bitumen also contains finely dispersed clay solids. During the separation of bitumen from oil sands, the transfer of mineral particles from the oil sands ore into an

aqueous phase is the critical step. When the mineral solids are completely hydrophilic and separated from bitumen by interstitial water, this process is relatively easy.

However, the presence of toluene-insoluble organic matter adsorbed onto mineral surfaces allows some small mineral particles ($< 30 \mu\text{m}$) to enter the bitumen product along with any free organic particles (Kotlyar et al., 1998). Any mineral particles not rejected after the froth treatment process remain with the bitumen and adversely affect its quality. Some of these particles are entrained into the gas oil fraction during distillation, and these entrained fine solids subsequently enter downstream hydrotreaters.

Filtration prior to the reactor bed can effectively remove particles larger than $20 \mu\text{m}$, but not the smaller fine particles. Although the concentration of these fine particles is quite low (at the level of several parts per million in weight), they may accumulate significantly in the packed-bed reactor and cause appreciable increase in pressure drop. This pressure drop buildup may finally be excessively high so that the reactor has to be shut down before the activity of the hydrotreating catalyst is fully used (Chan et al., 1994). Reactor shutdowns, especially unscheduled ones, are time-consuming and expensive by removing the catalyst that are still active.

1.4 Research Objectives and Methodology

1.4.1 Major Objectives

There are two major objectives in this study.

- (1) It was estimated that 30 wt % of the fines captured in Syncrude coker gas oil hydrotreaters were attributed to catalyst attrition, 5 % from coke-make, and the remaining 65 % attributed to the dispersed clay (Chan et al., 1994). The coke may be entrained from upstream cokers, or produced in-situ in the hydrotreaters. The first

objective was to determine the interactions between the organic toluene-insolubles and clays with different surface properties, and the impact of this interaction on the subsequent particle deposition.

(2) Fine particles in the hydrotreater feeds vary in their surface properties due to their processing history. Kaolin is the most abundant clay in Athabasca oil sands.

Asphaltene-treated kaolin was used to simulate the authentic mineral solids in the oil streams. The hydrotreating conditions (catalyst, hydrogen and elevated temperatures) may change the surface properties of fine particles. The vapor byproducts, i.e. water and ammonia, which were produced in hydrotreaters, and unconverted polar compounds in liquid phase, such as quinoline, may also interact with the organic coating on fine particles. The second objective was to determine the deposition mechanism for various solids with different surface properties, and the possible effects of the polar compounds on particle deposition.

1.4.2 Simulation of Commercial Hydrotreaters

Most packed-bed hydrotreaters are operated under one of the two common flow regimes, trickle or pulsed flow, depending on the gas and liquid fluxes and their corresponding physical properties, i.e. density, viscosity and surface tension. In the trickle flow regime, the interaction between liquid and gas is low, and they flow independently of each other. At higher gas and liquid flow rates, pulsed flow is observed. This flow regime is characterized by the intense interaction of the liquid and gas. Ideally, the fines capture tests should be conducted in a pilot unit at hydrogen pressure and flow rates of gas oil yielding the hydrodynamic conditions equivalent to the commercial reactors. As an alternative, rather than trying to reproduce both the chemistry and the

physics of the commercial reactor, a 500-mL batch reactor with internal circulation of liquid and gas was selected for tests of particle deposition at temperatures and hydrogen partial pressure similar to the commercial hydrotreaters. Although the hydrodynamics of the batch reactor are significantly different from the packed-bed hydrotreater, our study focused on the effect of surface chemistry of fine particles on their deposition. The selected apparatus gave controlled hydrodynamics, and allowed a systematic variation of the chemistry of the system at temperatures and pressures that are typical of hydrotreating.

1.4.3 Variables Studied in Particle Deposition in a Batch Reactor

In order to understand the role of the surface chemistry of fine particles on deposition and plugging in packed-bed hydrotreaters, a simplified experimental system was constructed. A model suspension of kaolin in gas oil was selected, and the surface properties of the kaolin were modified by pretreatment with asphaltenes. To study interactions between toluene-insoluble matter and mineral solids, coker gas oil was used because it is the feed for hydrotreaters and it has a low content of asphaltenes (0.6 wt %). In an oil stream, kaolin carries adsorbed organic matter on its surface (Kotlyar et al., 1998). Asphaltene-treated kaolin, with various concentrations of asphaltene coating, was used to simulate the fine kaolin solids in the oil streams. Carbon black was used because it is considered hydrophobic, similar to asphaltene-treated solids and coke materials. The filtered solids from the liquid product were analyzed with scanning electronic microscopy (SEM), energy dispersive X-ray analysis (EDX), and elemental analysis.

For particle deposition experiments, hydrotreated gas oil was used to minimize changes in fluid properties with time. Iron sulfide particles with and without

asphaltene-treatment were used to represent corrosion products in oil streams. Experiments were conducted with either glass beads or catalyst pellets as the bed packing, to serve as the collectors for the fine particles. The filtration of kaolin particles by the packed beds was determined as a function of time and reactor operation, including the introduction of liquid additives such as water, ammonia, and quinoline.

1.5 Structure of Thesis

In **Chapter 1** the entire thesis is introduced and some terminology used most often in the thesis is defined. Also, in this chapter the industrial background for this research is described and the main objectives of this thesis are identified. In **Chapter 2** presents an extensive review on the kinetics and mechanism of toluene-insoluble solids formation during processing of heavy oils and bitumen is presented. The toluene-insoluble solids that are discussed include coke in various processes, sediments during processing heavy oils, and fouling in downstream reactor vessels. Various parameters affecting the formation of solids are examined, and methods for mitigation of coke formation are discussed. Particle deposition in porous media is reviewed in **Chapter 3**, mainly in aqueous systems, but the concepts are extended to non-aqueous systems. Experiments are reported in **Chapter 4**, in which coker gas oil was thermally treated at temperatures (300-420 °C) under an atmosphere of hydrogen or nitrogen. Untreated kaolin, asphaltene-treated kaolin, and carbon black were introduced into the feed, independently. Two sizes of kaolin particles were used to give different specific external surface areas. The interactions of these solids with organic toluene-insoluble were studied with SEM and EDX by analyzing the solids filtered from liquid product. The carbon contents of all filtered solids were measured to determine the effect of introduced solids on coke yield.

Deposition of fine particles in packed beds at hydrotreating conditions was studied (**Chapters 5 & 6**), using untreated kaolin, asphaltene-treated kaolin, and iron sulfide. Iron sulfide was used to represent corrosion products. A draft tube loaded with glass beads or catalyst pellets was installed inside the batch reactor, and the two impellers were utilized to promote fluid circulation through the packed bed in the draft tube. This apparatus was employed to simulate fine capture in packed beds under a well-defined hydrodynamic condition. The deposit morphology on the top of the packed bed was recorded with a camera, and the specific deposit of fine particles on the collectors was determined. The relationship between the deposition behavior and surface chemistry of fine particles was determined. **Chapter 6** focuses on the effect of polar compounds on deposition of asphaltene-treated kaolin and authentic solids in oil streams. Water, ammonia, and quinoline were introduced into the batch reactor at the reaction temperatures (375 °C or higher). The carbon contents of filtered solids from liquid products were measured, so that the effects of liquid additives on removal of asphaltene coating from fine particles were determined. **Chapter 7** summarizes the key results and conclusions of the thesis. Some possible industrial implications and future research work in this area are suggested.

References

- Berkowitz, N.; Speight, J. G. The Oil Sands of Alberta. *Fuel* **1975**, *54*, 138-149.
- Chan, E. W.; Chung, K. H.; Veljkovic, M.; Liu, J. K. Hydrodynamics and Fines Capture in Packed-Bed Hydrotreaters. *Int. Petrol. Petrochem. Technol. Symp.*, Beijing, September 15-17, **1994**.
- Chung, K. H.; Xu, C.; Hu, Y.; Wang, R. Supercritical Fluid Extraction Reveals Resid Properties. *Oil Gas J.* **1997**, *95*(3), 66-69.
- Clark, K. A.; Pasternak, D. S. The Hot Water Separation of Bitumen from Alberta Bituminous Sand. *Ind. Eng. Chem.* **1932**, *24* (12), 1410-1416.
- Gray, M. R. "Upgrading Petroleum Residues and Heavy Oils." Marcel Dekker, Inc. New York, **1994**.
- Hocking, M. B. The Chemistry of Oil Recovery from Bituminous Sands. *J. Chem. Educ.* **1977**, *54*, 725-729.
- Kotlyar, L. S.; Sparks, B. D.; Chung, K. H. Organic Rich Solids from Oil Sands: Properties and Role in Processing. *Rev. Proc. Chem. Engr.* **1998**, *1*, 81-110.
- Liu, J. K.; Gunning, H. E. "Syncrude Analytical Methods Manual for Bitumen Upgrading," published by Alberta Oil Sands Technology and Research Authority, **1991**.
- Matar, S.; Hatch, L. F. "Chemistry of Petrochemical Processes." Houston: Gulf Pub. Co., **1994**.
- Speight, J. M. "The Chemistry and Technology of Petroleum." Marcel Dekker, Inc. New York, **1991**.

Chapter 2: Literature Review – Kinetics and Mechanism of Toluene-Insolubles Formation during Processing of Heavy Oils

2.1 Introduction

As the supply of conventional crude oils decreases and the demand for light product expands, processing of heavy oils and bitumen is becoming increasingly important. Formation of various toluene-insoluble organic solids, such as coke, is common in processing these heavy feeds. This chapter covers the formation of organic solids from heavy feeds. The formation of organic solids includes coke production, sediment formation during hydroconversion, and fouling occurring in subsequent processing and utilization. The purpose of this review is to emphasize how these three seemingly discrete phenomena are intimately linked in non-catalytic processes through free radical reaction chemistry and phase behavior. The effects of feedstock, hydrogen, solvents, and particulate in the feed on the formation of these organic solids are stressed as well. It will be helpful to our later discussion to first introduce some definitions associated with the formation of organic toluene-insolubles.

2.2 Definitions of Coking, Sediment Formation and Fouling

2.2.1 Coke Production

Coke is defined as a carbonaceous product of pyrolysis of organic material, at least parts of which have passed through a liquid or liquid-crystalline state during the carbonization process (Kochling et al., 1982). The term “liquid crystal” is used to describe fluids that have organized structure, giving anisotropy under cross-polarized light. Such fluids possess more structural order than that found in normal isotropic

liquids, but are not fully crystalline. The term “mesophase” is frequently used interchangeably with liquid crystalline state in the literature on coke growth and formation.

Petroleum coke is further defined as a carbonization product of high boiling carbon fractions obtained in petroleum processing (Kochling et al., 1983), which includes green coke, calcined coke and needle petroleum coke. However, even a cursory examination of the literature on processing of various fractions of petroleum shows that toluene-insoluble (TI), benzene-insoluble, quinoline-insoluble and tetrahydrofuran (THF)-insoluble carbonaceous materials are commonly referred to as “coke” (Belinko et al., 1977; Bisaria et al., 1993; Del Bianco et al., 1993a; Wiehe, 1996). Therefore, in this review coke is defined as a solubility fraction derived from petroleum that is insoluble in the above-mentioned solvents, among which toluene is most commonly used.

The upgrading of heavy oils or bitumens is carried out mainly in two ways: by coking and by hydrogen addition. From a chemical reaction viewpoint, coking can be considered a severe thermal cracking process in which the end products are carbon-rich residue, hydrogen-rich gas, and liquid distillate with a similar hydrogen/carbon ratio to the feed. Three types of coking processes (delayed coking, fluid coking and Flexicoking) are widely used in refining, and the detailed descriptions are provided elsewhere (Speight, 1991; Gray, 1994). The cokes from each process differ significantly with regard to their properties and end uses. However, conversion of a significant portion of the feed to coke is much less valuable than forming the same amount of distillate products. Hence, the importance of hydrogen addition processes is increasingly recognized, in which hydrogen gas is used to stabilize the reactive radical fragments

produced during the thermal cracking of the heavy oil feeds. Consequently, the coke formation is minimized and liquid yield is increased.

2.2.2 Sediment Formation and Fouling

Precipitation of insoluble organic material can occur under a variety of process conditions, and this kind of precipitate is often called sediment. For example, sediment forms in the liquid product of visbreaking and hydrocracking processes for upgrading vacuum residue or heavy crude oils (Storm et al., 1997). The sediment accumulates in downstream separators, heat exchangers and fractionating towers, limiting conversion in visbreaking and upgrading processes and eventually causing a shutdown. In this sense, sediment formation and fouling are closely linked, because fouling is generally defined as the formation of deposits on heat transfer surfaces, which interferes with heat transfer and/or fluid flow. Among many fouling mechanisms which may be present simultaneously, chemical reaction fouling and particulate fouling are most common in petroleum refining (Garrett-Price et al., 1985). Chemical reaction fouling gives deposits due to the chemical reactions within the process fluid. Particulate fouling, on the other hand, is the accumulation of particles (e.g. iron sulfide) from a liquid suspension onto heat-transfer surfaces.

It is noted that many processes have to contend with fouling problems related to localized coke formation during heating. Characterization of deposits from many heat exchangers for hundreds of crude oils and mixtures showed that fouling is closely related to the presence of asphaltenes (Dickakian and Seay, 1988). The mere presence of asphaltenes, however, does not necessarily dictate that a crude oil will foul. It is the incompatibility between the asphaltenes and the oil medium that initiates the precipitation

of some asphaltenes, which then adhere to the hot metal surface and react to form coke. The step of coke formation produces irreversible decreases in heat transfer coefficients and reduces the diameter of the available flow channel. One of the marked differences between coking and fouling could be that coke is mainly produced in the bulk phase of the oil, whereas fouling occurs by gradual deposition of trace amounts of asphaltenes followed by coking. Alternatively, fouling could be the immediately following step of coke formation in the bulk phase, which in turn is controlled by the incompatibility of asphaltenes in the aliphatic oil phase. Despite the fact that coke is a significant constituent of fouling deposits (Crittenden et al., 1992; Lemke and Stephenson, 1998), the incorporation of inorganic matter (e.g. iron-containing materials) into fouling deposits suggests other fouling mechanisms (e.g. particulate fouling). The presence of inorganic matter may indicate some interactions between inorganic materials and coke-precursors during the fouling process. The effects of fine mineral matter on TI solids formation will be discussed later in this review chapter.

The phenomena of coking, sediment formation and coke-related fouling could be related to the formation of a new liquid and then a solid phase from the petroleum. In order to understand these phenomena, we need to know which constituent of petroleum is the most important contributor to this new solid phase, and how this new solid phase is formed under various conditions. It will be useful to our further discussion to introduce the methods for fractionation of petroleum.

2.3 Fractionation of Petroleum

Petroleum is a mixture of hydrocarbons with very complicated composition and physical-chemical properties. Fractionation means to separate petroleum into many

fractions, where each fraction has similar composition and physico-chemical properties. Distillation is the primary method of fractionation, separating various fractions based on their different volatilities. The remaining materials (i.e. distillation residue) can be further fractionated into four classes of compounds: saturates, aromatics, resins, and asphaltenes (SARA), based on their solubility and adsorption ability (Gray, 1994). When the whole distillation residue is dissolved in an aromatic solvent such as toluene, addition of alkane such as n-pentane in excess will give precipitated asphaltenes. Saturates, aromatics and resins are separated according to their adsorption selectivity on a solid support such as silica. Of the four classes of compounds, only saturates are distinguishable from the rest of the hydrocarbons because saturates contain only aliphatic compounds. There are no clear demarcation lines between aromatics and resins, and between resins and asphaltenes. The mixture of aromatics, resins, and asphaltenes constitutes a compositional continuum with regard to both molecular weight and polarity (Altgelt and Boduszynski, 1994).

Asphaltenes differ from the remainder of the crude oil in being insoluble in light alkanes such as n-pentane but soluble in aromatic solvents such as benzene and toluene. A significant variation in the average chemical characteristics (e.g. molecular weight, aromaticity, functional groups, etc.) of asphaltenes may arise when they are isolated from oils of different sources. Even asphaltenes from the same source are composed of molecules that differ markedly in their chemical characteristics. Consequently, asphaltenes are the most heterogeneous solubility fraction in petroleum.

Asphaltenes and resins are the first and second contributors for coke formation in terms of importance (Karacan and Kok, 1997), and coke was formed most rapidly from

the asphaltenes fraction with the greatest aromaticity (Banerjee et al., 1986). Since asphaltenes are the principal coke precursor, it is important to analyze the structure of asphaltenes in petroleum and understand how coke is produced from petroleum, following the destruction of this structure.

2.4 Structure of Asphaltenes

Asphaltenes tend to form aggregates in hydrocarbon mixtures, and these aggregates are commonly referred to as micelles in the literature, based on an analogy with the behavior of surfactant molecules in solution (Pfeiffer and Saal, 1940). There is a fundamental difference, however, between the monomers of asphaltenes and common surfactants due to the polydispersity in molecular weight and chemical structure of asphaltenes. The asphaltene micellar system is conceptually equivalent to a mixed surfactant system with a nearly infinite number of components. Assuming that an asphaltene molecule is a cylinder when it adsorbs at the oil/air interface, the height of the cylinder is about 6.6 nm (Sheu, 1996). Based on their physical size, the micellar aggregates formed in hydrocarbon media were defined as colloids or microemulsions (Sheu, 1996). The models for the structure of asphaltenes in our discussion can be classified into steric-stabilization models and thermodynamic models. Steric-stabilization models assumes that asphaltenes are stabilized by a transition material (e.g. resins) in the oil, while thermodynamic models assume that dissolved asphaltenes are in balance with precipitated ones thermodynamically.

2.4.1 Steric-Stabilization Models

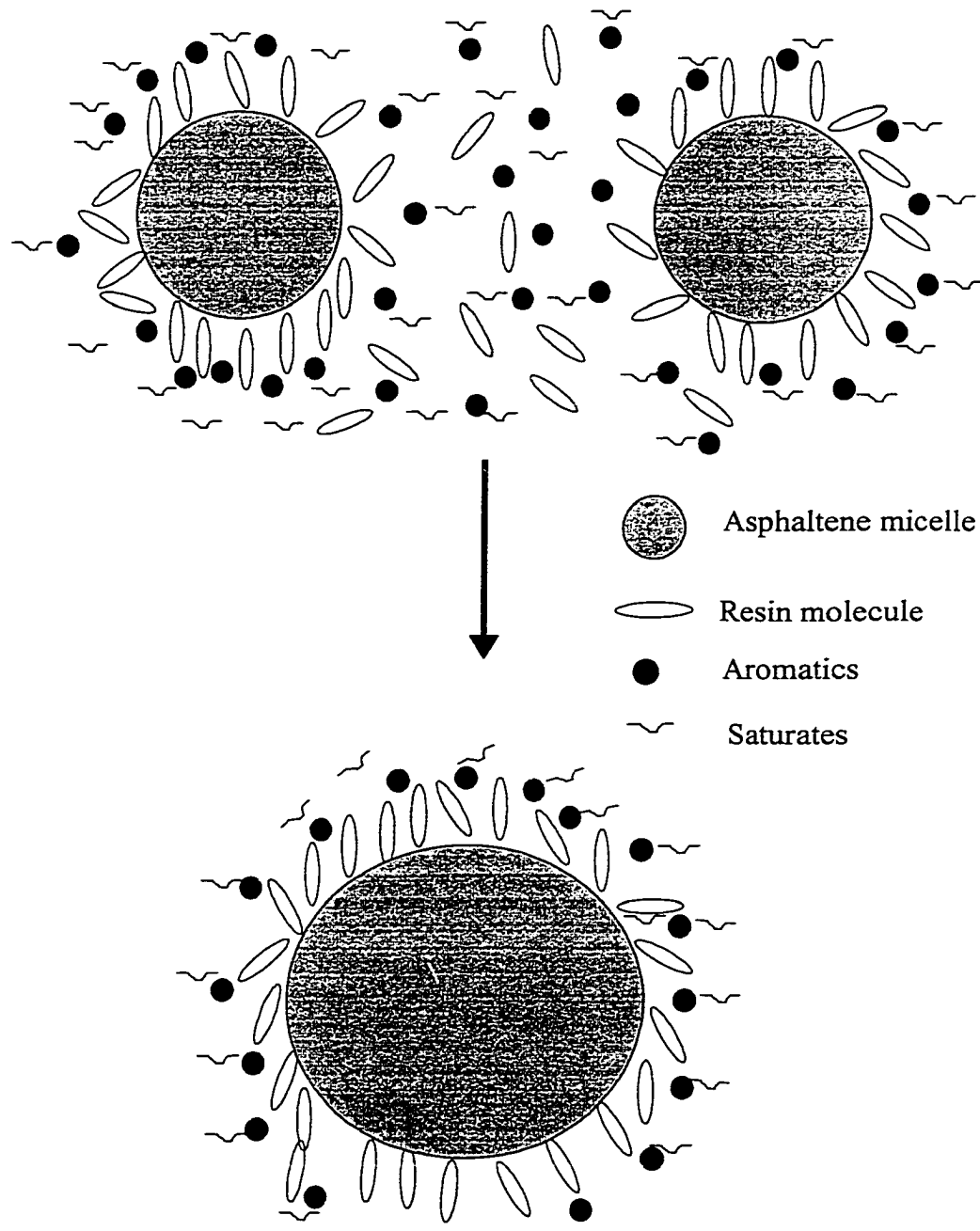
Pfeiffer and Saal (1940) originally devised the microemulsion model of petroleum to interpret rheological data. This model has been extensively accepted and modified

(Riggs and Diefendorf, 1980a and 1980b; Rand et al. 1989; Wiehe, 1996). In this model asphaltenes are dispersed by the surfactant-like resins, which in turn are held in solution by aromatics (*Figure 2-1*). The resins typically consist of long paraffinic groups, and highly polar end groups that often contain heteroatoms (e.g. oxygen, sulfur and nitrogen). The polar end groups in resins and asphaltenes attract each other in the form of hydrogen bonding and dipole-dipole interactions. The paraffinic chains of the resin molecules provide the transition to the relatively non-polar bulk phase of the oil where individual molecules are in the true solution (Hunt, 1996).

Since asphaltenes are incompatible with the oil fraction, dispersion of asphaltenes is attributed mainly to the resins, which provide steric stabilization against flocculation and precipitation. Thus, any factors resulting in solubilization of the resins will lead to dissociation of the resin-asphaltene complexes, which in turn gives phase separation of asphaltenes. For example, removal of the resin fraction from the micelles by thermal conversion at elevated temperatures or by dilution with alkane will cause asphaltene precipitation. A separate phase of asphaltenes occurs when the solvating power of the surrounding medium toward the asphaltene monomers and micelles is reduced to the point at which they are no longer fully compatible with the oil medium (*Figure 2-1*).

Another steric-stabilization model was proposed by Storm et al. (1995) in which a classical solvation shell forms around the hard asphaltenic particles and protects them from flocculation, because the adsorbed layer generates short-range repulsive forces at small inter-particle separations against the attractive dispersion forces. The thickness of the adsorbed layer is temperature dependent, and increasing the temperature above 200 °C will decrease the thickness of this protective layer and thus steric forces to such an

Figure 2-1. Hypothetical mechanism of asphaltenes aggregation from crude oils
(Pfeiffer and Saal, 1940)



extent that a separate phase of asphaltenes is formed by aggregation (Storm et al., 1996).

It is assumed in steric-stabilization models that asphaltene micelles are lyophobic dispersions, and resins are physically present at the interface between the asphaltene micelles and the oil medium. However, examples can readily be found to show that the inclusion of resins is not a necessary condition for the stabilization of asphaltenes micelles against further aggregation in hydrocarbon media. For example, the asphaltenes can be dissolved in good solvents, forming a stable dispersion against precipitation and giving no change in the dimensions of asphaltenes micelles (Cimino et al., 1995). The solutions of asphaltenes display these properties without the presence of a resin fraction.

2.4.2 Thermodynamic Models for Asphaltene Solubility and Separation

Solubility parameter has often been used in the thermodynamic approach to describing asphaltenes solubility in oil media. The difference in solubility parameter between asphaltenes and oil media results in a phase separation of asphaltenes from the medium. This difference in solubility parameter can be estimated using the Scatchard-Hildebrand equation (Griffith and Siegmund, 1985):

$$\ln a_1 = \ln x_1 + \frac{M_1}{RT\rho_1}(\phi_2(\delta_1 - \delta_2))^2 \quad (2-1)$$

where a_1 , x_1 , M_1 , and ρ_1 are the activity, the mole fraction solubility, the molecular weight, and the density of dry asphaltenes, respectively; R is the gas constant, T is the absolute temperature, ϕ_2 is the volume fraction of solvent, and $(\delta_1 - \delta_2)$ is the difference in solubility parameter between asphaltenes and solvent. Assuming that in a very dilute system insoluble asphaltenes are in equilibrium with asphaltenes in solution, and the

activity of the solute asphaltenes and the volume fraction of the solvent are both unity,

Equation (2-1) gives

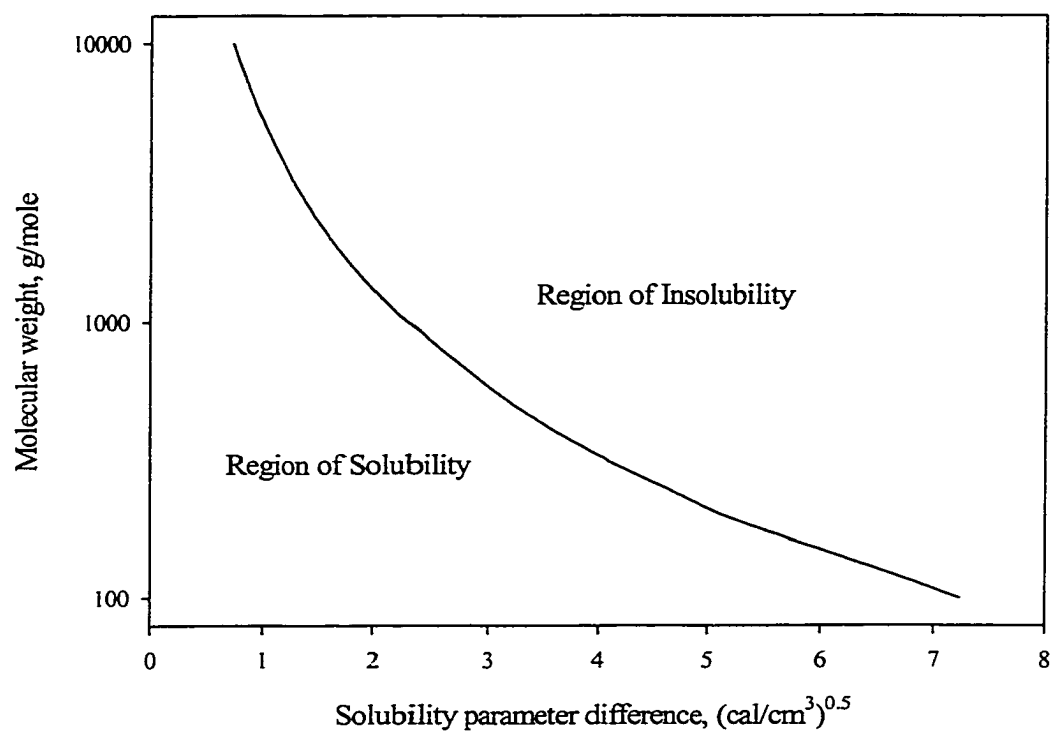
$$\ln x_1 = -\frac{M_1}{RT\rho_1}(\delta_1 - \delta_2)^2 \quad (2-2)$$

Schabron and Speight (1998) calculated the difference in solubility parameter from *Equation (2-2)* by changing the molecular weight of asphaltenes from 100 to 10,000 g/mole at the given maximum solubility of asphaltenes (i.e. 0.001 in mole fraction), and plotted a phase diagram with regions of insolubility and solubility that is a function of molecular weight and solubility parameter difference (*Figure 2-2*). This phase diagram shows that when the molecular weight of asphaltenes decreases, the tolerance of difference in solubility parameters between asphaltenes and oil medium to allow asphaltenes to remain dissolved is increased. Upon thermal cracking at elevated temperatures, asphaltenes become progressively more aromatic as the alkyl side chains are stripped from the aromatic cores. The side alkyl chains are reacted off from asphaltenes to enter the oil medium and to give asphaltene cores with less solubility and an oil medium with less solvency power (Mochida et al., 1990; Speight and Long, 1996). Thus, the difference in solubility parameters between the asphaltenes and the surrounding medium is constantly increasing until such a value is reached that a separate phase of asphaltenes is formed, usually followed by the formation of TI solids.

2.4.3 Multiphase Behavior of Hydrocarbon Mixtures at Elevated Pressures and Temperatures

The processes for bitumen and heavy oil upgrading have yet to be further optimized because the understanding of the phase behavior of these materials at elevated pressures

Figure 2-2. Phase diagram of asphaltene molecules in liquid oil media (Schabron and Speight, 1998)

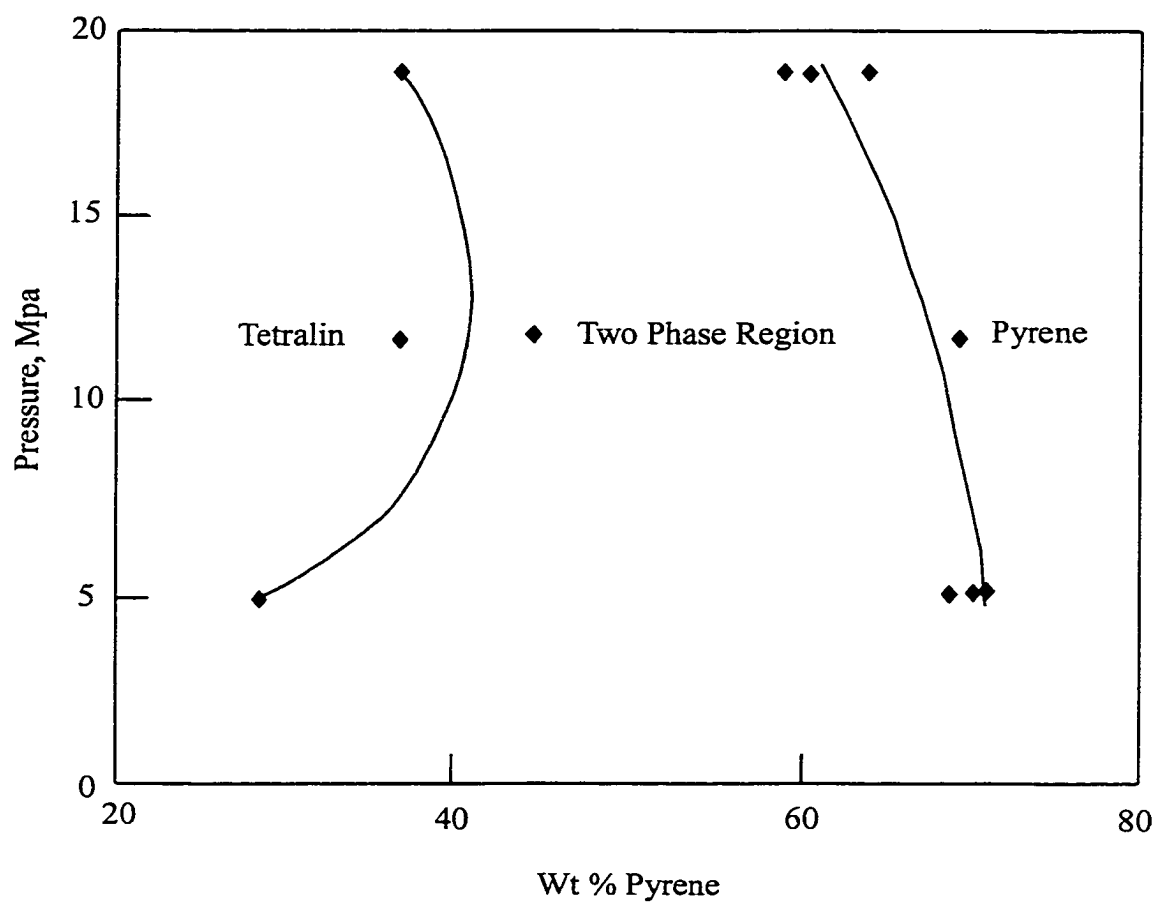


and temperatures and the connection between phase behavior and reaction kinetics are both poor. Shaw et al. (1988) observed that pyrene-tetralin mixtures exhibited liquid-liquid phase separation over a range of temperatures (347-427 °C) and hydrogen partial pressures (5-20 MPa). One liquid phase is predominantly pyrene, and the other is predominantly tetralin or related degradation products (*Figure 2-3*). The solubility of hydrogen in tetralin is approximately 8 times greater than in pyrene over the temperature interval of 400-427 °C, and compounds in the hydrogen deficient phase tend to polymerize “coke”.

Complex phase behavior such as liquid-liquid-vapor and solid-liquid-liquid-vapor were observed for heavy oil mixtures at temperatures and pressures ranging up to 450 °C and 7 MPa using a non-intrusive X-ray imaging system, although the nature of this “solid” phase is unclear (Cartlidge et al., 1996a and b). This multiphase behavior also arises at elevated temperatures and pressures in coal oil coprocessing (Dukhedini-Lalla et al., 1989) reaction environments. Heavy material that has separated and is not dispersed by mixing was referred to as solid (Cartlidge et al., 1996b). The enthalpy of “fusion” of the said solid is 7 kJ/kg, which overlaps the reported enthalpies of fusion for micelles, asphaltenes and liquid crystals (Cartlidge et al., 1996a).

Liquid phase separation at elevated temperatures suggested a transition from colloidal or micellar asphaltenes to bulk asphaltenes phases (Storm, 1991), giving a hydrogen lean phase as a precursor for coke formation (Wiehe, 1993). By preventing this phase separation, a greater conversion of the “bottom-of-the-barrel” can be obtained, with the immediate advantages of greater distillate yields and less byproduct coke. In fact, by adding sufficient quantities of polar aromatic solvents to disperse the asphaltenes,

Figure 2-3. Partial phase diagram for the pyrene-tetralin solvent system showing the two phase liquid region at 427 °C (Shaw, 1988)



Benham and Pruden (1996) managed to achieve more than 90% conversion of the 524 °C+ boiling fraction with minimal coke production.

All the above models may offer the same explanation for the formation of TI solids; destroying the balanced structure of asphaltenes in petroleum and forming a second hydrogen-lean and asphaltenes-rich phase constitute the key bases for the kinetics and mechanism of the formation of TI solids.

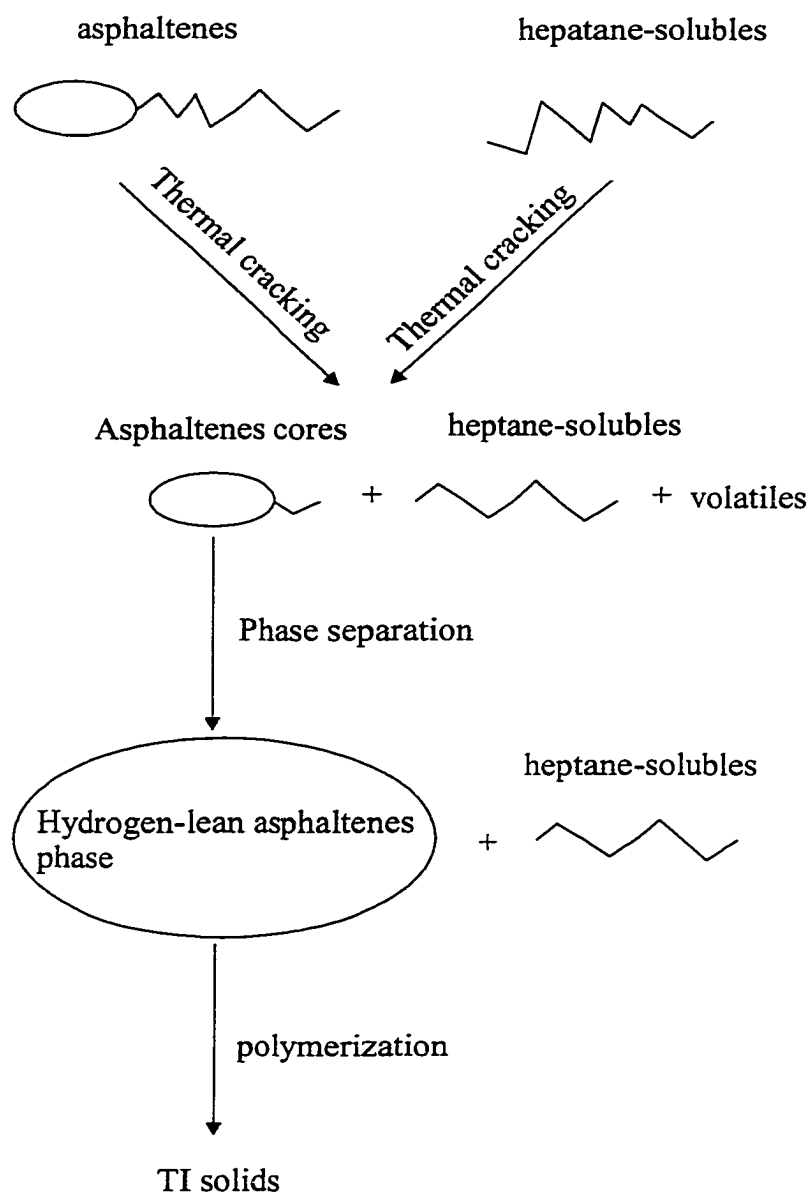
2.5 Kinetics and Mechanisms of TI Solids Formation

2.5.1 Wiehe's Phase-Separation Kinetic Model

Magaril and Aksenova (1968) first proposed that coke formation was triggered by the phase separation of asphaltenes. During thermal cracking of resins at 400 °C, a maximum concentration of asphaltenes is reached. The excess asphaltenes separate from the rest of the solution, condensing into coke in a hydrogen-deficient condition. The repeated observations of spherical particles in anisotropic solids after thermal cracking of various heavy feeds are now considered to be the evidence of liquid-liquid phase separation in coke formation (Brooks and Taylor, 1965; Nandi et al., 1978; Wiehe, 1993).

Wiehe (1993) proposed a kinetic model for coke formation and assumed that asphaltenes form a separate liquid phase once its concentration exceeds the maximum concentration allowed in the solution (*Figure 2-4*). Initially, heptane-solubles and asphaltenes are thermally cracked in an isotropic homogeneous phase, giving the loss of side chains from the asphaltenic cores and producing lower aromatic and higher aromatic fractions simultaneously. The production of coke exceeds the initial amount of asphaltenes during the thermal cracking of a vacuum residue, hence heptane-solubles are

Figure 2-4. Schematic diagram of chemical reactions and phase behavior in Wiehe's phase-separation kinetic model (1993).



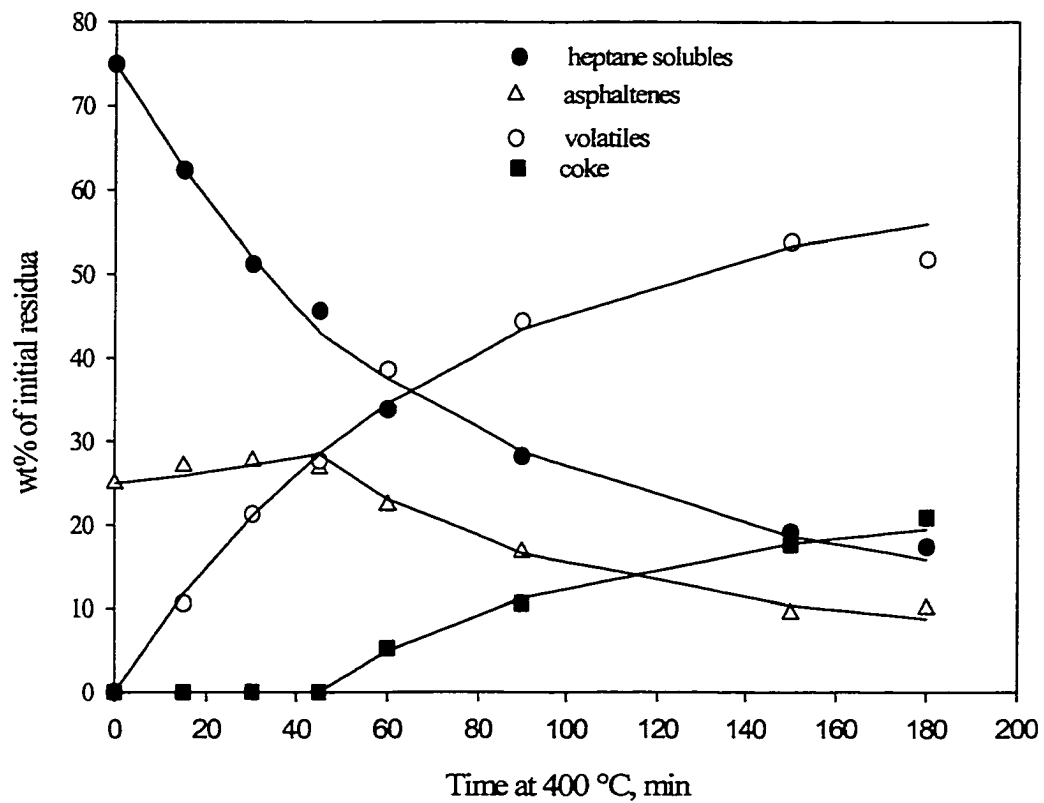
also involved in the cracking and then coking reaction (Del Bianco et al., 1993a). During the coke induction period, heptane-soluble materials can provide sufficient abstractable hydrogen to terminate asphaltene free radicals and to retard the recombination of these radicals. Once the asphaltenes exceed the solubility limit, they form a second liquid phase which undergoes a rapid reaction to form coke. The coke-forming reaction from the excess asphaltene cores is phase equilibrium controlled so that an infinite reaction rate is assumed. *Figure 2-5* shows the conversion of the full residuum (with 25% asphaltenes) to various fractions as a function of reaction time, characterizing a maximum concentration of asphaltenes, a coke-induction period, and a parallel decrease in the concentrations of asphaltenes and heptane solubles.

Phase separation leading to coke formation may also be applied to sediment formation and chemical reaction fouling of heat exchangers. Fouling in model solutions of indene, hexadecene, and dicyclopentadiene in kerosene and lube oil was caused by the formation of polyperoxide gums (Wilson and Watkinson, 1995). These polar gums exhibit solubility limits in aliphatic solvents and precipitate out of the solution beyond their solubility limit. Similarly, after the excess asphaltenes beyond the maximum asphaltene concentration form a separate liquid phase in oil streams, they could take two means to forming fouling deposit. They could either react to form coke and then deposit onto metal surfaces, or wet and spread onto the hot metal surfaces, followed by polymerization that gives fouling deposits.

2.5.2 Free Radical Reaction Mechanism

The phase separation kinetic model (Wiehe, 1993) proposed the initial thermal

Figure 2-5. Temporal variation in the four product classes from thermolysis of the full residuum. Curves were calculated from the phase-separation kinetic model (Wiehe, 1993).

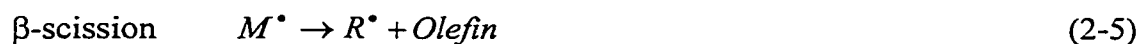


cracking of the feed during the coke-induction period (a period when there is no detectable coke formation), followed polymerization of the separate aromatic phase (Figure 2-4). While thermal cracking occurs from the start of thermal treatment, polymerization only occurs after a separate asphaltenes-rich phase appears. One thing in common between thermal cracking and polymerization is that these two reactions are both free radical chain reactions. Free radicals are highly reactive intermediates with an unpaired electron. The reaction pathways favor the formation of the most stable radical species such as aromatic radicals due to electron delocalization. Free radical chain reactions, leading to cracking and polymerization, were summarized in the following equations (Billmeyer, 1962; Gray, 1994), where I is the initiator, M is the parent compound, R^\bullet is the radical, and $R-(M-)_xM^\bullet$ is the polymer radical (x is a nonnegative integer).

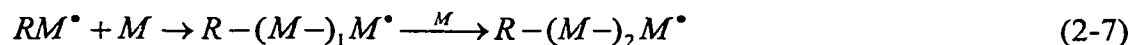


Intermediate reactions:

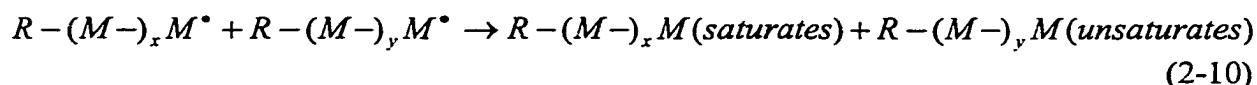
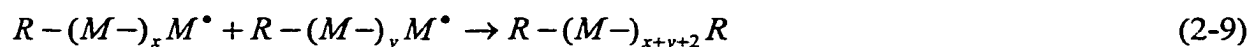
Cracking:



Polymerization:



Termination:



The three steps of initiation, intermediate reaction and termination are both necessary and sufficient for free radical chain reactions. The main difference between thermal cracking and polymerization is the step of intermediate reaction. In thermal cracking, molecules become smaller by chain transfer and β -scission, while in polymerization the addition of small molecules to free radicals produces larger free radicals.

The initial cracking of heavy oil feeds involves the cracking of largely aliphatic fragments away from a largely aromatic core. This mechanism is supported by a rapid decrease in average molecular size and an increase in aromaticity of asphaltenes that occurs during the initial cracking of heavy oils (Wiehe, 1993; Del Bianco, et al., 1993a; Heck and DiGuseppi, 1994). After the concentration of asphaltenes exceeds the maximum concentration that can be maintained by the surrounding medium, a separate phase of asphaltenes occurs in which the free radical aromatic cores could polymerize to form bigger molecules under hydrogen-deficient conditions. Considering this, conditions must be optimized so that the cracking rate does not significantly outpace the hydrogenation in order to achieve high conversion of petroleum residue to distillate without excessive formation of coke (Heck and DiGuseppi, 1994).

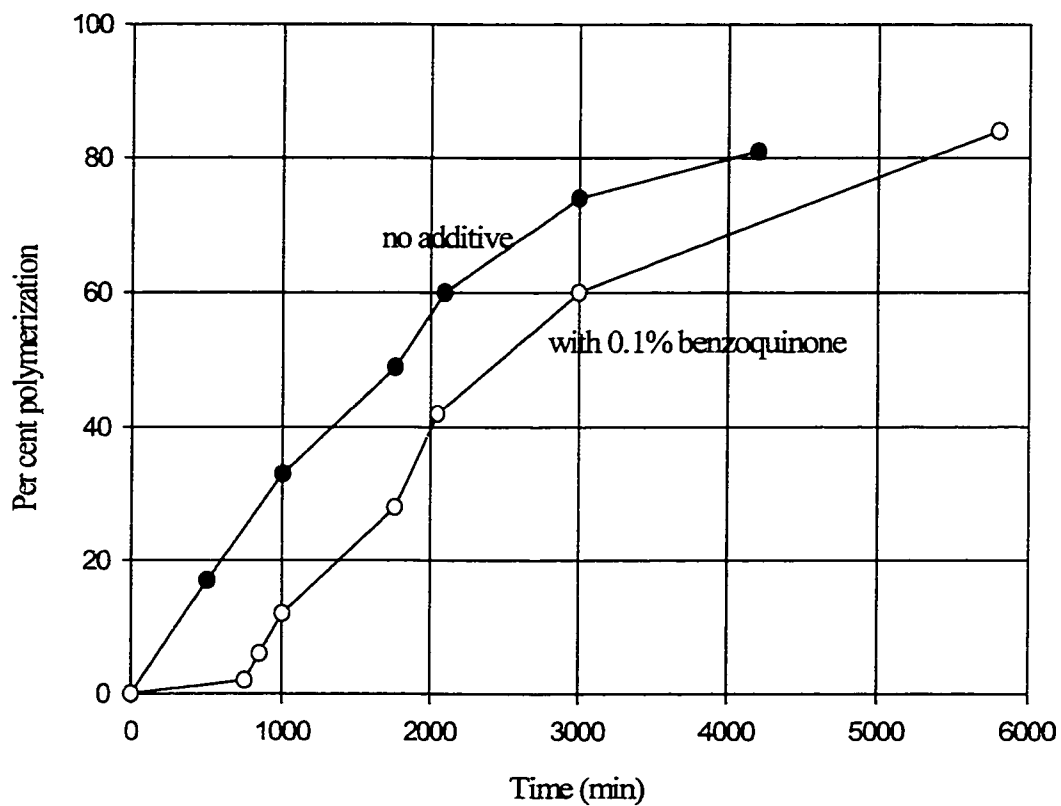
Other reactions may take place to hinder the polymerization of asphaltenes to form coke. In polymer science, a retarder is defined as a substance which can react with a free radical to form products incapable of adding monomer (Billmeyer, 1962). Possible retarders in the heavy oils may include fine solid particles and other free radical

scavengers such as hydrogen and hydrogen donating solvents. Although the widely-observed coke induction phenomena can be explained by the phase-separation kinetic model (*Figure 2-5*), it is also in agreement with the induction period in polymerization (*Figure 2-6*).

2.6 Factors Influencing the Formation of TI Solids

Reaction temperature can greatly affect the coke formation. For example, the coke induction period was appreciably decreased or even diminished for various petroleum feeds when the reaction temperature was raised (e.g. Srinivasan and McKnight, 1994). However, this review focuses on the effects of a range of reactants on coke formation, so no further efforts are exerted on discussing the influence of temperature on coking. Thermal cracking of heavy oil feeds involves the production of various radicals with varying aromaticity, due to the reactions that remove the alkyl groups from the aromatic cores of the feed molecules. The resulting free radicals and olefins are significantly more reactive than the feed molecules from which they come. Any factors that can selectively promote thermal cracking or prevent polymerization (see *Section 2.5.2*) of these free radicals will increase the distillate yield and decrease the coke yield. The concentration of asphaltenes in the feed oils is a very important parameter in affecting coke yield, but other reaction conditions such as the presence of hydrogen (including its introduction method), hydrogen donating solvents, and fine solids in the feed can affect the coke formation.

Figure 2-6. Thermal polymerization of styrene at 100 °C where benzoquinone was used as a retarder (Billmeyer, 1962)



2.6.1 Hydrogen, Solvents, and Asphaltenes Content

Hydrogen can react with the aromatic-carbon radicals to give a molecule and the hydrogen radical (Sanford, 1993). The hydrogen radical attacks the aromatic ring, decomposing the aromatic molecule and giving gases and distillate. Hydrogen can stabilize aromatic free radicals and prevent these radicals from reacting into coke. Higher hydrogen pressure could give a decreased rate of coke formation, for examples, for two petroleum-based feeds (Shigley and Fu, 1988). Hydrogen solubility in the hydrocarbon solvents with different aromaticity was correlated under the same hydrogen pressure (Shaw, 1987). The solubility of hydrogen in an aromatic phase is less than that in an aliphatic solvent. It is important to recognize that it is the hydrogen-deficient environment in the highly aromatic phase, forming from the rest of heavy feed upon thermal cracking, that allows the materials inside that phase to polymerize into coke (e.g. Wiehe, 1993).

The mere presence of hydrogen is not enough to prevent coke formation. It is the availability of hydrogen to interact with free radicals that really matters. Excellent mass transfer of hydrogen to the separated second liquid (coke precursors) through an intimate contacting of the second liquid phase with hydrogen is very effective in reducing coke formation (Shaw et al., 1988). Bubbling hydrogen through the liquid phase suppressed tetrahydrofuran insoluble coke to a much greater extent than merely adding hydrogen to the gas phase (Heck et al., 1992).

The introduction of solvents can decrease coke formation either by preventing the formation of a separate and more aromatic liquid phase from asphaltenes due to the increased solvency power of the solvent medium, or by providing sufficient abstractable

hydrogen atoms from hydrogen-donating solvents to the already separated asphaltenic phase. The reduced rates of the formation of both isotropic coke and mesophase droplets are attributed partly to the increased solvency power upon the addition of gas oils (Nowlan and Srinivasan, 1996). Aromatic solvents such as phenanthrene, 1-methylnaphthalene, and quinoline significantly reduce coke deposition during thermal cracking of a vacuum residue (Del Bianco et al., 1993b). The greater solvency power of the solvent or the smaller difference in the solubility parameters between solvent and coke precursors (e.g. asphaltenes) possibly shifts the reaction system from the region of insolubility to the region of solubility (*Figure 2-2*). Failure to form a second phase minimizes polymerization reactions that eventually leads to coke formation (*Section 2.5.2*). However, aromatic solvents are generally less significant than hydrogen-donating solvents in suppressing coke generation.

Radical fragments during thermolysis reaction may abstract hydrogen atoms from hydrogen donating solvents to be stabilized, giving increased yields of cracked distillate and gases. Partially hydrogenated aromatic compounds are often used as hydrogen donating solvents. Coke formation was considerably suppressed during visbreaking of a vacuum residuum upon the addition of tetralin, accompanied by a significant increase in the maximum conversion without coke formation (Que et al., 1990). The conversion of Athabasca bitumen to TI solids was about 8 wt% under nitrogen atmosphere, which decreased to 4 wt% by introducing either hydrogen or tetralin, and was further reduced to 2 wt% by the combined use of hydrogen and tetralin (Sanford and Xu, 1996). Similarly, 20 wt% of dihydrophenanthrene hinders coke formation during thermal cracking of a vacuum residue and increases the maximum distillate production by more than 10 wt%

(Del Bianco et al., 1993b). However, the insufficient radical-scavenging abilities of those hydrogen-donor solvents require a large amount of such solvents to satisfactorily reduce coke formation, which increases operation costs (Anon, 1993). Antioxidants, like many other powerful radical scavengers, are not heat resistant enough to be used under severe thermal cracking conditions. Hence the addition of vast amounts of hydrogen-donating solvents into thermal cracking feeds has seen limited commercial application, although suitable solvents have been derived from petroleum (Kubo, 1992). These very stable hydrogen-donating solvents with high radical-scavenging abilities are the heavy hydroaromatics from petroleum that include partially hydrogenated products of condensed aromatic rings. Addition of such solvents in small amounts (3 wt % of the feed) was sufficient to inhibit coke formation (Kubo et al., 1996).

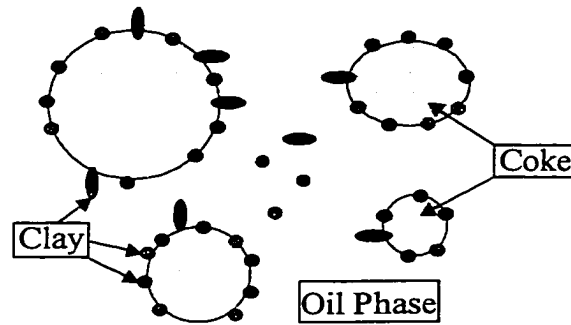
The concentration of asphaltenes in the feed oils was well correlated with their propensity of coke formation. Wiehe (1993) reported that the length of coke induction period decreases with the increasing amount of asphaltenes in the feeds. When the asphaltenes content in the feed oil is higher, the reaction system will be closer to the maximum solubility limit of asphaltenes, and there will be less abstractable hydrogen available in the reaction mixture. Therefore, the asphaltenes content in the feed, the presence of aromatic solvents, and the availability of hydrogen and hydrogen donating solvents are linked by their influence on the phase separation, the polymerization in the separated phase of asphaltenes and eventually the coke formation. Besides these organic compounds, fine mineral solids, naturally occurring in some oil feeds, may also play an important role in reducing the production of coke.

2.6.2 Fine Solid Particles

Depending on the geological location and processing history, heavy oils may contain some mineral materials. For example, the ash content of Athabasca bitumen is about 0.8 wt %, and gas oils derived from this bitumen typically contain minerals (Chung et al., 1997). Wolk (1974) first suggested that fine mineral particles inhibit coke. One marked characteristic of these fine solids is the high surface area. The effects of these solid particles on coke formation can be grouped into physical interaction and chemical reactivity.

Physical interactions may include a role for fine solids as the nucleating centers for coke development. For example, the benzene-insoluble material near the outlet of a hydroconversion reactor had inert mineral matter encapsulated by a layer of coke material (Belinko et al., 1977), indicating that fine mineral matter may be a nucleating center. However, enhanced nucleation by fine particles would give an increased coke production, which was opposed to the observations during thermal cracking of a vacuum residue (Tanabe and Gray, 1997). Another physical interaction may be that these mineral solids appear at the interface of the coke precursor and oil medium to prevent agglomeration of these coke precursors. At reactor conditions coke-precursor in a liquid phase may be stabilized by adsorbing fine solids on it, provided that the size of fine solids is significantly smaller than that of coke precursor spheres. Coalescence of the coke-precursors is thereby prevented, and the rate of formation of solid coke is reduced (*Figure 2-7*). This stabilization mechanism with fine solids was widely observed in emulsion systems (e.g. Yan and Masliyah, 1996). This stabilization mechanism was used to explain the observations that fine solids postponed the onset of coke formation, and

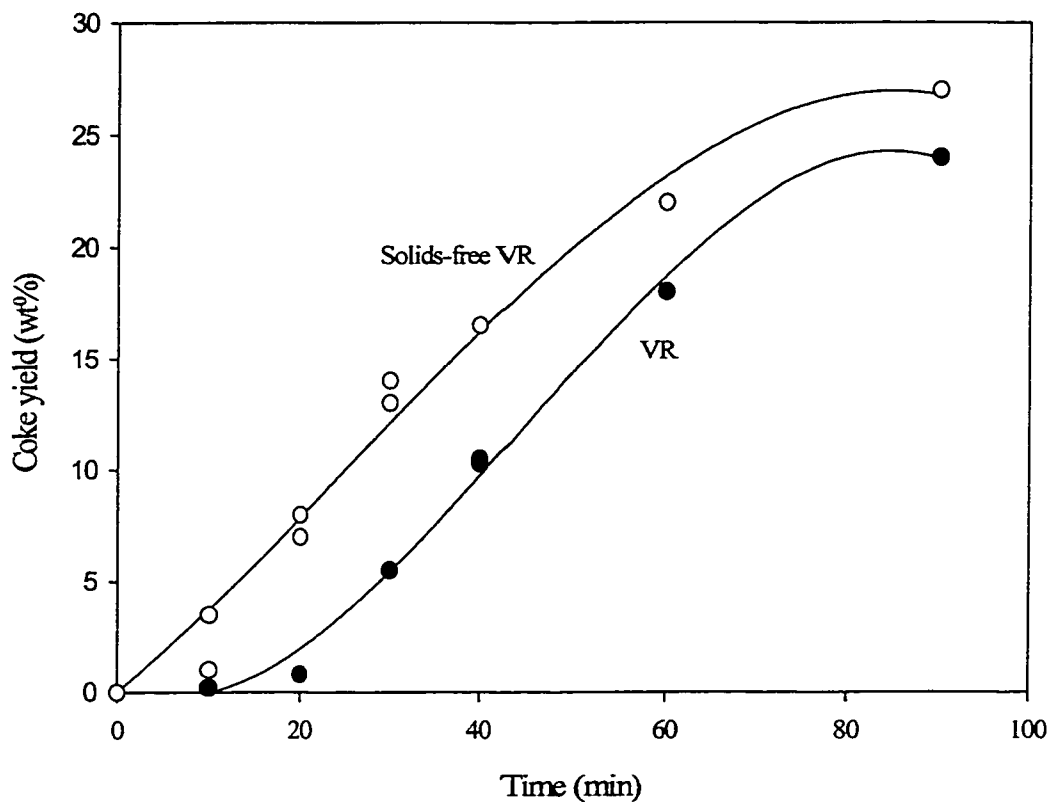
Figure 2-7. Schematic diagram of clays at interfaces of thermoplastic coke dispersed in oil (Tanabe and Gray, 1997)



decreased the coke yield at short reaction times during the thermal cracking of a vacuum residue and an asphaltene fraction from Athabasca (*Figure 2-8*). Similar interactions between fine solids and mesophase were also observed. Insoluble particles are found to be associated with the mesophase as soon as transformation commences, although they are never incorporated into the body of mesophase and are thus swept along in the mesophase-matrix interfaces as the transformation progresses (Brooks and Taylor, 1968). The similar interference of fine solids with the coalescence of the mesophase was also observed in coal tar (Dubois et al., 1970; Bradford et al., 1971).

At room temperature, coke exists as TI solids, but Wiehe's model (1993) suggested that coke precursors are in a separate aromatic liquid phase during coke formation. Fine solids give a large surface area, compared with the inner surfaces of the process equipment. This separate liquid phase may wet certain surfaces such as mineral matter and metal surfaces, which would affect the coke formation and fouling. The wetting of a solid by a liquid (α) in the presence of another fluid (β) is often characterized by the equilibrium contact angle, θ , which is related by Young's equation (i.e. $\gamma_{\alpha\beta} \cos\theta + \gamma_{s\alpha} = \gamma_{s\beta}$) to the solid-liquid (α) interfacial tension, $\gamma_{s\alpha}$, solid-fluid (β) interfacial tension, $\gamma_{s\beta}$, and liquid (α)-fluid (β) interfacial tension, $\gamma_{\alpha\beta}$. The criterion for wetting is that the contact angle is less than 90° , i.e. $\gamma_{s\alpha} < \gamma_{s\beta}$. The fluid (β) can be a liquid phase different than liquid (α), or a vapor phase. The contact angle decreases with increasing temperature at temperatures above the softening point of pitch, pretreatment of the carbon surface with pitch vapors, and addition of surface-active agents (Greenhalgh and Moyses, 1970). This kind of study may be suggestive for the wettability of the separate aromatic liquid phase (i.e. coke precursors) on other surfaces at elevated

Figure 2-8. Yield of coke from thermal cracking of Athabasca vacuum residue and solids-free Athabasca vacuum residue at 430 °C under a nitrogen atmosphere (Tanabe and Gray, 1997)



temperatures, which in turn affects the morphology and yield of TI carbonaceous solids upon thermal treatment of heavy oil feeds.

Chemical reactivity of fine inorganic solids towards coke formation could give prevention or retardation of the polymerization reaction in the separated phase of asphaltenes. Fine mineral solids may be viewed as impurities in the feed oil, which could be considered free radical scavengers to selectively terminate the asphaltenic radicals. It can be deduced that the length of the induction period before coke forms is directly proportional to the concentration of fine solids initially present in the feed (Billmeyer, 1962). An alternate mechanism is that the mineral matter may have some catalytic activity towards hydrogenation reactions, promoting hydrogen transfer to asphaltene free radicals in the separate liquid phase. The presence of mineral solids resembles the beneficial effect of increased hydrogen pressure, minimizing the need for hydrogen-donors and delaying the coke formation (Belinko et al., 1977). Coal acted as a good hydrogen donor or shuttle in co-processing with bitumen, resulting in increased production of light oils (Yoshida et al., 1995). This is analogous to the catalytic effect of metal compounds (e.g. $\text{FeSO}_4 \cdot \text{H}_2\text{O}$) on thermal cracking of heavy oil feeds (Kriz and Ternan, 1984), which enhance hydrogen transfer at their surface to unstable intermediates formed by thermal cracking.

2.7 Concluding Remarks

Steric-stabilization models and thermodynamic models have been proposed for the structure of asphaltenes in petroleum. All the models show that a disturbance of the balanced petroleum system would break the delicate equilibrium between the asphaltenic phase and deasphalted oil, leading to the formation of a second liquid phase of

asphaltenes cores. Free radical polymerization reactions in the resulting asphaltenic phase during thermolysis of petroleum would give aromatic molecules with increased molecular weight and polarity and finally coke. The phase-separation kinetic model of Wiehe (1993) best explained the coke induction period, the parallel decrease in concentrations of asphaltenes and heptane-solubles, and the maximum concentration of asphaltenes during the thermolysis of full residuum and a heptane-soluble fraction. Mesophase spheres in the coke products were commonly used to verify the existence of a separate liquid phase in the course of coke formation. However, this is inductive evidence rather than a direct proof. A better understanding of the wettability of coke precursors (i.e. a liquid asphaltenic phase) on different surfaces may benefit from further fundamental research.

Any factor that inhibits the route for coke formation may decrease the coke yield and enhance the distillate yield. Generally, lowering asphaltene content and adding aromatic solvents or finely dispersed solids to the feed will delay the onset of phase separation, while the presence of hydrogen or hydrogen donating solvents, and fine mineral solids with catalytic activity, will retard the polymerization of aromatic radicals.

References

Altgelt, K. H.; Boduszynski, M. M. "Composition and Analysis of Heavy Petroleum Fractions." Marcel Dekker, New York, **1994**.

Anon. Petroleum-Derived Additive Reduces Coke on Hydrotreating Catalyst. *Oil Gas J.* **1993**, 91(52), 100-101.

Banerjee, D. K.; Laider, K. J.; Nandi, B. N.; Patmore, D. J. Kinetic Studies of Coke Formation in Hydrocarbon Fractions of Heavy Crudes. *Fuel* **1986**, 65, 480-484.

Belinko, K.; Nandi, B. N.; Denis, J. M. The Distribution of Coke Precursors in the Reactor during Thermal Hydrocracking of Athabasca Bitumen. Presented in 'The Oil Sands of Canada-Venezuela 1977' (D. A. Redford and A. G. Winestock (Eds)) CIM Special Vol. 17, CIM, Calgary, **1977**, pp. 189-194.

Benham, N. K.; Pruden, B. B. CANMET Residuum Hydrocracking Advances Through Control of Polar Aromatics. NPRA Ann. Meeting, San Antonio, Texas, **1996**, March 17-19, Paper AM-96-58.

Billmeyer, Fred W., Jr. *Textbook of Polymer Science*. John Wiley & Sons, Inc., **1962**.

Bisaria, M. K.; Bakhshi, N. N.; Ranganatha, R. Nonhydrogenative Processing of a Saskatchewan Heavy Oil under Mild Conditions Using Disposable Additives. *Can. J. Chem. Eng.* **1993**, 71 (5), 746-755.

Braford, D. J.; Greenhalgh, E.; Kingshott, R.; Senior, A.; Bailey, P. A. Interaction of Carbon Black with Coal Tar Pitch. *Third Conference on Industrial Carbons and Graphite*; Society of Chemical Industry: London, **1971**, pp. 520-527.

Brooks, J. D.; Taylor, G. H. The Formation of Graphitizing Carbons for the Liquid Phase. *Carbon* **1965**, 3, 185-193.

Brooks, J. D.; Taylor, G. H. The Formation of Some Graphitizing Carbons. *Chem. Phys. Carbon*. **1968** (4), 243-286.

Cartlidge, C. R.; Dukhedin-Lalla, L.; Rahimi, P.; Shaw, J, M. Preliminary Phase Diagrams for ABVB+n-dodecane+hydrogen. *Fluid Phase Equilibria* **1996a**, 117, 257-264.

Cartlidge, C. R.; Dukhedin-Lalla, L.; Rahimi, P.; Shaw, J, M. Preliminary Phase Diagrams for Bitumen/Heavy Oils and Related Mixtures. *Fuel Sci. Technol. Int.* **1996b**, 14(1&2), 163-178.

Chung, K. H.; Xu, C.; Hu, Y.; Wang, R. Supercritical Fluid Extraction Reveals Resid Properties. *Oil Gas J.* **1997**, 95(3), 66-69.

Cimino, R.; Correra, S.; Del Bianco, A.; Lockhart, T. P.; Enricerhe, S. P. A. Chapter III: Solubility and Phase Behavior of Asphaltenes in Hydrocarbon Media. in *Asphaltenes: Fundamentals and Applications*, Edited by E. Y. Sheu and O. C. Mullins. Plenum Press, New York, 1995.

Crittenden, B. D.; Kolaczowski, S. T.; Downey, I. L. Fouling of Crude Oil Preheat Exchangers. *Chem. Eng. Res. Des.* **1992**, 70A, 547-557.

Del Bianco, A.; Panariti, M. A.; Beltrame, P. L.; Carniti, P. Thermal Cracking of Petroleum Residue. 1. Kinetic Analysis of the Reaction. *Fuel* **1993a**, 72, 75-80.

Del Bianco, A.; Panariti, M. A.; Beltrame, P. L.; Carniti, P. Thermal Cracking of Petroleum Residue. 2. Hydrogen-donor Solvent Addition. *Fuel* **1993b**, 72, 81-85.

Dickakian, G.; Seay, S. Asphaltene Precipitation Primary Crude Exchanger Fouling Mechanism. *Oil Gas J.* **1988**, 86(10), 47-50.

Dubois, J.; Ahache, C.; White, J. L. The Carbonaceous Mesophase Formed in the Pyrolysis of Graphitizable Organic Materials. *Metallography* **1970**, 3, 337-369.

Dukhedine-Lalla, L.; Yushun, S.; Shaw, J. M. Phase Splitting of Complex Hydrocarbon Mixtures. *Fluid Phase Equilibria* **1989**, 53, 415-422.

Garrett, B. A. et al. Chapter 2. Overview of Fouling. In *Fouling of Heat Exchangers: Characteristics, Costs, Prevention, Control, and Removal*. Noyes Publications, Park Ridge, New Jersey, USA, **1985**, pp. 9-19.

Gray, M. R. "Upgrading Petroleum Residues and Heavy Oils." Marcel Dekker, New York, **1994**.

Greenhalgh, E.; Moyse, M. E. Contact Angle of Pitch on Carbon Surfaces. *Proc. 3rd Conf. on Industrial Carbon and Graphite* (Soc. Chem. Ind.), London. **1970**, 539-549.

Griffith, M. G.; Siegmund, C. W. "Controlling Compatibility of Residual Fuel Oils." *Marine Fuels*, ASTM STP 878, Jones, C. H. (Ed.), American Society for Testing and Materials, Philadelphia, **1985**, pp. 227-247.

Heck, R. H.; DiGuseppi, F. T. Kinetic Effects in Resid Hydrocracking. *Energy Fuels* **1994**, 8, 557-560.

Heck, R. H.; Rankel, L. A.; DiGuseppi, F. T. Conversion of Petroleum Resid from Maya Crude: Effect of H-Donors, Hydrogen, Hydrogen Pressure and Catalyst. *Fuel Process. Technol.* **1992**, 30(1), 69-81.

- Hunt, A. Uncertainties Remain in Predicting Paraffin Deposition. *Oil Gas J.* **1996**, 94(31), 96-103.
- Karacan, O.; Kok, M. V. Pyrolysis Analysis of Crude Oils and Their Fractions. *Energy Fuels* **1997**, 11, 385-391.
- Kochling, K. H.; McEnaney, B.; Rozploch, F.; Fitzer, E. International Committee for Characterization and Terminology of Carbons "First Publication of 30 Tentative Definitions." *Carbon* **1982**, 20(5), 445-449.
- Kochling, K. H.; McEnaney, B.; Neumann, S.; Fitzer, E. International Committee for Characterization and Terminology of Carbon "First Publication of Further 24 Tentative Definitions." *Carbon* **1983**, 21(5), 517-519.
- Kriz, J. F.; Ternan, M. "Hydrocracking Heavy Hydrocarbon Feedstocks: Aspects of Catalyst Related to Feedstock Coking Tendency," in "Studies in Surface Science and Catalysis," Vol. 19: "Catalysis on the Energy Scene," S. Kaliaguine and A. Mahay, Eds., Elsevier Publishing Co., Amsterdam (1984), pp. 545-552.
- Kubo, J.; Higashi, H.; Ohmoto, Y.; Arao, H. Heavy Oil Hydroprocessing with the Addition of Hydrogen-Donating Hydrocarbons Derived from Petroleum. *Energy Fuels* **1996**, 10, 474-481.
- Kubo, J. Radical Scavenging by Hydroaromatics in the Presence of Oxygen. *Ind. Eng. Chem. Res.* **1992**, 31, 2587-2593.
- Lemke, H. K.; Stephenson, W. K. Deposit Formation in Industrial Delayed Coker/Visbreaker Heaters. *Petrol. Sci. Technol.* **1998**, 16(3&4), 335-360.
- Magaril, R. Z.; Aksenora, E. I. Study of the Mechanism of Coke Formation in the Cracking of Petroleum Resins. *Int. Chem. Eng.* **1968**, 8, 727-729.
- Mochida, I.; Zhao, X.; Sakanishi, K. Suppression of Sludge Formation by two-stage hydrocracking of Vacuum Residue at High Conversion. *Ind. Eng. Chem. Res.* **1990**, 29, 2324-2327.
- Nandi, B. N.; Belinko, K.; Ciavaglia, L. A.; Pruden, B. B. Formation of Coke during Thermal Hydrocracking of Athabasca Bitumen. *Fuel* **1978**, 57, 265-268.
- Nowlan, V. J.; Srinivasan, N. S. Control of Coke Formation from Hydrocracked Athabasca Bitumen. *Fuel Sci. Technol. Int.* **1996**, 14(1 & 2), 41-54.
- Pfeiffer, I.; Saal, R. N. J. Asphaltic Bitumen as Colloid System. *J. Physical Chem.* **1940**, 44, 139-149.

- Que, G.; Sun, B.; Liang, W. Hydrovisbreaking of Gudao Vacuum Residue in the Presence of Hydrogen Donor. *Am. Chem. Soc. Div. Petrol. Chem. Prepr.* **1990**, 35(4), 626-634.
- Rand, B.; Hosty, A. J.; West, S. Physical Properties of Pitch Relevant to the Fabrication of Carbon Materials. In *Introduction to Carbon Science* (Ed. H. Marsh), Butterworth, Toronto, **1989**, pp. 75-106.
- Riggs, D. M.; Diefendorf, R. J. A Phase Diagram for Pitches. *Preprints of 3rd International Carbon Conference, Baden-Baden*, **1980a**, pp. 326-329.
- Riggs, D. M.; Diefendorf, R. J. Factors Controlling the Thermal Stability and Liquid Crystal Forming Tendencies of Carbonaceous Materials. *Preprints of 3rd International Carbon Conference, Baden-Baden*, **1980b**, pp. 330-333.
- Sanford, E. C. Mechanism of Coke Formation by Hydrogen during Residuum Hydrocracking. *Am. Chem. Soc. Div. Petrol. Chem. Prepr.* **1993**, 38(2), 413-416.
- Sanford, E. C.; Xu, C. M. Relationship between Solids Formation, Residuum Conversion, Liquid Yields and Losses during Athabasca Bitumen Processing in the Presence of a Variety of Chemicals. *Can. J. Chem. Eng.* **1996**, 74(3), 347-352.
- Shaw, J. M. Correlation for Hydrogen Solubility in Alicyclic and Aromatic Solvents. *Can. J. Chem. Eng.* **1987**, 65(2), 293-298.
- Shaw, J. M.; Gaikwad, R. P.; Stowe, D. A. Phase Splitting of Pyrene-Tetralin Mixtures under Coal Liquefaction Conditions. *Fuel* **1988**, 67, 1554-1559.
- Sheu, E. Y. Physics of Asphaltene Micelles and Microemulsions - Theory and Experiments. *J. Phys.: Condense Matter* **1996**, 8 (25A), A125-A141.
- Shigley, J. K.; Fu, T. W. Coke Formation Reaction Kinetic Study on Petroleum Based Feeds. *Am. Chem. Soc. Div. Petrol. Chem. Prepr.* **1988**, 33(3), 420-426.
- Speight, J. G.; Long, R. B. The Concept of Asphaltenes Revisited. *Fuel Sci. Technol. Int.* **1996**, 14 (1 & 2), 1-12.
- Speight, J. G. "The Chemistry and Technology of Petroleum." Marcel Dekker Inc., New York, **1991**.
- Srinivasan, N. S.; McKnight, C. A. Mechanism of Coke Formation from Hydrocracked Athabasca Residuum. *Fuel* **1994**, 73, 1511-1517.
- Storm, D. A. Colloidal Nature of Vacuum Residue. *Fuel* **1991**, 70: 779-787.

Storm, D. A.; Barresi, R. J.; Sheu, E. Y. Rheological Study of Ratawi Vacuum Residue in the 298-673 K Temperature Range. *Energy Fuels* **1995**, *9*, 168-176.

Storm, D. A.; Barresi, R. J.; Sheu, E. Y. Flocculation of Asphaltenes in Heavy Oil at Elevated Temperatures. *Fuel Sci. Technol. Int.* **1996**, *14*(1 & 2), 243-260.

Storm, D. A.; Decanio, S. J.; Edwards, J. C.; Sheu, E. Y. Sediment Formation During Heavy Oil Upgrading. *Petrol. Sci. Technol.* **1997**, *15* (1&2), 77-102.

Tanabe, K.; Gray, M. R. Role of Fine Solids in the Coking of Vacuum Residues. *Energy Fuels* **1997**, *11*, 1040-1043.

Wiehe, I. A. A Phase-Separation Kinetics Model for Coke Formation. *Ind. Eng. Chem. Res.* **1993**, *32*, 2447-2454.

Wiehe, I. A.; Liang, S. Asphaltenes, Resins, and Other Petroleum Macromolecules. *Fluid Phase Equilibria* **1996**, *117*, 201-210.

Wilson, D. I.; Watkinson, A. P. Model Experiments of Autoxidation Reaction Fouling I: Mechanisms. *Chem. Eng. Res. Des.* **1995**, *73*, 59-68.

Wolk, R. H. Hydroconversion of Tar Sand Bitumens. U. S. Patent 3,844,937; **1974**.

Yan, N.; Masliyah, J. H. Effect of pH on Adsorption and Desorption of Clay Particles at Oil-Water Interface. *J. Colloid Interface Sci.* **1996**, *181*, 20-27.

Yoshida, T.; Nagaishi, H.; Sasaki, M.; Yamamoto, M.; Kotanigawa, T.; Sasaki, A.; Idogawa, K.; Fukuda, T.; Yoshida, R.; Maekawa, Y. Addition Effects of Coal-Derived Oil and Coal on Upgrading of Oil Sand Bitumen. *Energy Fuels* **1995**, *9*, 685-690.

Chapter 3: Literature Review – Particle Deposition in Porous Media

3.1 Background

As mentioned in **Chapter 1**, one of the major objectives of this study is to find out the deposition mechanism for various solids with different surface properties, and the possible effects of the polar compounds on particle deposition. Although toluene-insolubles are produced in hydrotreaters, in **Chapter 2** only the kinetics and mechanism of toluene-insoluble formation in heavy oil processing in the absence of catalyst was reviewed. Deposition of fine particles, including those toluene-insolubles, in hydrotreaters is analogous to deep-bed filtration, in which removal of colloidal particles is achieved by deposition onto the filter grains constituting the bed (Chowdiah, 1981). The particles are transported to the filter grain surface by the mechanisms of interception, sedimentation and Brownian diffusion (Masliyah, 1994). Whether or not a particle finally attaches itself to the collector surface depends on the net result of the short-range forces, which are the attraction due to London-van der Waals forces, and the force due to electrical double layer interactions. Repulsive double layer forces between particles with the same charge as the filter medium can be strong enough to prevent deposition.

Packed-bed reactors are widely used in the petroleum industry for hydrotreating different distillate fractions. As discussed in *Section 1.3.3*, natural clay particles, coke and corrosion products are entrained into hydrotreaters. The gradual accumulation of these particles gives an increasing pressure drop across the reactor over time. This pressure drop may finally force unscheduled shutdowns (Chan et al., 1994). In the

hydroprocessing of crude oil residue fractions, solids such as iron sulfide contained in the non-distillable fraction of the crude oils can deposit in the catalyst bed, leading to premature reactor shutdown before the catalyst is fully used (Koyama et al. 1995). Fine particles are also responsible for fouling and erosion in downstream processing units (Menon et al. 1987). In general, the presence of fines from any sources necessitates the cleaning of the oils prior to further processing.

Several methods have been tried to filter these fine particles from reactor feeds (Christopherson, 1994). Electrostatic separation had good success in removing clay from the oil feed, but it was rejected because of the high cost. Sand bed filters have been used to remove coke fines from coker products prior to hydrotreating. The typical sizes of the coke particles to be removed are 25-50 μm , although smaller particles can also be removed. Sand bed filters were most useful for handling process upsets rather than the oil stream with a steady concentration of solids. Chan et al. (1994) found that the fine capture efficiency of a packed-bed reactor increased with increasing gas rate at ambient conditions under trickle bed operation. However, it is not considered an acceptable long-term solution because reducing the fine capture efficiency of the reactor will cause more fines in the product sent to the refineries. The pressure drop buildup problem, therefore, is not resolved but transferred to the downstream refineries. Hence it is extremely important to understand the mechanism of particle deposition in a packed-bed filter so that ultimately the fine particles can be removed from the hydrotreater feeds.

There have been numerous studies on particle deposition in aqueous systems, but there is very scanty literature for non-aqueous systems. The following sections focus on

particle deposition mainly associated with aqueous systems, with some attempt to extend the pertinent concepts to non-aqueous systems.

3.2 Difference between Aqueous and Non-aqueous Systems

Removal of fine particles by the catalyst packing in hydrotreaters is analogous to deep-bed or granular filtration of aqueous suspensions, wherein liquid flows through a granular bed with particles depositing on the bed packing. However, there are marked differences between aqueous and non-aqueous media with a hydrocarbon liquid in particular. Based on dielectric constant (ϵ) non-aqueous media fall into three groups (Hoeven et al. 1992): apolar range ($\epsilon < 5$), low-polarity ($5 < \epsilon < 11$), and semi-polar to polar ($\epsilon > 11$). Most hydrocarbons have dielectric constants that are much smaller than that of water (78.5 at 25 °C). In liquid non-aqueous media with low dielectric constant, electrolytes are poorly dissociated and often the ionic strengths are much lower than 10^{-6} M. Therefore, the electric conductivity is also much lower for a non-aqueous solution than an aqueous solution. By virtue of the low dielectric constant and low electrical conductivity of non-aqueous systems, charged particles give very thick electrical double layers in non-aqueous liquids as compared to aqueous solutions.

3.3 Stabilization of Colloids

Colloidal particles have a size range from 0.1 to 10 μm . Colloidal particles can be stabilized against coagulation (or flocculation) by electrostatic repulsion due to the presence of ions near their surfaces or by steric effects arising from polymer chains attached to the surface of the particles. The properties of a colloidal system, i.e., its rheology, shear stability and stability to added electrolyte or polymer are much affected

by the nature of the stabilizing mechanism (Walbridge, 1987). The stabilization of colloids may be important in controlling the ability of fine particle to remain in the oil streams, thus affecting the deposition of these particles in hydrotreaters.

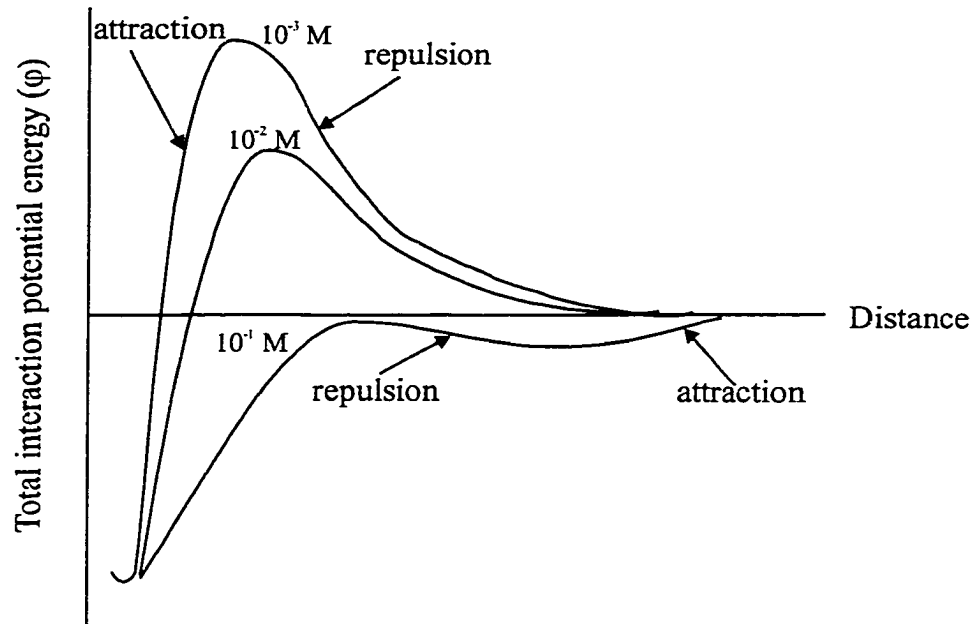
Electrostatic stabilization plays a dominant role in aqueous systems. Electrostatically stabilized particles can be flocculated by the addition of an electrolyte and by shear.

Figure 3-1 shows that increasing the electrolyte concentration changes the shape of the interaction potential energy, leading to a weak repulsive force and a possible attractive force at a large separation distance between the particles. However, electrostatic stabilization is still under dispute in non-aqueous media. From theoretical considerations it appears that the extent of the electrostatic stabilization in non-aqueous media is extremely sensitive to the dielectric constant of the liquid, affecting stability in particular through the degree of dissociation of the stabilizing electrolyte (Hoeven and Lyklema, 1992).

One illustration is the frequently cited theoretical study of Féat and Levin (1976). They considered a system consisting of a non-polar solvent ($\epsilon = 2-3$) with TiO_2 particles as the dispersed solid and sodium Aerosol OT (NaAOT) as the electrolyte. The concentration of the negative ions, contributed by the dissociation of NaAOT, was of the order of 1×10^{-7} M. They concluded that “double layer effects alone will not stabilize a highly concentrated dispersion in a hydrocarbon medium.” For a similar system, only when the ion concentration is greater than 1×10^{-5} M will repulsive forces be sufficient to ensure colloidal stabilization (Kitahara, 1973).

However, for media with ϵ between 2 and 5, a number of authors have reported indications of the role of electrostatic stabilization in non-aqueous media (Lyklema,

Figure 3-1. Variation of the total potential energy at different electrolyte molarity for charge-stabilized particles (Masliyah, 1994)



1968; Parfitt and Peacock, 1978; Kitahara, 1984). Fowkes (1984) went even further by saying that readers should be “wary of any claims of steric stabilization unless the electrostatic contribution has been measured.” Recently it was theoretically shown that smaller energy potentials are required for stabilization of larger particles than smaller ones (Morrison, 1991).

A colloidal dispersion can be stabilized in either an aqueous or non-aqueous media by solvated polymeric moieties adsorbed on the colloidal particle surface. The polymeric chains attached to the surface can be regarded as a barrier around each particle, preventing their close approach to each other. For sterically stable colloidal systems, the continuous medium must be a good solvent to the polymer attached to fine solid particles. Two steric stabilization mechanisms are shown in *Figure 3-2*: (a) entropic stabilization theory based on strict statistics; (b) osmotic repulsion stabilization theory based on statistical thermodynamics of polymer solution.

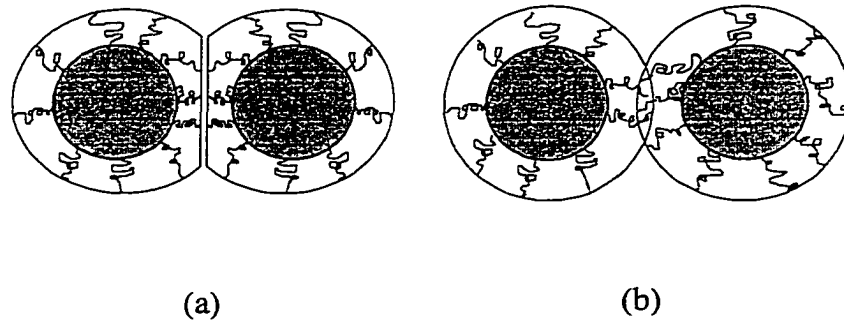
When two particles with adsorbed polymer layers approach each other at a distance of separation of less than twice the thickness of the adsorbed layer, interaction of the two layers takes place. The Gibbs free energy change ΔG of the overlap interaction of the adsorbed layer is expressed as

$$\Delta G = \Delta H - T\Delta S \quad (3-1)$$

where ΔH is the enthalpy change, and ΔS is the entropy change. If ΔG is negative upon the overlap of the adsorbed layers, flocculation or coagulation will result, and if ΔG is positive, stabilization will result.

A second surface approaching the adsorbed layer is impenetrable in the entropic stabilization theory (*Figure 3-2(a)*). The polymer segments occupy fewer possible

Figure 3-2. Highly sterically stabilized colloidal particles: (a) compression of adsorbed layer; (b) interaction of adsorbed layers (Sato and Ruch, 1980)



configurations in the compressed state than in the uncompressed state. The reduction in entropy leads to an increased ΔG , producing a net effect of repulsion between particles and thus preventing particles from flocculating.

In contrast, the osmotic repulsion stabilization theory assumes that the adsorbed layers of two particles can overlap each other and no desorption of polymer occurs upon collision (*Figure 3-2(b)*). The stability of the suspension depends on the total free energy change, ΔG_M , which is given by

$$\Delta G_M = \Delta H_M - T\Delta S_M \quad (3-2)$$

where ΔH_M and ΔS_M are the enthalpy and entropy of mixing, respectively. The contact between polymer segments and dispersion medium is reduced as a result of the overlap of adsorbed layers, which gives the enthalpy of mixing ΔH_M . Due to the increase of polymer segment concentration in the overlapped region, the configurational entropy of the adsorbed molecules ΔS_M is also decreased, like in the first theory.

Sterically stabilized colloidal particles are usually very stable over a wide range of particle size and shear rate, and at high concentrations of the dispersed phase. These particles may flocculate by decreasing the solvency of the continuous phase or desorbing the attached polymeric moieties. In practice, molecular weights above 1,000 are desirable for the stabilizing polymer (Walbridge, 1987).

3.4 Electroseparation

Today the removal of submicron particles from process or waste streams often involves granular filtration. While mechanically simple and energy efficient, this filtration primarily relies on physical interactions such as interception, sedimentation,

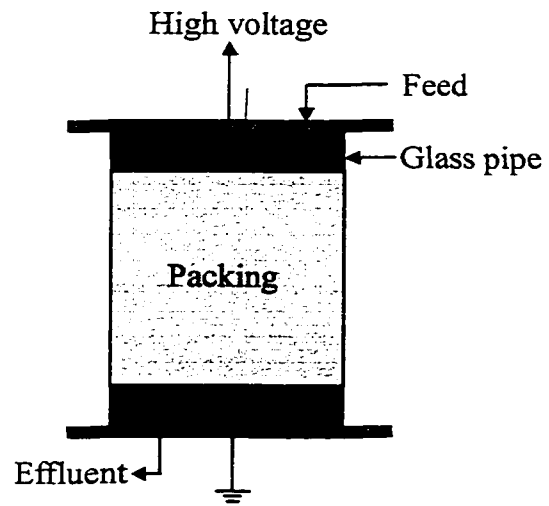
inertial, and van der Waals forces – hence, such filters are inefficient, particularly with submicron particles. To retain their effectiveness, large volume filters are required.

Electrostatic separation had great success in removing clay from hydrotreater feed, although the cost for implementing this technology was prohibitively high (*Section 3.1*). A broad definition for electroseparation was proposed (Byers and Amarnath, 1995) as “the use of electricity, or electromagnetic fields to produce and enhance chemical or physical separation.” Electric potential can serve as the primary driving force itself or enhance other driving forces, thus promoting separations. Universal availability, consistent quality, benign environmental impact, great flexibility, and an economic price render electroseparation attractive.

Barker et al. (1991) conducted electrofiltration research by passing a non-conducting liquid with suspended submicron particles through the packed bed and found that the particles were collected with very high efficiency on the packing surface (*Figure 3-3*). The electric field polarizes charges on the solid packing, causing charged or polarizable particles in the flowing liquid to be captured on the packing surface. The filter is easily cleaned by turning off the magnetic field, followed by backflushing. Filtration of aerosols in granular beds has also been improved by applying an electric field to the filter media (Harriot and Saville, 1980).

Critical to filter efficiency is the dielectric constant of the packing material, which must be higher than that of the continuous liquid phase, and the effectiveness of the filter goes up linearly as the dielectric constant of the packing material increases (Barker et al., 1991). For example, rutile ($\epsilon \cong 150$) has led to vastly enhanced performance, compared with glass beads ($\epsilon \cong 5$). This finding could propel dielectric filtration

Figure 3-3. The schematic diagram of a dielectric filter (Barker et al., 1991)

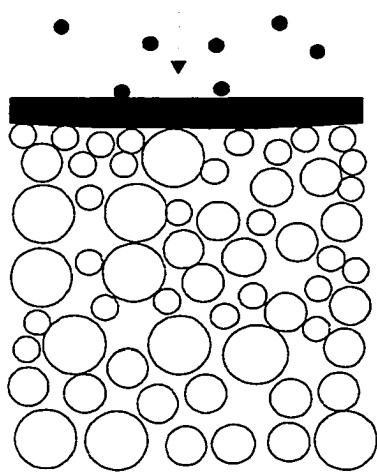


technology toward more widespread industrial application.

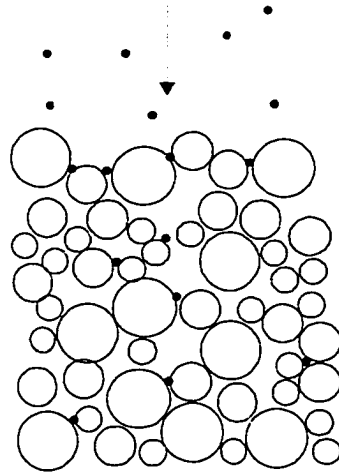
3.5 Filtration Mechanisms

Three filtration mechanisms (cake filtration, straining filtration, and physical chemical filtration) are schematically shown in *Figure 3-4* according to the relative sizes of particles (or particle aggregates) and collectors (McDowell-Boyer et al., 1986). When particles are too large to penetrate into the filter media, particles and aggregates are collected above the porous media to form a filter cake, which is termed cake filtration. Particles small enough to enter the porous media can be mechanically removed by straining in smaller pore spaces. Particle straining has limited capacity for particle accumulation, and little decrease in permeability is expected. Sakthivadivel (1969) conducted experiments with large plastic particles suspended in mineral oil to minimize any particle-particle and particle-collector interactions, and showed that the critical factor determining straining within porous media was the ratio of the collector diameter, d_m , to the particle diameter, d_p . For $\frac{d_m}{d_p}$ less than 10, or relatively large particles compared to the media size, no particle penetration into the media was observed, that is cake filtration. For relatively small particles, $\frac{d_m}{d_p} > 20$, only 2-5% of the pore volumes were occupied by retained particles under equilibrium conditions. If the influent particles contained a broad distribution in sizes from $\frac{d_m}{d_p} < 10$ to $\frac{d_m}{d_p} > 20$, then retained larger particles acted as strainers for smaller particles, leading to effective particle filtration at or near the media surface in a combination of surface and straining filtration. Particles much smaller than

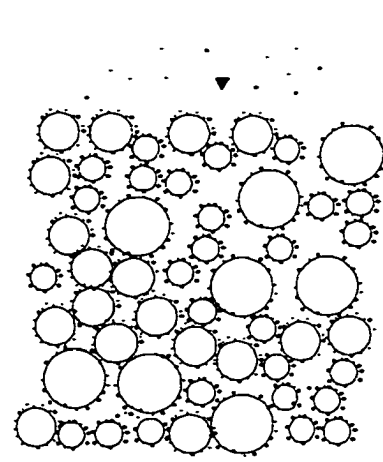
Figure 3-4. Variation of filtration mechanisms with particle size and difference in deposit morphology in each filtration mechanism (McDowell-Boyer et al., 1986)



(1) Cake Filtration



(2) Straining Filtration



(3) Physical Chemical Filtration

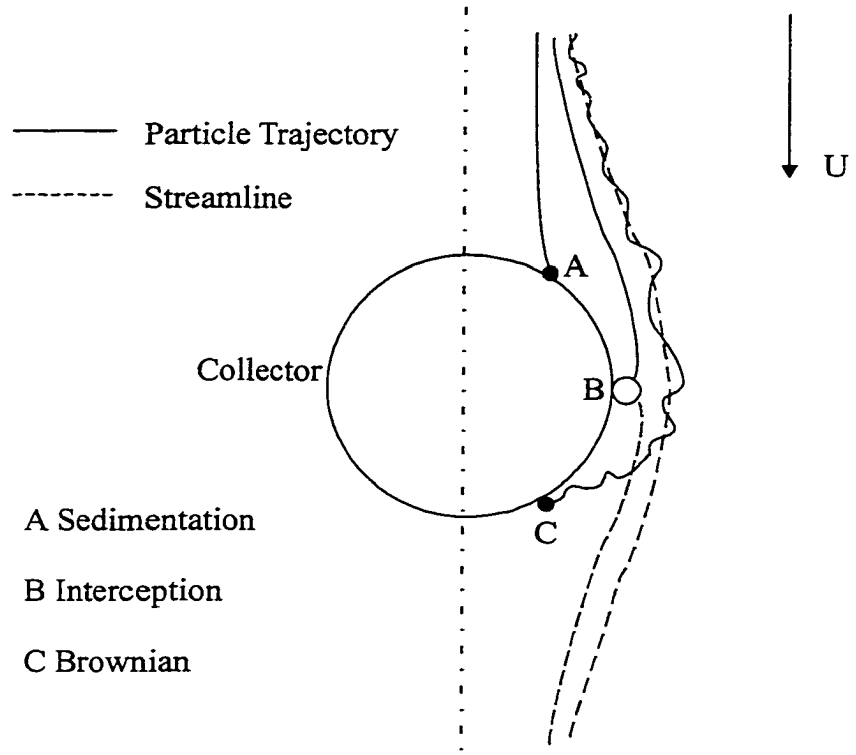
the collector diameter are retained only if physical or chemical attractive forces dominate when particles collide with the porous media.

3.6 Process of Particle Deposition

The process of particle deposition from flowing suspensions onto collector surfaces is conveniently divided into several steps: transport, attachment and reentrainment. In the first step, the particles are transported from the bulk of the fluid to the vicinity of a stationary surface. Brownian particles are mainly transported through convection and diffusion, while the transport of the larger particles is controlled by gravity and fluid drag (Tien, 1989). *Figure 3-5* illustrates the three dominant mechanisms for capturing suspended particles flowing through porous media (Yao et al., 1971). Attachment, on the other hand, is dominated by various chemical-colloidal interactions that act between particles and collector surfaces at short distances. These colloidal interactions include electrical double layer and van der Waals interactions, hydrodynamic interactions, hydration forces, hydrophobic interactions for hydrophobic surfaces, and steric forces. However, hydration forces and hydrophobic interactions can be ignored in a non-aqueous system. Particles attached to the collector surfaces can be removed from the surfaces, reentering the bulk flow of the fluid. The reentrainment is caused by the shear stress due to the velocity gradient within the boundary layer (Kern and Seaton, 1959). Although there are slight differences between the processes of particle reentrainment, detachment, and resuspension, they are all used so frequently in related literature that they are used interchangeably in this thesis.

Attachment of particles is determined by the magnitude of the colloidal interactions between particles and collectors. These, in turn, are controlled by the chemical

Figure 3-5. Three dominant mechanisms for capturing suspended particle to a collector surface (Yao et al., 1971)



characteristics of the solution phase, the suspended particles and the collectors. The critical role of solution chemistry and colloidal interactions in the attachment step is poorly understood (O'melia, 1987; Tobiabson and O'melia, 1988). The deposition rate may increase when deposited particles act as additional collectors, which is termed "ripening" (Liu et al. 1995). Song and Vigneswaran (1990) used two different suspensions to study the effect of ionic strength on the particle removal efficiency, and quantitatively related the clean filter bed efficiency and removal efficiency during the ripening period for various ionic strengths to the two model coefficients in the O'melia-Ali Model (1978). Both concentration and type of electrolyte in water influence the dynamics of particle deposition in porous media. A single deposited particle may block an area which is many times larger than its geometric cross-section, which gives a reduced deposition rate with time (Dabros, 1989). This excluded area effect, or blocking effect, is produced when charged particles are deposited. However, because the ionic strength in non-aqueous solutions is very low, the effects of electrolyte on particle deposition in aqueous systems are not likely to apply to a non-aqueous system.

Dabros and van de Ven (1992 and 1993) studied particle deposition on partially coated surfaces. They showed that colloidal interactions, rather than hydrodynamic interactions between deposited and flowing particles, have a significant influence on blocking. Vasak et al. (1995) rendered glass collector surfaces positively charged by coating them with a cationic polymer while the suspended particles were negatively charged. The initial deposition rates in turbulent flow decreased with increasing Reynolds number, indicating that deposition was no longer mass transfer controlled and that particle attachment played an increasingly important role in deposition as Reynolds number was increased.

Most early studies did not consider particle detachment in filtration. However, experiments showed that particle detachment does occur in the later stages of filtration. Mints et al. (1967) showed in an experimental run that more larger particles leave a filter than those entering the filter. They used this observation as evidence for particle detachment. Particle detachment was also used to explain the shifting of particle size distribution of the effluent toward larger size during filtration (Ginn et al. 1992). Using fiber optics, Ives and Clough (1985) were able to observe events within the filter to demonstrate deposition and reentrainment. Using clay suspensions, these investigators observed dome-shaped deposits on top of the grains and detachment of these deposits. Moran et al. (1993) reported the occurrence of particle detachment and its dependence on particle size. Bai and Tien (1997) further confirmed the dependence of particle detachment upon the particle size and the collector grain size. Particle detachment in filtration was a result of either the flow shear forces overcoming the attachment forces (Payatakes et al. 1981) or instabilities caused by arriving particles (Ives 1989).

A kinetic model of particle reentrainment by fluid drag force in a turbulent flow has been developed by Vainshtein et al. (1997). Now it is generally believed that increases in interstitial velocity due to the buildup of deposit are instrumental in particle detachment. Titanium dioxide particles that were strongly attached to glass beads under weak shear, for example, were observed to detach when the shear rate is increased (Newman and Stolzenbach, 1996). Mints (1966) described particle detachment as being directly proportional to the specific deposit. Others (Adin and Rebhun, 1977; Vigneswaran and Song, 1986) assumed that particle detachment was directly proportional to the product of the hydraulic gradient and the specific deposit.

3.7 Transient Behavior of Filtration

Deep-bed filtration is inherently unsteady in nature, because both the collection efficiency and the permeability of the filter media change with time (Choo and Tien, 1995). In the past a large number of investigators have examined the transient behavior of deep-bed filtration. During the initial stage of deposition, while collector surfaces are essentially devoid of particles, a constant rate of particle deposition is generally observed. During the later stages of deposition, variations in the rate of particle deposition arise as particles accumulate on the collector surfaces. Accumulation of particles will cause either a rise or decline in the deposition rate, depending on the solution chemistry and the surface chemistry of particles and collectors. In many deposition processes, declining deposition rates arise when excluded area effects of deposited particles hinder subsequent attachment of particles. Excluded area effects are produced when repulsive electrostatic forces emanating from charged particles deposited on collector surfaces create an energy barrier which inhibits subsequent deposition (Rajagopalan and Chu, 1982). Baghdikian et al. (1987) studied the transient behavior of the flow of clay suspensions through porous media at different flow rates, pH values, ionic strengths, and particle concentrations. The particle and pore size distributions together with the surface charges on the particles and pores were used to estimate theoretically the declining rates of permeability. It was concluded that permeability reduction occurs more rapidly as the clay concentration increases, the solution pH decreases and the ionic strength increases. Many deposition processes occurring in aqueous media are restricted to single layer coverage of collector surfaces, because of the prevalence of repulsive interparticle electrostatic forces that prevent contact of particles (Johnson and Elimelech, 1995). However, Matijevic and

Ryde (1995) elaborated on the possibility of inducing deposition by magnetic field under conditions where particles and collector surfaces bear the same sign of charge. Under favorable particle-particle interactions (i.e. in the absence of interparticle repulsion), on the other hand, the particle deposition rate usually increases with time. O'melia and Ali (1978) attributed the increased rate in particle collection to the fact that deposited particles functioned as additional collectors. However, since the particle deposition in hydrotreaters occurs over a prolonged period of time, the transient behavior of particle deposition is not of major concern.

3.8 Particle Deposition on Coated Collector Surfaces

The packed column technique serves as a useful tool in the investigation of the deposition and removal mechanisms of particles dispersed in a liquid in contact with a solid substrate. The effect of surfactants on adhesion of particles onto glass beads has been studied by a few investigators using this technique. Negatively charged surface-active agents are known to mask favorable sites for particle attachment and to significantly reduce particle deposition rates (Hull and Kitchener, 1969). The lowest deposition rates of particles coated with humic materials in packed beds were attributed to the greatest steric interaction forces by Amirbahman and Olson (1993). Litton and Olson (1994) suggested that particle attachment is enhanced by uncharged, hydrophobic regions of quartz. Ryde and Matijevic (1995) studied the adhesion phenomena of hematite particles on gelatin-coated glass beads and compared with the same system in the absence of the protein. They argued that the interaction between hematite and glass is affected by physical forces only, whereas in the presence of gelatin, chemical bonds are formed between the particles and the substrate. Matijevic and Ryde (1995) further proved

that the rate of deposition, in the absence of a repulsion barrier, is governed by a convective diffusion mechanism. If a repulsion barrier exists, the deposition rate depends on the ionic strength in a manner consistent with colloidal stability. Zelenev and Matijevic (1997) found that sodium 4-octylbenzenesulfonate of sufficiently high concentrations causes charge reversal of hematite particles to negative values and a restabilization of the suspension, preventing their deposition under such conditions.

3.9 Particle Deposition in Non-aqueous Systems

The deposition process has been studied extensively in aqueous systems, but relatively few studies have considered non-aqueous suspensions. Chowdiah et al. (1981) studied the filtration of carbon black from tetralin through a bed of sand. The streaming potential across the filter bed was used to monitor the initial deposition of particles. The initial capture efficiency was very high and a distinct breakthrough curve was observed in particle concentration. The initial deposition was attributed to the electrostatic attraction between the particles and the packing. Once the charge on the collector surfaces was neutralized, continued deposition at much lower filter efficiency was ascribed to other mechanisms such as straining and interception, which may not be affected by electrical double layers. Lo et al. (1983) studied the cross-flow electrofiltration of $\alpha\text{-Al}_2\text{O}_3$ particles suspended in tetralin and presented the effects of feed rate, driving pressure and electrical field strength on the filtration rate and the efficiency of the filter. Byers and Amarnath (1995) suggested that placing a high voltage across the packed bed can enhance the capture of particles, especially when the bed packing has a much higher dielectric constant than that of the liquid. The deposition of carbon black in kerosene was studied by Narayan et al. (1997) in columns packed with glass beads and catalyst. The

efficiency of trapping of fine particles decreased with the amount of deposit in the bed and decreased with increasing Reynolds number. Equivalent results were obtained with glass beads and hydrotreating catalyst. Low Reynolds number gave a more pronounced increase in pressure drop because deposits accumulated in the flow channels between beads or pellets in the bed.

The surface chemistry of suspended particles and the collector plays an important role in deposition onto collector surfaces. It has been reported that cleaning methods of glass surfaces, used as collectors in deposition experiments, can significantly influence the rate of particle deposition in water under unfavorable chemical conditions (Dabros and van de Ven, 1983). When mineral materials such as clays are present in Athabasca bitumen or its products, their interactions with polar compounds alter their surface characteristics and surface behavior. The partially hydrophilic and partially oleophilic nature of the mineral particles leads to their partitioning at the oil/water interface resulting in a solids-stabilized emulsion (Prudich and Henry, 1978; Gelot et al., 1984; Yan and Masliyah, 1996) and a significant oil loss during the separation of fine particles (Menon et al. 1987). The asphaltene content of crude oil varies from about 1% or less in light crudes to as much as ten percent in heavy crudes. The high asphaltene contents coupled with relatively high solid contents of synthetic crudes make separation of solids a very difficult problem. Marlow et al. (1987) found that adsorbed asphaltenes enhances stability of illite suspensions in toluene, and concluded that the colloidal stability is due to a combination of electrostatic and steric repulsive forces. Furthermore, asphaltenes and preasphaltenes in coal liquids have been found to affect the suspended particle size (Briggs et al. 1980), and Rodgers (1980) has related this phenomenon to the changes in particle charge caused

by asphaltenes depositing on the particle surface. However, the effect of adsorbed asphaltenes (or resins) on fine particles or free asphaltenes (or resins) in liquid phase on particle deposition has not been studied, let alone in simulated hydrotreaters.

3.10 Hydrodynamics of Packed-Bed Reactors

In packed-bed hydrotreaters several flow regimes are observed (Ng and Chu, 1987). According to the flow rates of the liquid and gas, they are referred to as trickling flow, spray flow, bubble flow, dispersed bubble flow, and pulsing flow regimes. Trickle-bed reactors are used extensively in industrial practice, due to the wide range of operating conditions that they can accommodate. The behavior of this type of reactor is complex due to hydrodynamic characteristics arising from the gaseous and liquid flow through the packed bed. A large number of variables, such as reaction kinetics, bed porosity, size and shape of catalyst particles, interfacial tension, wettability, gas and liquid flow rates and viscosities, seem to have a considerable effect on the reactor operation (Wu et al., 1996). The fluid flow pattern adjacent to collector surfaces plays an important role in particle transport and deposition. Flow patterns are not necessarily uniform in a trickle-bed reactor. For example, liquid maldistribution occurs in reactors with highly exothermic reactions. As the liquid film flows down the column from particle to particle, vaporization takes place and the particles near the bottom are even dry. Hence some parts of the catalyst bed are not in contact with the liquid, whereas other parts are overloaded. It has been suggested that without a liquid film to carry away the heat generated, these non-wetted or dry catalyst particles can lead to hot spot formation (Ng and Chu, 1987).

Deposition of fine particles in commercial hydrotreaters occurs at extreme conditions of temperature and pressure. In laboratory-scale trickle beds packed with the commercially used catalyst, the ratio of the reactor diameter and catalyst particle diameter is undesirably low, and low liquid velocity is frequently used in order to match the liquid hourly space velocity of the commercial unit (Wu et al., 1996). These conditions give rise to wall effects, axial dispersion, maldistribution, and incomplete external catalyst wetting which are not observed to the same extent in commercial reactors. Therefore, scaling up of the trickle-bed reactor is very difficult, even when the scaling correlation is based on the same packings and similar fluids, because the flow pattern in a commercial reactor may differ markedly from that of the laboratory-scale reactor. However, a systematic study on the chemistry of particle deposition in a simulated hydrotreater under the identical hydrodynamic conditions may help to better understand the deposition profile and the deposition mechanism in commercial hydrotreaters.

References

- Adin, A.; Rebhun, M. A Model to Predict Concentration and Head-Loss Profiles in Filtration. *AWWA J.* **1977**, 69 (8), 444-453.
- Amirbahman, A.; Olson, T. M. Transport of Humic Matter-Coated Hematite in Packed Beds. *Environ. Sci. Technol.* **1993**, 27 (13), 2807-2813.
- Baghdikian, S. Y.; Sharma, M. M.; Handy, L. L. "Flow of Clay Suspensions through Porous Media." SPE (Society of Petroleum Engineers) International Symposium on Oilfield Chemistry, San Antonio, Texas, Feb. 4-6, **1987**.
- Barker, R. E.; Brunson, R. R.; Clinton, S. D.; Watson, J. S. Granular Electrofiltration. *Separations Technology* **1991**, 1, 166.
- Biran, R.; Tang, Y. Z.; Brook, J. R.; Vincent, R.; Keeler, G. J. Aqueous Extraction of Airborne Particulate Matter Collected on Hi-Vol Teflon Filters. *Intern. J. Environ. Anal. Chem.* **1996**, 63 (4), 315-322.
- Bai, R.; Tien, C. Particle Detachment in Deep Bed Filtration. *J. Colloid Interface Sci.* **1997**, 186, 307-317.
- Briggs, D. E.; Cameron, J. R.; Ho, B.; Islip, P. N.; Mckeen, J. A. Filtration of Slurries from Coal Liquefaction Processes. *Separation Sci. Technol.* **1980**, 15 (3), 223.
- Byers, C. H.; Amarnath, A. Understand the Potential of Electroseparation. *Chem. Eng. Prog.* **1995**, 91 (2), 63-69.
- Chan, E. W.; Chung, K. H.; Veljkovic, M.; Liu, J. K. Hydrodynamics and Fines Capture in Packed-Bed Hydrotreaters. *Int. Petrol. Petrochem. Technol. Symp.*, Beijing, September 15-17, **1994**.
- Choo, Chang-Upp; Tien, C. Analysis of the Transient Behavior of Deep-Bed Filtration. *J. Colloid Interface Sci.* **1995**, 169, 13-33.
- Chowdiah, P.; Wasan, D. T.; Gidaspow, D. Electrokinetic Phenomena in the Filtration of Colloidal Particles Suspended in Non-aqueous Media. *AIChE J.* **1981**, 27 (6), 975-984.
- Christopherson, P. "Plant 18-1 Reactor Pressure Drop Buildup Status Report #3." Primary Upgrading Technology Inter-Office Correspondence, Syncrude Canada Ltd. Dec. 19, **1994**.
- Dabros, T.; van de Ven, T. G. M. Direct Method for Studying Particle Deposition onto Solid Surfaces. *Colloid Polym. Sci.* **1983**, 261 (8), 694-707.

Dabros, T.; van de Ven, T. G. M. Hydrodynamic Interactions between Two Spheres near a Solid Plane. *Int. J. Multiphase Flow* **1992**, 18 (5), 751-764.

Dabros, T.; van de Ven, T. G. M. Particle Deposition on Partially Coated Surfaces. *Colloids and Surfaces A: Physicochemical and Engineering Aspects* **1993**, 75, 95-104.

Féat, G. R.; Levine, S. The Double-layer Interaction of Two Charged Colloidal Spherical Particles of a Concentrated Dispersion in a Medium of Low Dielectric Constant. III. Approximation of Perfectly Conducting Particles. *J. Colloid Interface Sci.* **1976**, 54(1), 34-44.

Fowkes, F. J.; Pugh, R. J. *Steric and Electrostatic Contributions to the Colloid Properties on Non-aqueous Dispersions*. In *Polymer Adsorption and Dispersion Stability*. Am. Chem. Soc. Symposium Series **1984**, pp.240.

Gelot, A.; Friesen, W.; Hamza, H. A. Emulsification of Oil and Water in the Presence of Finely Divided Solids and Surface-Active Agents. *Colloids Surfaces* **1984**, 12, 271-303.

Ginn Jr., T. M.; Amirtharajah, A.; Karr, P. R. Effects of Particle Detachment in Granular-Media Filtration. *AWWA J.* **1992**, 84 (2), 66-76.

Harriott, G. M.; Saville, D. A. Electrically Stimulated Aerosol Filtration in Packed Beds. *AIChE J.* **1980**, 26(3), 398-402.

Hoeven, PH. C. Van Der; Lyklema, J. Electrostatic Stabilization in Non-Aqueous Media. *Advances in Colloid and Interface Science* **1992**, 42, 205-277.

Hull, M.; Kitchener, J. A. Interaction of Spherical Colloidal Particles with Planar Surfaces. *J. Chem. Soc. Faraday Trans.* **1969**, 65, 3093-3104.

Ives, K. J. Filtration Studied with Endoscopes. *Wat. Res.* **1989**, 23 (7), 861-866.

Ives, K. J.; Clough, G. *Optical Fiber Investigations of Filtration Processes*. 4th IAWPRC Workshop on Instrumentation and Control of Water and Wastewater Treatment and Transport Systems, Houston, TX, April **1985**.

Johnson, Philip R.; Elimelech, M. Dynamics of Colloid Deposition in Porous Media: Blocking Based on Random Sequential Adsorption. *Langmuir* **1995**, 11, 801-812.

Kern, D. Q.; Seaton, R. E. A Theoretical Analysis on Thermal Surface Fouling. *Br. Chem. Engng* **1959**, 4, 258-262.

Kitahara, A. Zeta Potential in Non-aqueous Media and its Effect on Dispersion Stability. *Progr. Org. Coatings.* **1973**, 2, 81-98.

- Kitahara, A. *Non-aqueous Systems*. Chapter 5 in *Surfactant Science Series*. Vol. 1. *Electrical Phenomena at Interfaces. Fundamentals, Measurements and Applications*. Ed. Kitahara, A.; Watanabe, A. Marcel Dekker, **1984**.
- Koyama, H.; Nagai, E.; Torri, H.; Kumagai, H. Japanese Refiner Solves Problems in Resid Desulfurization Unit. *Oil Gas J.* **1995**, 93 (46), 82-90.
- Litton, G. M.; Olson, T. M. Colloid Deposition Kinetics with Surface-Active Agents: Evidence for Discrete Surface Charge Effects. *J Colloid Interface Sci.* **1994**, 165, 522-525.
- Liu, D.; Johnson, P.; Elimelech, M. Colloidal Deposition Dynamics in Flow through Porous Media: Role of Electrolyte Concentration. *Environ. Sci. Technol.* **1995**, 29 (12), 2963-2973.
- Lo, Y. S.; Gidaspow, D.; Wasan, D. T. Separation of Colloidal Particles from Nonaqueous Media by Cross-flow Electrofiltration. *Sep. Sci. Technol.* **1983**, 18 (12 & 13), 1323-1349.
- Lyklema, J. Principles of the Stability of Lyophobic Colloidal Dispersion in Non-aqueous Media. *Advan. Colloid Interface Sci.* **1968**, 2, 65-114.
- Marlow, B. J.; Sresty, G. C.; Hughes, R. D.; Mahahan, O. P. Colloidal Stabilization of Clays by Asphaltenes in Hydrocarbon Media. *Colloids and Surfaces* **1987**, 24, 283-297.
- Masliyah, J. H. *Electrokinetic Transport Phenomena*; AOSTRA Technical Publication Series #12, Edmonton, AB, **1994**.
- Matijevic, E.; Ryde, N. Kinetics of Particle Deposition and Detachment. *Journal of Adhesion* **1995**, 51 (1-4), 1-14.
- McDowell-Boyer, L. M.; Hunt, J. R.; Sitar, N. Particle Transport through Porous Media. *Water Resources Research* **1986**, 22 (13), 1901-1921.
- Menon, V. B.; Nagarajan, R.; Wasan, D. T. Separation of Fine Particles from Nonaqueous Media: Free Energy Analysis and Oil Loss Estimation. *Sep. Sci. Technol.* **1987**, 22 (12), 2295-2322.
- Mints, D. M. *Modern Theory of Filtration*; Special Subject No. 10, Int. Wat. Supply Assoc. Congress (Barcelona), **1966**.
- Mints, D. M. ET AL. Mechanism of the Filtration Process on Rapid Water Treatment Filters (in Russian). *Zh. Priklad. Khimii*, 8 (**1967**).

Moran, M. C.; Moran, Daniel C.; Cushing, Robert S.; Lawler, D. F. Particle Behavior in Deep-Bed Filtration (Part 2): Particle Detachment. *American Water Works Association Journal* **1993**, 85 (12), 82-93.

Morrison, Ian D. Criterion for electrostatic Stability of Dispersions at Low Ionic Strength. *Langmuir* **1991**, 7, 1920-1922.

Ng, K. M.; Chu, C. F. Trickle-Bed Reactor. *Chemical Engineering Progress* **1987**, 83 (11), 55-63.

Narayan, R.; Coury, Jose R.; Masliyah, J. H.; Gray, M. R. Particle Capture and Plugging in Packed-Bed Reactors. *Ind. Eng. Chem. Res.* **1997**, 36 (11), 4620 -4627.

Newman, K. A.; Stolzenbach, K. D. Kinetics of Aggregation and Disaggregation of Titanium Dioxide Particles and Glass Beads in a Sheared Fluid Suspension. *Colloids and Surfaces A: Physicochemical and Engineering Aspects* **1996**, 107, 189-203.

O'melia, C. R. In "Aquatic Surface Chemistry;" Stumm, W., Ed.; Wiley-Interscience: New York, **1987**.

O'melia, C. R.; Ali, W. The Role of Retained Particles in Deep Bed Filtration. *Prog. Wat. Tech.* **1978**, 10 (5), 167-182.

Parfitt, G. D.; Peacock, J. Stability of Colloidal Dispersion in Non-aqueous Media. Vol. 10: *Surface and Colloid Science*. Ed. Matijevic, E. Plenum Press (**1978**).

Payatakes, A. C.; Park, H. Y.; Petrie, J. A Visual Study of Particle Deposition and Reentrainment during Depth Filtration of Hydrosols with a Polyelectrolyte. *Chem. Eng. Sci.* **1981**, 36, 1319-1335.

Prudich, M. E.; Henry, J. D. Jr. The Mechanism of Transfer of Hydrophobic Coated Mineral Matter Particles from a Hydrocarbon to an Aqueous Phase. *AIChE J.* **1978**, 24, 788-795.

Rajagopalan, R; Chu, R. Q. Dynamics of Adsorption of Colloidal Particles in Packed Beds. *J. Colloid Interface Sci.* **1982**, 86, 299-317.

Rodgers, B. R. "Stability of Coal Derived Particles in Organic Media," Report No. ORNL-5631, Oak Ridge National Laboratory, Oak Ridge, TN , Aug., **1980**.

Ryde, N.; Matijevic, E. Particle Adhesion on Gelatin-Coated Glass Surface. *J. Colloid Interface Sci.* **1995**, 169, 468-475.

Sakthivadivel, R. Clogging of a Granular Porous Medium by Sedimentation. *Rep. HEL* 15-7, 106 pp., Hydraul. Eng. Lab., University of Calif., Berkeley, **1969**.

- Song, C. J.; Vigneswaran, S. Ionic Strength in Deep Bed Filtration. *Wat. Res.* **1990**, 24 (11), 1425-1430.
- Tien, C. *Granular Filtration of Aerols and Hydrosols*; Butterworths-Heinemann, Boston, MA, **1989**.
- Tobiabson, J. E.; O'melia, C. R. Physicochemical Aspects of Particle Removal in Depth Filtration. *American Water Works Association Journal* **1988**, 80 (12), 54-64.
- Vainshtein, P.; Ziskind, G.; Fichman, M.; Gutfinger, C. Kinetic Model of Particle Resuspension by Drag Force. *Physical Review Letters* **1997**, 78 (3), 551-554.
- Vasak, F.; Bowen, B. D.; Chen, C. Y.; Kastanek, F.; Epstein, N. Fine Particle Deposition in Laminar and Turbulent Flow. *Canadian Journal of Chemical Engineering* **1995**, 73 (6), 785-792.
- Vigneswaran, S.; Song, C. J. Mathematical Modeling of the Entire Cycle of Deep Bed Filtration. *Water Air Soil Pollut.* **1986**, 29, 155-164.
- Walbridge, D. J. Preparations of Solid/Liquid Dispersions. Chapter 2 in *Solid/Liquid Dispersions* (ed. Tadros, Th. F.), Academic Press, London, **1987**.
- Wu, Y.; Khadilkar, M. R.; Al-Dahhan, M. H.; Duduković, M. P. Comparison of Upflow and Downflow Two-Phase Flow Packed-Bed Reactors with and without Fines: Experimental Observations. *Ind. Eng. Chem. Res.* **1996**, 35, 397-405.
- Yan, N.; Masliyah, J. H. Effect of pH on Adsorption and Desorption of Clay Particles at Oil-Water Interface. *J. Colloid Interface Sci.* **1996**, 181, 20-27.
- Yao, K. M.; Habibian, M. T.; O'Melia, C. R. Water and Wastewater Filtration: Concepts and Application. *Environ. Sci. Technol.* **1971**, 5(11), 1105-1112.
- Zelenev, A.; Matijevic, E. Effects of Surfactants on Particle Adhesion Part 1. Interactions of Monodispersed Colloidal Hematite Particles with Glass Beads in the Presence of Sodium 4-Octylbenzenesulfonate. *Colloids and Surfaces A: Physicochemical and Engineering Aspects* **1997**, 125, 171-179.

Chapter 4: Toluene-Insoluble Fraction from Thermal Cracking of Athabasca Gas Oil: Formation of an Emulsified Liquid That Wets Hydrophobic Dispersed Solids*

4.1 Introduction

The formation of solids from petroleum fractions during processing is of significant interest, both in coking processes and in fouling of furnace tubes, heat exchangers and other process vessels. The tendency to form insoluble solids varies significantly with the properties of the feedstock, but it is commonly correlated with asphaltene content (Kriz, 1994). The chemical reactions that are involved in forming solids and ultimately petroleum coke have received considerable attention. Magaril et al. (1968) linked coke formation explicitly with asphaltene content by suggesting that coke formed *via* condensation and polymerization reactions in a new solid phase that formed by precipitation of the asphaltenes. Storm et al. (1995) suggested a similar process, wherein interactions between asphaltenic molecules in the oil give molecular aggregates, which can eventually react to give coke. The model for coke formation suggested by Wiehe (1993) is based on phase behavior rather than molecular aggregation. He suggested that coke forms from an asphaltenic phase that has separated from the rest of the oil. Phase separation is driven by the cracking of side chains from asphaltenes, leaving a progressively more aromatic core. Shaw et al. (1988) observed liquid-liquid phase separation in a mixture of tetralin, pyrene and hydrogen over a range of temperature and

* A version of this chapter appeared as Wang, S.; Chung, K.; Masliyah, J.H.; Gray, M. R. *Fuel*, 1998, 77(14), 1647-1653.

pressure typical of hydroconversion processes, and suggested that such phase separation could lead to coke formation. The observation of phase separation with such simple mixtures suggests that the macromolecular behavior that is so useful in understanding the precipitation of asphaltenes in paraffinic solvents (Mannistu et al., 1997) may be inappropriate at reactor conditions.

Although many of the concepts of asphaltene behavior are guided by observations of flocculation at room conditions, the behavior of these components of residual oils may be significantly different at reactor conditions. For example, coke precursors exhibit fluid properties such as coalescence and deformation by shear at temperatures in excess of 400 °C. The observation of mesophase by Brooks and Taylor (1968) is another excellent example. Micron-sized spheres of liquid-crystalline mesophase form and coalesce with time, clearly exhibiting the behavior of one fluid suspended in a second, less viscous fluid. Highly structured coke materials, such as needle coke, can form due to the action of shear from rising gas bubbles on the mesophase liquid (Mochida et al., 1988). The plastic properties of cokes from petroleum and coal indicate that although these materials are solid at room temperature, their properties can change significantly at elevated temperatures.

Carbonaceous material frequently deposits on the inner surfaces of process equipment and causes fouling (Garett-Price et al., 1985), particularly in processing of heavy oils and bitumen (Crittenden, 1992). One of the important processes in fouling is the attachment of the material to the walls of the process equipment. The current understanding of fouling due to chemical reactions is largely driven by studies of adhesion of particles to metal surfaces, rather than adhesion of plastic or fluid materials (Watkinson and Wilson,

1997). When fluids deposit on a surface, their ability to wet the surface will determine the structure of the deposit. Although adhesion to metal surfaces is important in process equipment, the presence of fine solids in an oil stream can provide a high surface area dispersed throughout the liquid phase. Several studies have indicated that physical interactions between coke materials and particle surfaces may be important. Belinko et al. (1977) investigated the benzene-insoluble residue at the bottom of a hydroconversion reactor by optical microscopy, and observed a layered coating of coke material on inert mineral particles. Mineral solids tend to be concentrated in coke products, which indicates significant physical interaction (Gray, 1994). Both Dubois et al. (1970) and Bradford et al. (1971) observed that the addition of fine solids interfered with the coalescence of mesophase coke, indicating that the ability of coke materials to wet surfaces can result in different properties. Tanabe and Gray (1997) suggested that fine particles inhibited the coalescence of plastic coke particles, thereby altering the kinetics of coke formation. Conversely, surface coatings of carbonaceous material may alter the behavior of mineral particles. Solid deposits in hydrotreating reactors are often accretions of carbonaceous material and iron sulfides (Koyama et al., 1995). Gas oils from Athabasca bitumen typically contain clay minerals, which also deposit in hydrotreating reactors to give undesirable increases in pressure drop (Narayan, 1996). If the mineral particles are wetted by a carbonaceous phase, then this organic film could enhance adhesion and cementation of particles. These studies suggest that the fluid-phase properties of insoluble fractions at reactor conditions, such as wettability and surface tension, may be important in the performance of upgrading processes.

The objective of this study was to observe the formation of a toluene-insoluble (TI) fraction, and then study its physical interactions with solid surfaces at reactor conditions. Measurement of contact angles is not possible at the temperatures typical for formation of TI solids; therefore, the surface chemistry of fine solids added to the reactor was defined as either non-polar or polar. Toluene insolubles were formed by heating Athabasca coker gas oil, at temperatures ranging from 300 to 420 °C, in a batch reactor under a hydrogen atmosphere. The TI fraction was defined throughout this study as the carbonaceous solid which was insoluble in toluene, and hence recoverable by filtration. The yield and morphology of the TI solids were examined, and then the physical interactions with solid surfaces were studied by adding finely divided particles to the reactor. This approach was intended to enhance our understanding of how interactions between the TI fraction and particulates could alter deposition of solids in packed-bed catalytic reactors.

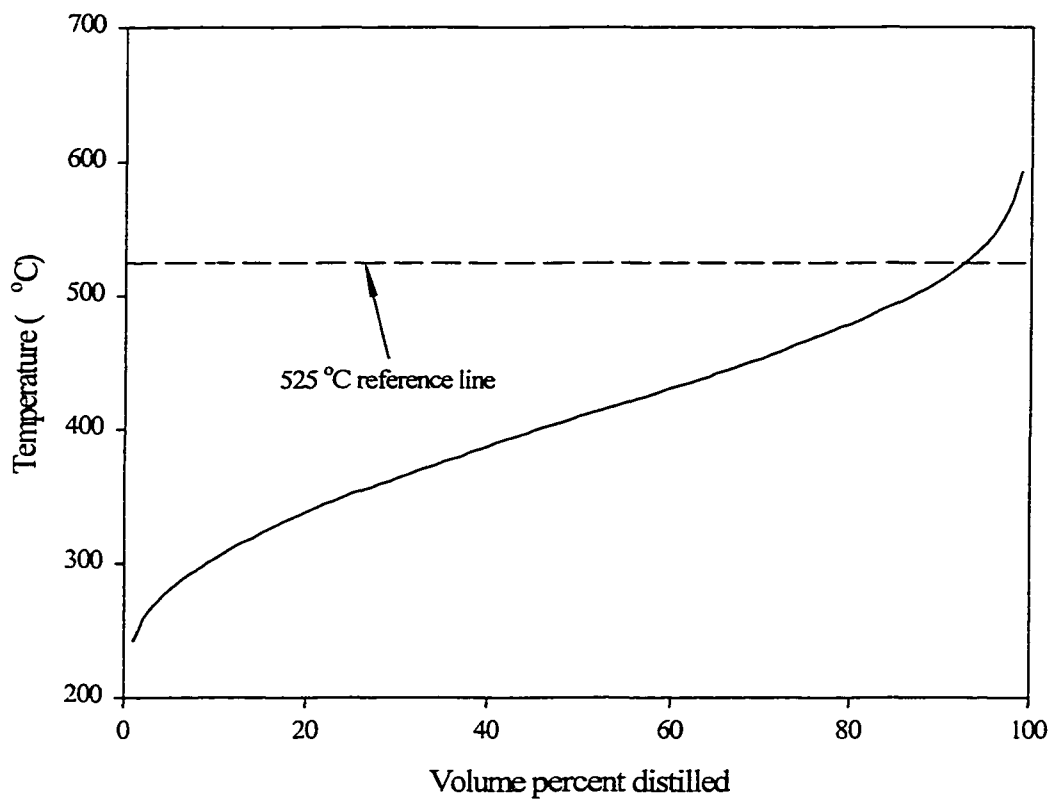
4.2 Experimental

The feed to the reactor was the Coker gas oil produced from Athabasca bitumen by fluid coking, provided by Syncrude Canada Ltd. from its plant at Mildred Lake, Alberta, Canada. The properties of the gas oil are listed in *Table 4-1*. The boiling point distribution curve for this coker gas oil is shown in *Figure 4-1*. Only the temperature range from the 5% boiling point to the 95% boiling point, not from the initial boiling point (IBP) and the final boiling point (FBP), is reported in *Table 4-1*. The contents of oxygen and metals were not determined. Three different solids were suspended in the gas oil prior to some reaction experiments. Kaolin, the most abundant clay mineral in the Athabasca oil sands, was selected as a material with polar functional groups on its surface. The data of the composition and physical properties

Table 4-1. Composition and properties of Athabasca coker gas oil

Elemental composition	weight %
C	83.5
H	10.5
S	4.15
N	0.34
Properties	
Asphaltene, weight %	0.6
Density, kg/m ³ at 15 °C	990.2
Viscosity, mPa-s at 20 °C	492
Boiling range, °C	275 - 540
Filterable solids, wppm	250

Figure 4-1. Boiling point distribution curve of Athabasca coker gas oil



of the kaolin was given in the material safety distribution sheet from Georgia Hydrite (*Table 4-2*). Two mean particle sizes were used: 5 μm and 0.2 μm . Carbon black (Fisher Scientific Co.) was selected as a material with mainly non-polar functional groups on its surface. With a mean particle size of 0.2 μm , its elemental composition was 97.44 wt% C, 0.86 wt% S, 0.39 wt % H, and 0.31 wt% N. All reagents were from Fisher Scientific (Toronto, Canada) unless otherwise specified.

Samples of 5 μm kaolin were treated to cover the surface with non-polar groups by coating the particles with asphaltenes, following the method of Yan and Masliyah (1996). An asphaltene fraction of Athabasca bitumen (0.5 g, prepared by supercritical fluid extraction (Chung et al., 1997)) was dissolved in 125 mL toluene and sonicated (Aquasonic 150 HT, VWR Scientific, Toronto, Canada) for 30 min. Heptane (125 mL) was added to the solution and the mixture was sonicated for 10 min. Kaolin (2.5 g) was added and the mixture was stirred at 200 rpm for 24 h. The mixture was then filtered through a 0.22 μm membrane filter (Millipore) to recover the kaolin, which was dried under vacuum at 50 °C for 24 h to constant weight.

The solids were dispersed in the gas oil by mixing in a blender (Waring Corp.) for three minutes. Each reaction experiment used 240 g feed with solid concentration of 4 g/kg oil. The oil or oil/solid mixture was poured into a 500-mL autoclave (Model 4575, Parr Instrument Company). Detailed information about this autoclave is presented in *Appendix 1*. The reactor was pressure tested with nitrogen at 12 MPa and then pressurized with hydrogen at 12 MPa and purged three times. The initial hydrogen pressure at room temperature was 7 MPa and the impeller speed was normally 560 rpm. The reaction time (normally 1 h) began when the preset reaction temperature in the range

Table 4-2. Composition and properties of kaolin

Component	Weight percent (%)
Aluminum oxide	38.38
Calcium oxide	0.05
Silicon dioxide	45.30
Magnesium oxide	0.25
Sodium oxide	0.27
Iron oxide	0.30
Potassium oxide	0.04
Titanium dioxide	1.44
Ignition loss at 950 °C (combined water)	13.97
Physical properties	
Density (kg/m ³)	2,580
BET surface area (m ² /g) for kaolin of different median particle size (μm)	
0.20	21
0.68	12
5.0	7

of 300 – 420 °C was first reached. The total pressure during the reaction of the gas oil was ca. 13 MPa. The impeller was operated for one hour at the end of the reaction time to prevent local overheating. The reactor was then removed from the heater and allowed to cool for 24 h before opening.

About 20 mL of well-mixed liquid product was filtered through a 0.22 μm membrane filter (Millipore), and 100-mL methylene chloride was used to wash the filtered solids on the filter paper. The filter cake was weighed, photographed, and sent for elemental analysis after being dried in the vacuum oven at 80 °C for 24 h. The same method was used to determine the solids content of the gas oil prior to reaction. The yield of the solids was insensitive to the choice of solvent; equivalent results were obtained with toluene, methylene chloride and xylene. Solubility in toluene is the most common criterion to distinguish solids in petroleum processing, therefore, the insoluble fraction is called “toluene-insoluble” as the most familiar terminology. The yield of toluene-insoluble (TI) material was determined as follows:

$$TI \text{ yield} = \frac{m_p w_{s,p} w_{i,p} - m_f w_{s,f} w_{i,f}}{m_f w_{s,f} w_{i,f}} \quad (4-1)$$

where m_p and m_f are the masses of product and feed, $w_{s,p}$ and $w_{s,f}$ are the mass fractions of solids in the product and feed oils, and $w_{i,p}$ and $w_{i,f}$ are the mass fractions of the tie element in the solids filtered from the product and the feed. Carbon was used as a tie component in determining the yield of TI in experiments with kaolin, while sulfur was used to determine TI yields in experiments with carbon black. In both cases, TI yield was calculated on a mineral-free basis.

Elemental analysis was performed by the University of Alberta Microanalytical Laboratory. Analysis was performed on an elemental analyzer (Carlo Erba Stumentazione Elemental Analyzer 1108) by combustion of the sample, followed by gas chromatographic separation of the combustion products and analysis by thermal conductivity detection. The method has limitations in use due to the operating temperature of ca. 1,100 °C, which may not be high enough for such inorganic compounds as metal oxides to decompose.

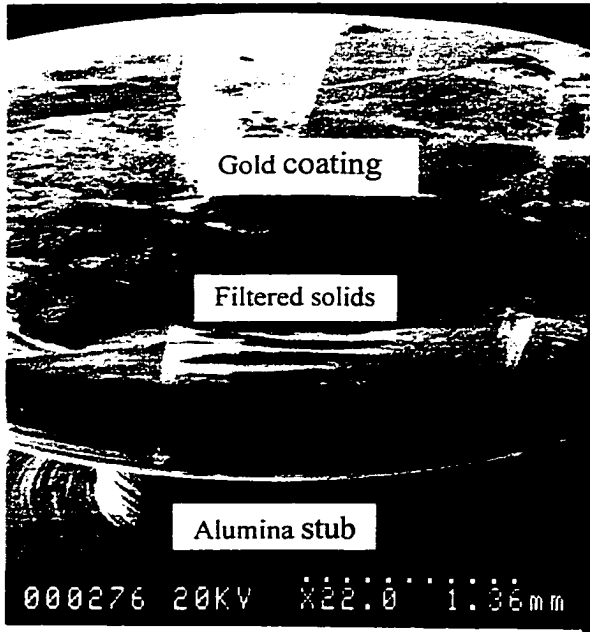
Specimens for scanning electron microscopy (SEM) and energy dispersive x-ray (EDX) analysis were prepared by filtering five or six drops of the well-mixed liquid products through 0.2 µm polycarbonate filter, and then washing with xylene and then isopropanol. The filter cakes were dried in the air, stuck to the aluminum stub, and sputter coated with gold under vacuum (*Figure 4-2(a)*). SEM and EDX analyses were done at Syncrude Research Center (Edmonton, AB) using a Hitachi S-2500 SEM with a Princeton Gamma-Tech EDX.

4.3 Results

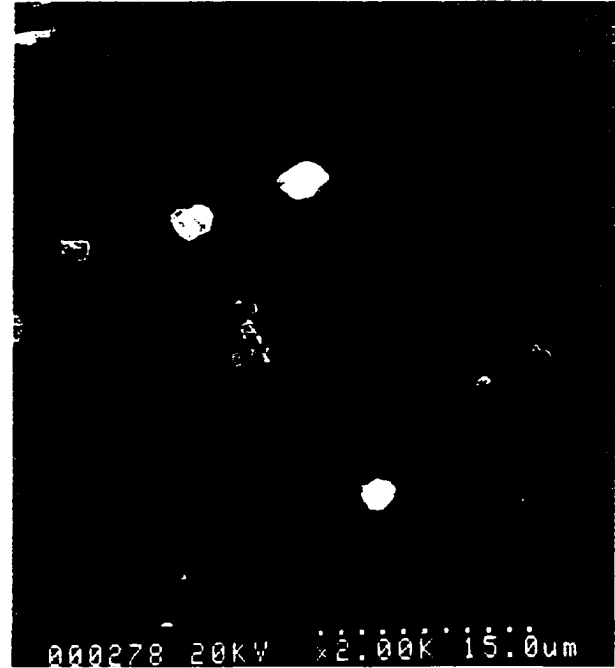
4.3.1 Formation of a TI Emulsion from Coker Gas Oil

A small portion of coker gas oil had a boiling point exceeding the upper boiling point limit of distillate, which is 525 °C (*Figure 4-1*). This is in agreement with the small asphaltene concentration in coker gas oil (*Table 4-1*), because asphaltene was not distillable. The clean micrograph of a blank filter paper (*Figure 4-2(b)*) suggested little interference from the SEM sample preparation process. Coker gas oil contained a small amount of very fine particles (*Figure 4-2(c)*), mostly less than 1 µm, in conformity with the concentration of filterable solid in gas oil (*Table 4-1*). Thermal treatment of the gas

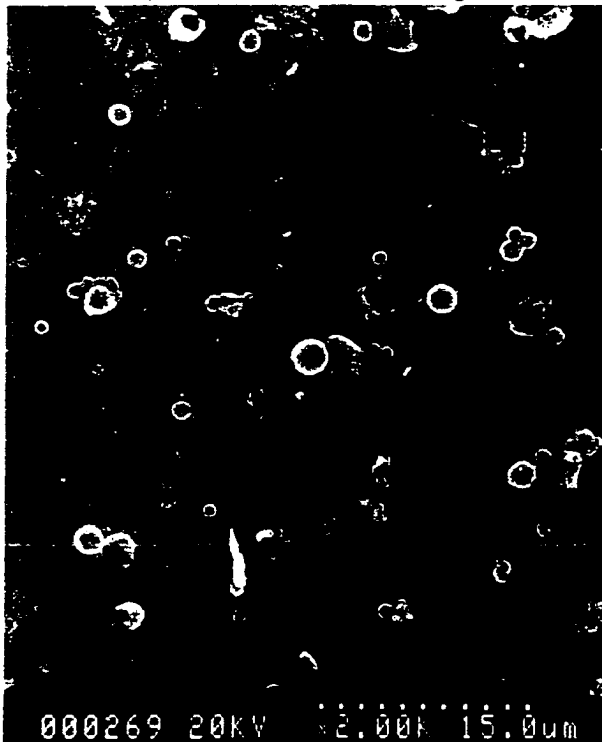
Figure 4-2. Micrographs of filtered solids SEM sample setup, blank filter paper and coker gas oil feed. The scale at the bottom of each micrograph indicates a length of 1.36 mm, 15 μ m, and 15 μ m, respectively.



(a) Filter cake SEM sample



(b) Blank filter



(c) Coker gas oil feed

oil at 300 °C gave filtered solids that were identical to those present in the feed oil; a low concentration of irregular particles. When the gas oil was reacted at 375 °C and higher temperatures, spherical particles of TI were observed, as illustrated in *Figure 4-3(a)*. The spheres had a mean diameter of 2.5 μm (*Table 4-3*). The yield of TI increased with temperature, but the appearance and size of the particles were unaffected. Most of the spheres were separate from each other, but some spheres were fused together (*Figure 4-3(b)*), giving evidence for coalescence and liquid behavior at reaction conditions. When the agitation in the reactor was reduced from 560 RPM to 100 RPM, the size of the spheres was unchanged (*Figure 4-4(a)* and *(b)*). With the same impeller stirring speed, the increase of reaction time from 60 min to 2 h did not bring a significant increase in the size of TI spheres (*Figure 4-4(b)* and *(c)*). Consequently, mechanical stirring beyond 100 rpm was not a factor in maintaining the dispersion of small-diameter spheres, and a 60-min reaction time was sufficiently long for TI spheres to grow to the maximum size. No experiments were conducted at lower stirring speed, say, 0 rpm. Energy dispersive x-ray analysis showed that the spheres contained carbon and sulfur, consistent with a carbonaceous material that originated from the gas oil in the reactor (*Figure 4-5*). Chlorine was present in the gas oil due to entrainment of chloride salts from the upstream extraction of bitumen from the oil sands ore. The presence of iron can be attributed to corrosion products in the gas oil. The EDX data suggest that both of these inorganic materials, present in the gas oil as fine particles, were incorporated into the TI phase. Smooth and rough spheres coexisted in the products, but there was no difference in their composition.

Figure 4-3. SEM micrographs of the filtered TI solids from thermally treated coker gas oil without solids added (375 °C, 1 h reaction time). (a) Solid particles showing spheres with both rough and smooth surfaces. The scale at the bottom indicates a length of 10 μm ; (b) Coalescing spheres. The scale at the bottom indicates a length of 1 μm .

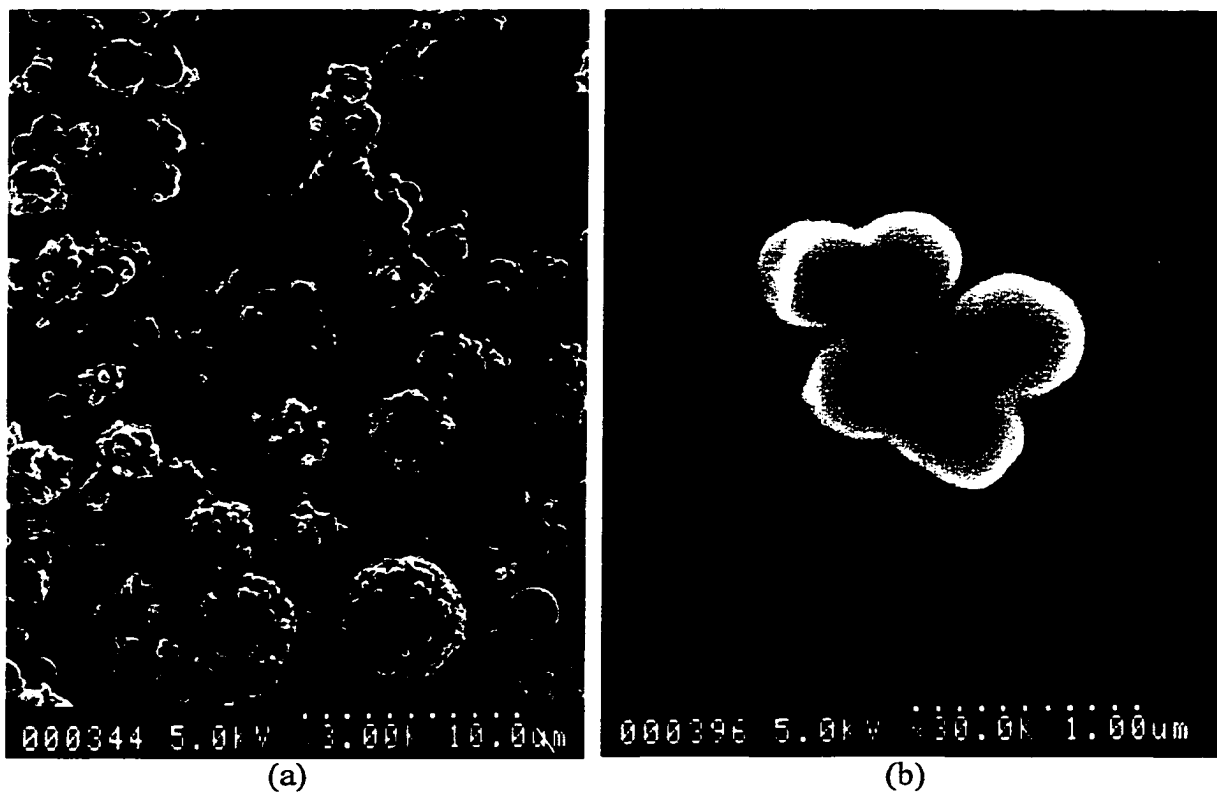
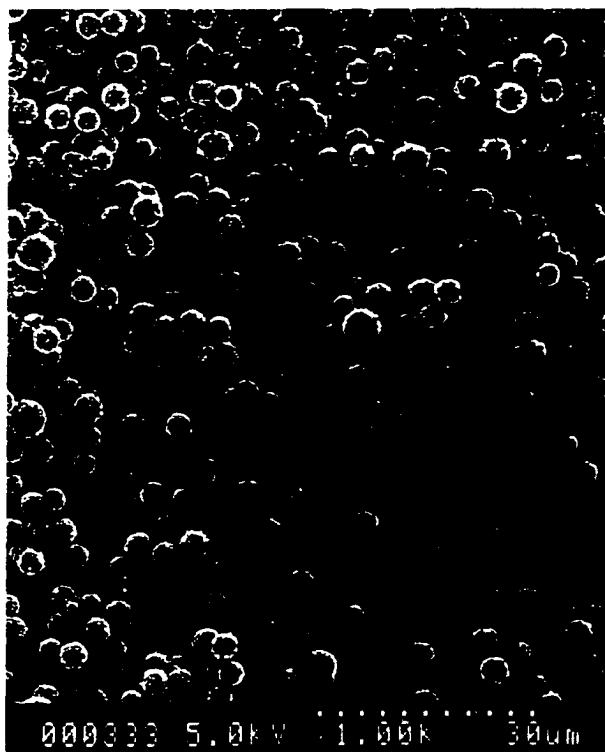
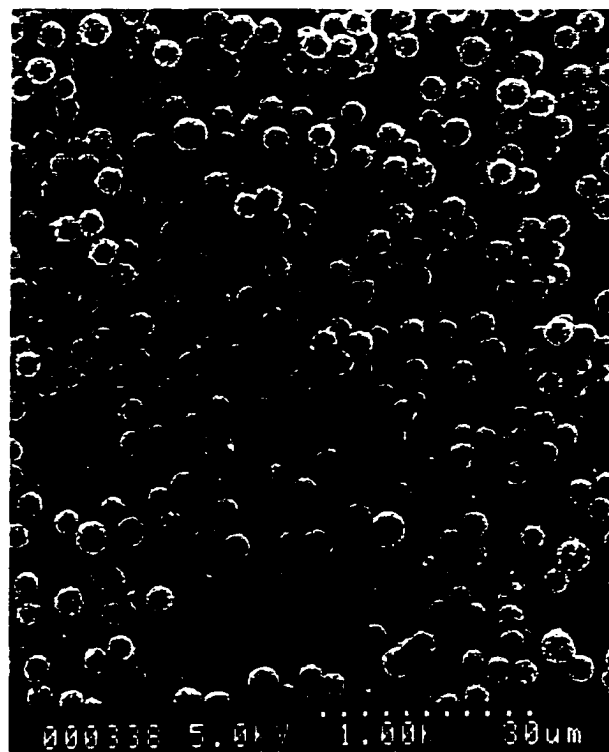


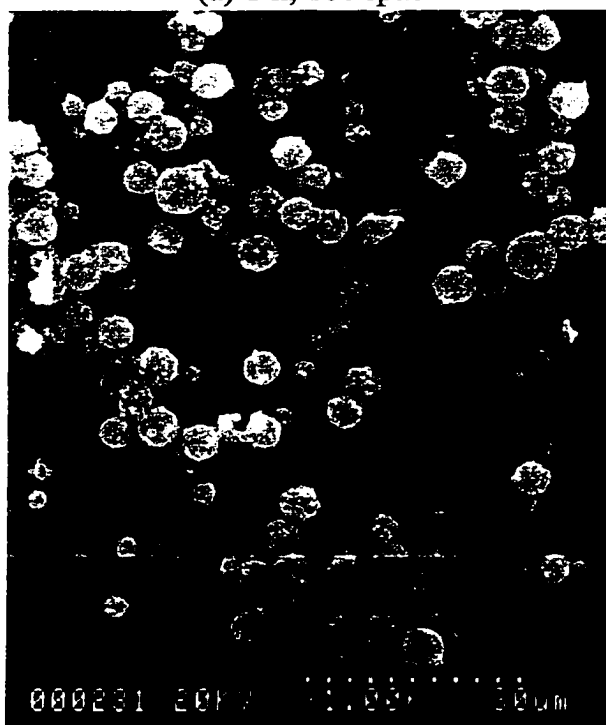
Figure 4-4. Effects of impeller speed and reaction time on the growth of TI spheres when coker gas oil was heated at 375 °C under H₂ atmosphere



(a) 1 h, 100 rpm

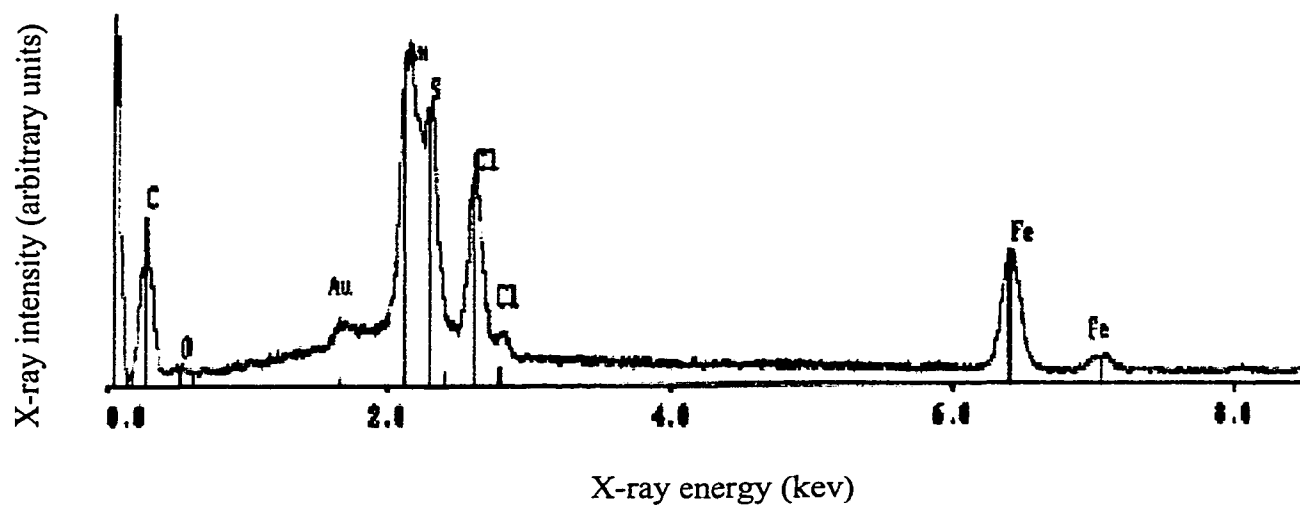


(b) 1 h, 600 rpm



(c) 2 h, 600 rpm

Figure 4-5. EDX spectrum from the spherical particles of TI in products from runs without solids added (375 °C, 1 h reaction time).



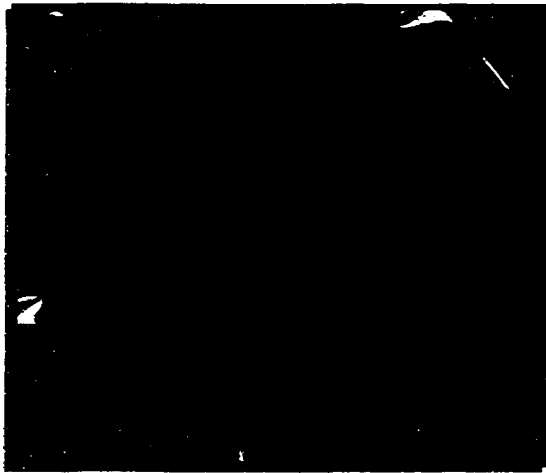
4.3.2 Photographs of Filter Cakes

The color of the filtered solids changed from brown to black upon the increase of reaction temperature from 25 to 420 °C when the kaolin concentration in the feed was 4 g/kg (*Figure 4-6*). A reaction temperature of 300 °C gave almost the identical color of the filtered solids with the solids in the feed oil. Apparently, the increase in the darkness of the filter cake was due to coke formation at elevated temperatures. This observation was in agreement with the fact that the carbon content of the corresponding filter cakes increased from 2.2% in the feed to 3.5% at 375 °C, and then to 17.7% at 420 °C. It was also consistent with the SEM micrographs (*Figure 4-7*). No spherical toluene-insolubles appeared until the reaction temperature was 375 °C or above. Only kaolin granules were observed in filtered solids under SEM when the reaction was at 300 °C and below.

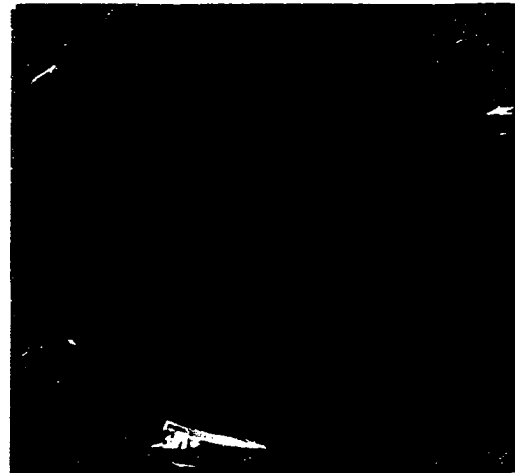
4.3.3 Interactions of TI with Added Solids

The addition of 5 µm kaolin particles had no effect on the appearance of TI spheres at reaction temperatures of 375 °C and above (*Figure 4-8(a)*). The addition of the kaolin did give a small reduction in the mean size of the spheres (*Table 4-3*). The TI did not cause agglomeration and adhesion of the clay particles, nor did the TI appear to wet the clay surface. EDX analysis of the TI spheres and the clay platelets showed a distinctly different composition, as illustrated in *Figure 4-9*. The TI particles showed strong signals of carbon and sulfur, as well as some aluminum and silicon (*Figure 4-9 (a)*). The clay particles showed strong signals from aluminum and silicon as expected (*Table 4-2*), but little evidence for deposition of carbonaceous material due to the absence of a signal from sulfur. These data confirmed that the spheres were carbonaceous particles with some clay

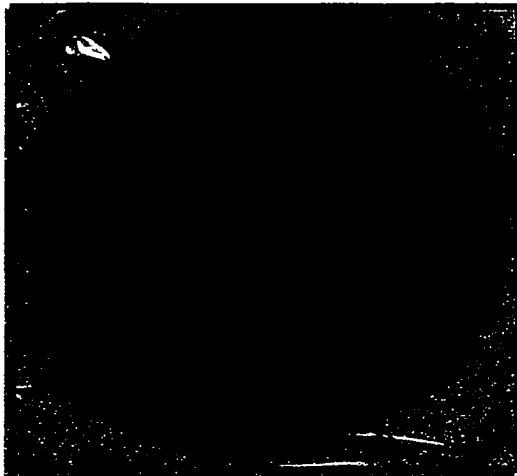
Figure 4-6. Variation of filter cake color with reaction temperature when 4 g untreated kaolin/kg was present in the coker gas oil feed



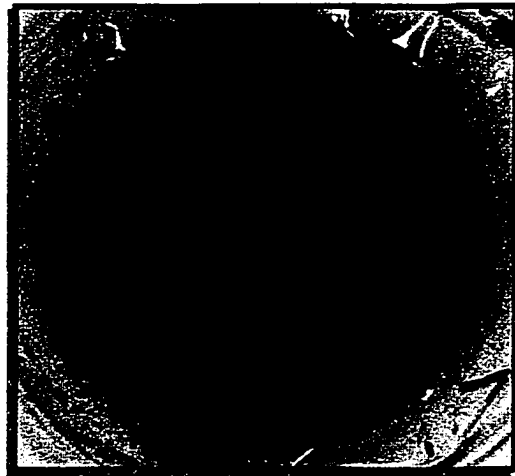
(a) 25 °C



(b) 300 °C



(c) 375 °C



(d) 420 °C

Figure 4-7. Development of TI spheres in the liquid product as a function of reaction temperature when 4 g untreated kaolin/kg was present in the coker gas oil feed.

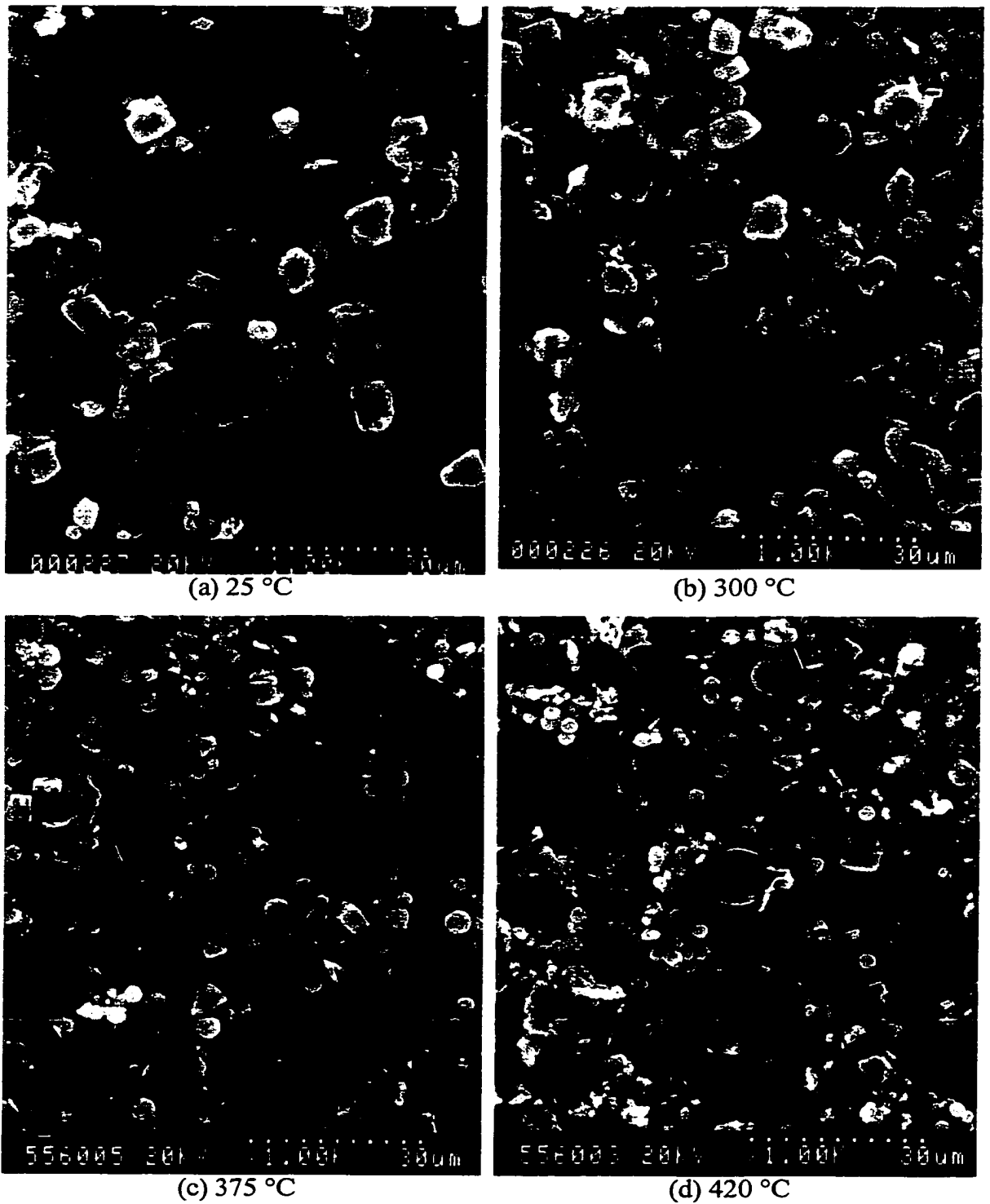


Figure 4-8. SEM micrographs of solids from liquid products from experiments with different solids added. All were reacted at 375 °C for 1 hr.: (a) 5 μm kaolin; (b) 0.2 μm kaolin; (c) 0.2 μm carbon black; (d) 5 μm asphaltene-coated kaolin.

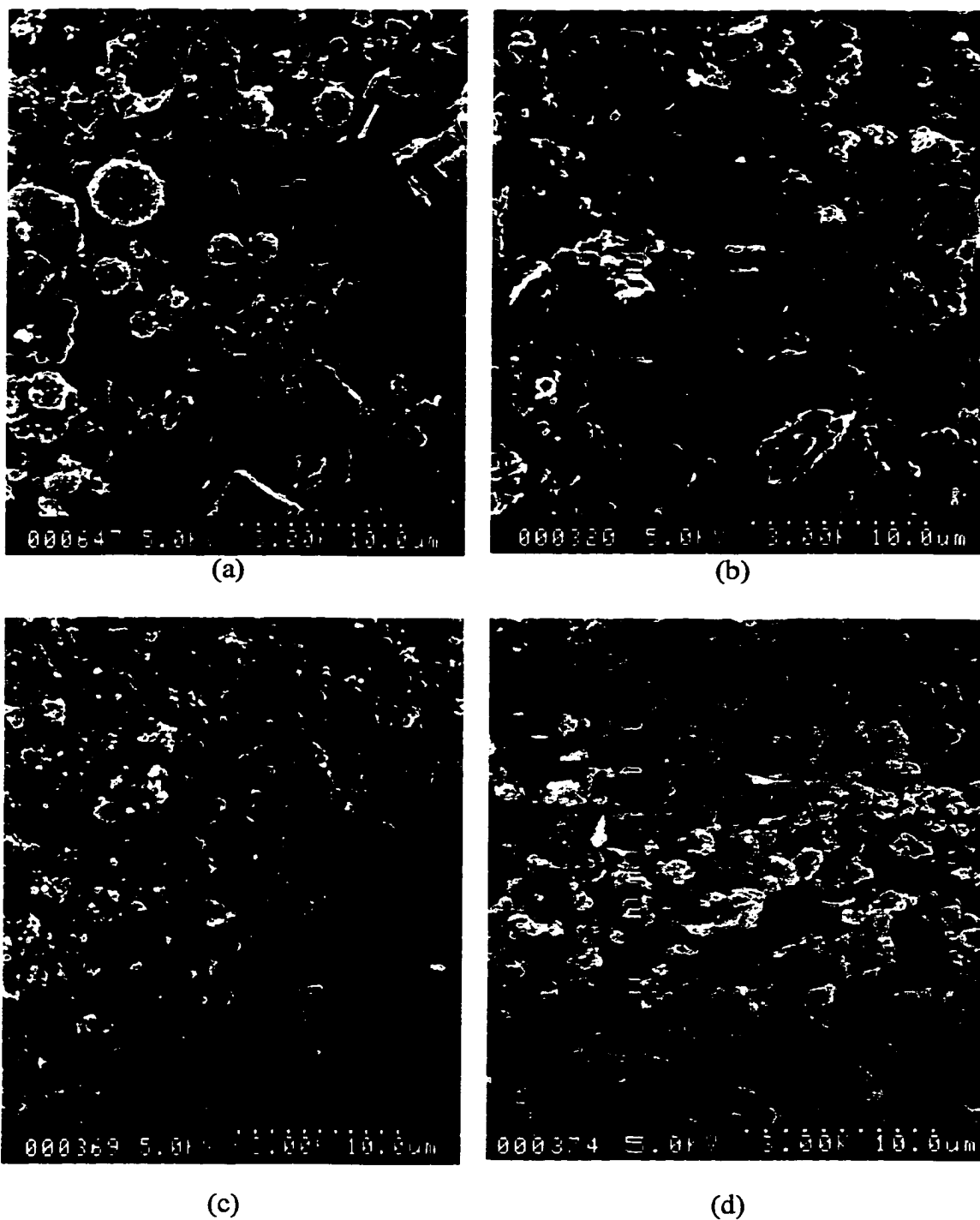
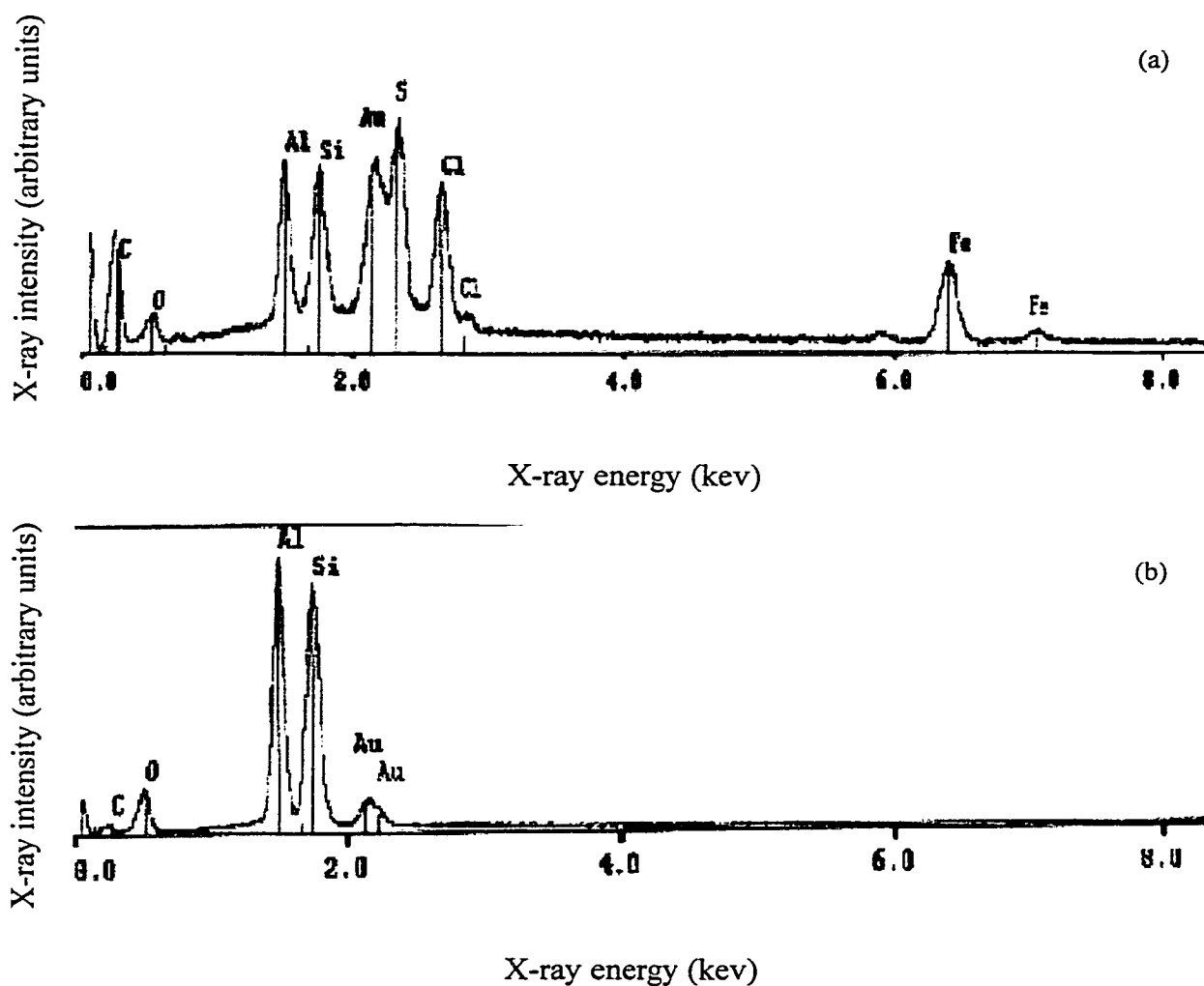


Table 4-3. TI fraction formed from thermal reactions of gas oil (Reaction at 375 °C for 1 h; Solid concentration of 4 g/kg)

Solids added	Yield of carbon in TI (g/kg feed)	Yield of sulfur in TI (g/kg feed)	Mean diameter of TI spheres (μm)*
No solids added	0.181	0.031	2.5 ± 0.2
5 μm kaolin	0.170	0.063	1.9 ± 0.2
0.2 μm kaolin	0.167	0.047	not observed
0.2 μm carbon black	not applicable	0.028	not observed

* - Error bounds give the 95% confidence interval based on a count of at least 100 particles

Figure 4-9. EDX spectra for spherical and granular particles in liquid products from runs with 5 μm kaolin added to coker gas oil, reacted for 375 $^{\circ}\text{C}$, 1 h: (a) spherical particles; (b) granular particles



trapped inside or adsorbed on the surface, while the kaolin clay was unchanged from its original appearance and composition.

When fine clay particles (0.2 μm kaolin) were added to the gas oil at the same reactor conditions, no spheres were observed in the product solids (*Figure 4-8(b)*). This result suggests that with a sufficient surface area, the formation of TI spheres can be suppressed. Addition of particles of 0.2 μm carbon black, which had non-polar groups on the surface, gave agglomerates of carbon black and TI in the product, with adhered spheres of TI (*Figure 4-8(c)*). Separate TI spheres were not observed, unlike the samples without added kaolin or with 5 μm kaolin.

The experiment with 0.2 μm carbon black had two significant differences from the experiments with 5 μm kaolin: a change in surface chemistry and a significant increase in surface area. In order to distinguish the two factors, gas oil was mixed with asphaltene-coated 5 μm kaolin then reacted at 375 °C. The filtered solids contained no TI spheres (*Figure 4-8(d)*).

4.3.4 Effect of Addition of Solids on TI Yield

Carbon and sulfur concentrations in the filtered solids were used to determine yield of TI from experiments with added solids, because direct gravimetric determinations were unreliable. The data are listed in *Table 4-3*. The data for yield on a carbon basis showed that the addition of either 5 μm or 0.2 μm kaolin had no effect on the overall yield of toluene insoluble carbonaceous solids. The yields of TI on a sulfur basis were less reliable, due to the low concentration of sulfur in the filtered solids from the experiments with added clay. Within the uncertainty of the analysis, these data show that the addition of 0.2 μm carbon black had no significant effect on overall yield of TI

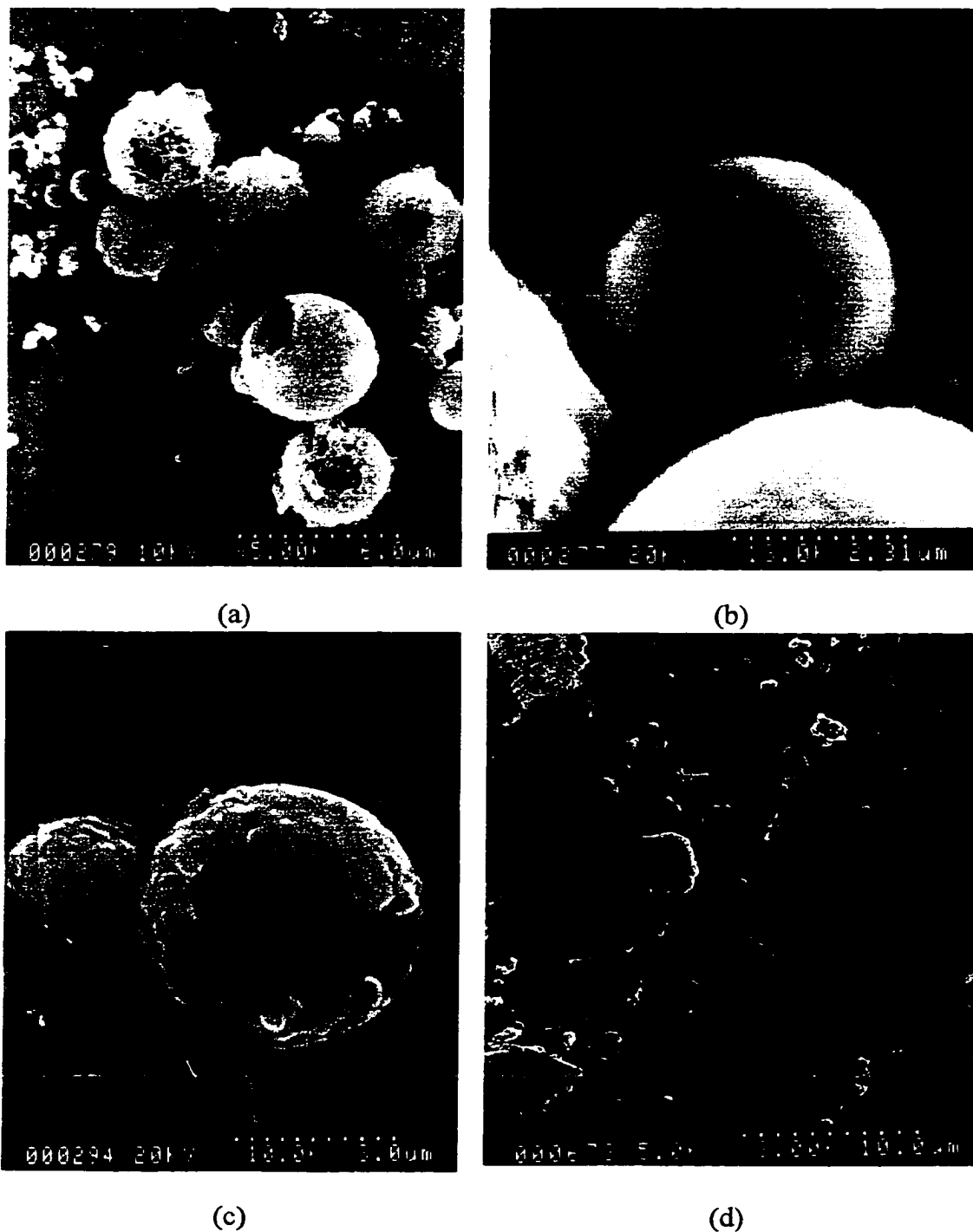
solids. The total yield of TI from the experiment with asphaltene-coated kaolin could not be determined because the asphaltenes interfered with both the carbon and the sulfur determinations, giving a significant background concentration in the feed solids. Overall, the data for carbon and sulfur yields in the filtered solids led to the conclusion that the addition of fine solids affected the distribution and morphology of TI, but not its total yield.

4.3.5 TI Spheres versus Mesophase

Mesophase forms as spheres in a liquid medium of pitch, which can then grow and coalesce depending on the reaction conditions and composition of the oil (Brooks and Taylor, 1968; Mochida et al., 1988; Dubois et al., 1970; Bradford et al., 1971). While both the pitch and the mesophase are insoluble in toluene, the mesophase is distinguished by its insolubility in strong solvents such as quinoline (Brooks and Taylor, 1968; Mochida et al., 1988). Previous work has shown that a significant portion of the benzene-insoluble solids from thermal hydrocracking of Athabasca bitumen is soluble in quinoline (Nandi et al., 1978).

In order to determine the solubility of the TI spheres, solids were collected from liquid product from the most severe reaction conditions (temperature of 420 °C, 2 h reaction time, 560 rpm agitation, and 5 µm clay at a concentration of 4 g/kg). When the filtered solids were only washed with excess toluene, some TI spheres were etched (*Figure 4-10(a)*). Some hollow TI spheres were also observed in the same sample (*Figure 4-10 (b) and (c)*). One possible explanation is that gas molecules were trapped inside the TI matter at reaction temperature due to the multiphase flow in the reactor. Some of these molecules may not escape, because the TI layer became very viscous

Figure 4-10. Effect of solvent etching on morphology of TI microspheres. Microspheres in sample (a), (b) and (c) were produced from coker gas oil after 2 h reaction at 420 °C and under H₂ atmosphere. Sample (d) was quinoline extracted.



when it cooled down. Part of the TI shell was etched due to the repeated washing of the filtered solids with quinoline. Quinoline is a stronger solvent than toluene for carbonaceous material. A portion of the filtered solids was sonicated in quinoline for 6 h. The solids with and without quinoline treatment were examined by SEM. No spheres were observed in the quinoline-extracted sample (*Figure 4-10(d)*), although large numbers were observed in the untreated sample (*Figure 4-8(a)*). The complete solubility of the TI spheres in quinoline showed that they did not consist of mesophase coke.

4.4 Discussion

The observations of TI spheres suggest that this material was liquid or plastic at reactor conditions. To minimize the surface energy, a liquid TI phase dispersed in a continuous oil phase would be expected to exist as an emulsion of spheres, analogous to spheres of mesophase in pitch at similar temperatures (Brooks and Taylor, 1968) and analogous to oil in water at room temperature. The combination of agitation during the cooling period and a low solids concentration would allow the TI phase to retain its spherical shape and remain dispersed as it cooled and solidified. Observation of spheres in the process of coalescing (*Figure 4-3 (b)*) is another argument for fluid behavior at reactor conditions. The TI spheres were not mesophase, because they were soluble in quinoline, but the literature on mesophase formation and behavior can be taken as another argument for the existence of liquid toluene-insoluble phases at reactor temperatures.

The physical interactions observed between TI and fine solids provided additional evidence for liquid behavior at reactor conditions. When 5 μm kaolin was added, TI spheres were still observed, therefore, the TI phase did not wet the clay surface. When

the kaolin was treated with asphaltenes to give non-polar groups on the surfaces of the particles, the formation of TI spheres was completely suppressed, consistent with complete wetting of the clay surface. The behavior of the carbon black was also consistent with wetting of the carbon surface by TI material, leading to adhesion and agglomeration of the coated carbon particles.

Although the untreated kaolin had polar surface functional groups, the data provide evidence for some physical interactions with the TI phase. Addition of 5 μm kaolin gave some incorporation of clay into the spheres, based on the EDX analysis (*Figure 4-9(a)*), and a reduction in the size of the spheres (*Table 4-3*). The clay surfaces could adsorb the TI precursors from the oil, preventing the formation of a separate phase, or nucleate the formation of droplets in the oil. The latter process would account for the changes in EDX composition and size of spheres. Addition of 0.2 μm kaolin completely suppressed the formation of TI spheres, likely because the 10-fold increase in the surface area of the clay was sufficient to adsorb all of the TI fraction. Tanabe and Gray (1997) have suggested that fine particles may prevent coalescence of coke droplets, as observed in mesophase formation (Dubois et al., 1970; Bradford et al., 1971). In the present study, however, the solid particles were too large relative to the TI spheres to give such stabilization. The small size of the TI spheres, with a mean diameter of 2 μm , suggests that the combination of agitation and low interfacial tension between the TI phase and the gas oil allowed the formation of a micro-emulsion.

Only the carbon black particles showed agglomeration with the TI phase under the reaction conditions. Although both the 0.2 μm kaolin and the 0.2 μm carbon black prevented the formation of TI spheres, the kaolin did not exhibit agglomeration.

Similarly, the asphaltene-coated 5 μm kaolin did not exhibit agglomeration, although it also suppressed the formation of TI spheres. Further study is required, therefore, to determine why a layer of surface TI promoted the agglomeration of carbon black and not the two types of kaolin.

The observed behavior of the TI spheres was consistent with the formation of a liquid microemulsion at reactor conditions, in agreement with proposals that liquid-liquid phase separation may be an important step in eventual coke formation (Wiehe, 1993; Shaw et al., 1988; Mochida et al., 1988). An alternate mechanism would be successive adsorption of toluene-insoluble components onto a growing sphere, similar to dispersion polymerization of monomers such as styrene in non-aqueous solvents (Akmed and Poehlein, 1997). If dispersion polymerization were carried out above the melting point of the polymer, then liquid droplets of polymer would form and grow in emulsion in the non-aqueous solvent. Either mechanism would give a liquid emulsion at 375 $^{\circ}\text{C}$, which would then set upon cooling to give solid particles. The present study cannot distinguish whether reactions of the TI precursors were a prerequisite to forming an emulsion phase.

4.5 Conclusions

An emulsion of a TI fraction was formed from coker gas oil during thermal reactions under a hydrogen atmosphere at 375 - 420 $^{\circ}\text{C}$. The TI fraction existed as spheres with a mean size of 2 - 2.5 μm , and was completely quinoline-soluble. The physical interaction between the TI and the fine solids depended on the surface chemistry of the solids. The formation of TI spheres was suppressed by presence of either non-polar

particle surfaces or a very large particle surface area. In either case, the distribution of the TI fraction was altered but not its total yield.

References

- Ahmed, S. F.; Poehlein, G. W. Kinetics of Dispersion Polymerization of Styrene in Ethanol. 2. Model Validation. *Ind. Eng. Chem. Res.* **1997**, *36*, 2605-15.
- Belinko, K.; Nandi, B. N.; Denis, J. M. In 'The Oil Sands of Canada-Venezuela 1977' (D. A. Redford and A. G. Winestock (Eds)) CIM Special Vol. 17, CIM, Calgary, **1977**, pp. 189-194.
- Bradford, D. J.; Greenhalgh, E.; Kingshott, R.; Senior, A.; Bailey, P.A. Interaction of Carbon Black with Coal Tar Pitch. *Proc. 3rd Conf. Ind. Carbons and Graphite*, S.C.I., London, **1971**, pp. 520-527.
- Brooks, J. D.; Taylor, G. H. In "Chemistry and Physics of Carbon" (P. L. Walker, Jr., Ed.), Marcel-Dekker, New York, **1968**, *4*, 243.
- Chung, K. H.; Xu, C.; Hu, Y.; Wang, R. Supercritical Fluid Extraction Reveals Resid Properties. *Oil Gas J.* **1997**, *95*(3), 66-69.
- Crittenden, B. D.; Kolaczowski, S. T.; Downey, I. L. Fouling of Crude Oil Preheat Exchangers. *Chem. Eng. Res. Des.* **1992**, *70*(A6), 547-557.
- Dubois, J.; Ahache, C.; White, J. L. The Carbonaceous Mesophase Formed in the Pyrolysis of Graphitizable Organic Materials. *Metallography* **1970**, *3*, 337-369.
- Garett-Price, B.A.; Smith, S.A.; Watts, R.L.; Knudsen, J.G.; Marner, W.J.; Sutor, J.W. *Fouling of Heat Exchangers*, Noyes Publications, Park Ridge, New Jersey, USA, **1985**.
- Gray, M. R. "Upgrading Petroleum Residues and Heavy Oils" Marcel Dekker, New York, **1994**.
- Koyama, H.; Nagai, E.; Torii, H.; Kumagai, H. Simple Changes Reduce Catalyst Deactivation, Pressure-Drop Buildup. *Oil Gas J.* **1995**, *93*(47), 68-71.
- Kriz, J. F. Coking Threshold in Hydroprocessing of Asphaltenic Oils. *Can. J. Chem. Eng.* **1994**, *72*, 85-90.
- Magaril, R. Z.; Aksenova, E. I. Study of the Mechanism of Coke Formation in the Cracking of Petroleum Resins. *Inter. Chem. Eng.* **1968**, *8*(4), 727-729.
- Mannistu, K. D.; Yarranton, H. W.; Masliyah, J. H. Solubility Modeling of Asphaltenes in Organic Solvents. *Energy Fuels* **1997**, *11*, 615-622.

Mochida, I.; Oyama, T.; Korai, Y.; Fei, Y. Q. Study of Carbonization Using a Tube Bomb: Evaluation of Lump Needle Coke, Carbonization Mechanism and Optimization. *Fuel* **1988**, *67*, 1171-1181.

Nandi, B. N.; Belinko, K.; Ciavaglia, L. A.; Pruden, B. B. Formation of Coke during Thermal Hydrocracking of Athabasca Bitumen. *Fuel*, **1978**, *57*, 265-268.

Narayan, R. 'Particle Capture from Non-Aqueous Media on Packed Beds'. MSc. Dissertation, University of Alberta, **1996**.

Shaw, J. M.; Gaikwad, R. P.; Stowe, D. A. Phase Splitting of Pyrene-tetralin Mixtures under Coal Liquefaction Conditions *Fuel* **1988**, *67*, 1554-1559.

Storm, D. A.; Barresi, R. J.; Sheu, E. Y. Rheological Study of Ratawi Vacuum Residue in the 298-673 K Temperature Range. *Energy Fuels* **1995**, *9*, 168-176.

Tanabe, K.; Gray, M. R. The Role of Fine Solids in the Coking of Vacuum Residues. *Energy Fuels* **1997**, *11*, 1040-1043.

Watkinson, A. P.; Wilson, D. I. Chemical Reaction Fouling: A Review. *Exp. Thermal Fluid Sci.* **1997**, *14*, 361-374.

Wiehe, I. A. A Phase-Separation Kinetics Model for Coke Formation. *Ind. Eng. Chem. Res.* **1993**, *32*, 2447-2454.

Yan, N.; Masliyah, J. H. Effect of pH on Adsorption and Desorption of Clay Particles at Oil-Water Interface. *J. Colloid Interface Sci.* **1996**, *181*, 20-27.

Chapter 5: Filtration of Fine Clays by Packed Beds at Hydrotreating Conditions: Role of Surface Treatment with Asphaltenes*

5.1 Introduction

The surface chemistry of suspended particles and the collector plays an important role in particle deposition onto collector surfaces. For example, Amirbahman and Olson (1993) attributed the low deposition rates of particles treated with humic materials in packed beds in aqueous systems to the steric interaction forces between the coatings on the particles. Humic materials had the similar composition as those of asphaltenes and other organic matter fractions from different oil sands sources (Kotlyar et al., 1998).

When fine particles of minerals, or metal sulfides from corrosion products are present, interactions of inorganic surfaces with asphaltenes, humic matter, or polar compounds will alter the surface properties such as contact angle (Yan and Masliyah, 1996).

Asphaltenes adsorb onto minerals primarily by interactions between their polar functional groups and the polar groups present on the mineral surface. Fendel and Schwochau (1988) found that extraction of clays from Athabasca oil sands with methylene chloride gave ca. 3 wt % of organic carbon still sorbed on the clays, particularly components containing oxygen groups. Marlow et al. (1987) found that adsorbed asphaltenes enhanced the colloidal stability of illite clay suspended in toluene due to a combination of

* A version of this chapter appears as Wang, S.; Chung, K. H.; Masliyah, J. H.; Gray, M. R. *Ind. Eng. Chem. Res.*, in press, 1999.

electrostatic and steric repulsive forces. Briggs et al. (1980) observed that the mean size of the suspended mineral particles from coal liquefaction was significantly decreased by the presence of asphaltenes. They suggested that the asphaltenes stabilized the fine particles, reducing flocculation and aggregates. Rodgers (1980) suggested that the asphaltenes adsorbed on the particle surfaces may equalize the surface charges on each particle, resulting in stronger electrostatic repulsive forces and a more stable suspension of mineral particles in organic media. These studies show that suspensions of minerals, such as clay in non-aqueous solvents, can be stabilized by polar compounds, but these interactions have not been studied at conditions typical of hydrotreating reactors.

Chung et al. (1998) showed that the mineral particles in Athabasca bitumen were coated with humic matter, which had similar surface chemistry to asphaltene solids. During distillation these particles are entrained into distillate products at low concentration, along with high-boiling point components such as asphaltenes. Consequently, asphaltenes can serve as a model material for polar, high molecular weight components that will tend to adsorb to mineral surfaces and stabilize them in non-aqueous suspensions.

Filtration of fine particles in hydrotreaters may involve both hydrodynamic and chemical processes. Several flow regimes are observed in packed-bed reactor operation (Ng and Chu, 1987), due to the complex hydrodynamic interactions between the flowing gas and liquid and the packed bed. The flow pattern adjacent to the collector surfaces will play a key role in particle transport and deposition, but the gas-liquid flows in hydrotreaters give time-varying flow at any given point on the surface of a catalyst pellet.

At the same time, the chemistry of the liquid phase and possibly the entrained particles can be altered by the hydrogenation reactions promoted by the catalyst.

In order to understand the role of the surface chemistry of fine particles on deposition and plugging in packed-bed hydrotreaters, a simplified experimental system was required. A model suspension of kaolin in a hydrotreated light gas oil was selected, and the surface properties of the kaolin were modified by pretreatment with asphaltenes. Rather than trying to reproduce both the chemistry and the physics of the commercial reactor, a batch reactor with internal circulation of liquid and gas was selected. The flow regime in this test reactor was different from the trickle-bed operation, but it allowed a systematic variation of the chemistry of the system at temperatures and pressures that are typical of hydrotreating. In this study the total reaction pressure was ca. 11 MPa at a reaction temperature of 375 °C. Experiments were conducted with either glass beads or catalyst pellets as the bed packing, to serve as the collectors for the kaolin particles. A hydrotreated light gas oil was used to minimize changes in fluid properties with time. The filtration of kaolin particles by the packed beds was determined as a function of time and reactor operation.

5.2 Materials and Methods

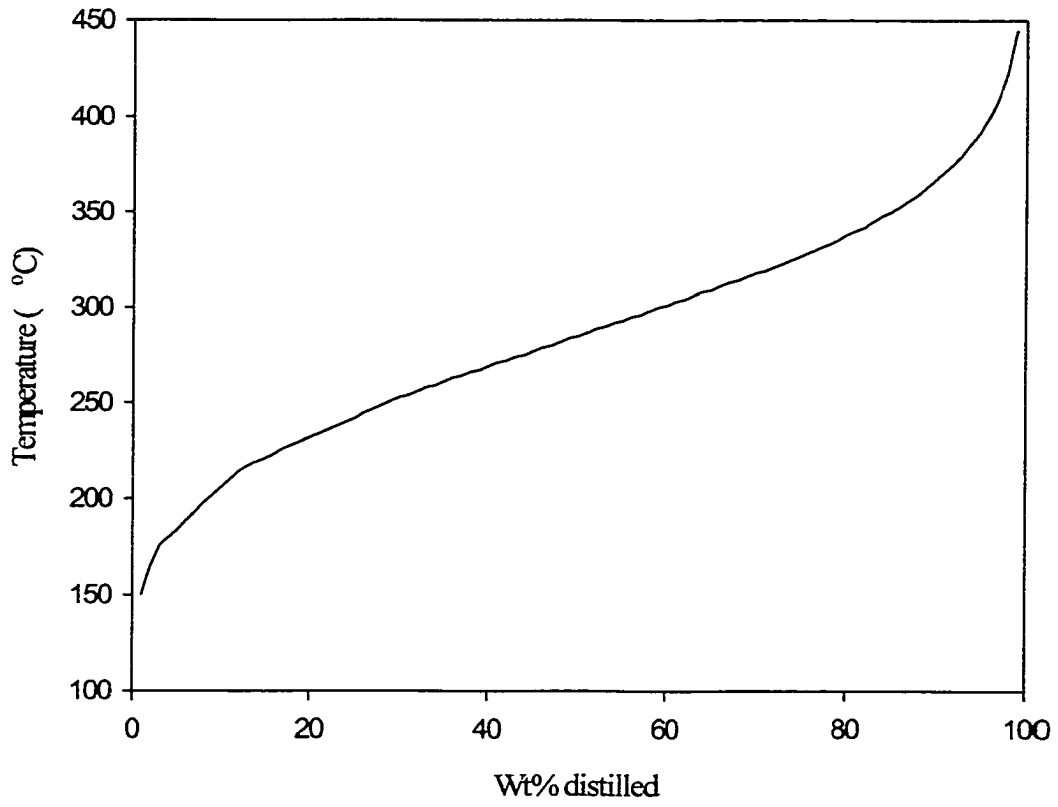
5.2.1 Feed and Packing Materials

The treated light gas oil (TLGO) was a hydrotreated product from Athabasca bitumen in the Syncrude plant at Fort McMurray, Alberta. The properties of TLGO are provided by Syncrude Research Center (Edmonton, Alberta) and tabulated in *Table 5-1*. Its boiling point distribution is drawn in *Figure 5-1*. Solids were removed from the TLGO by filtering it through a 0.22 µm Millipore membrane filter. Two sizes of kaolin were

Table 5-1. Composition and properties of Athabasca hydrocarbons

Elemental composition	Treated light gas oil	Solids-free asphaltenes
weight %		
C	86.0	80.4
H	12.9	8.4
wppm		
S	301	70,600
N	5.0	11,400
Asphaltene, weight %	0	100
Density, kg/m ³ at 15 °C	892	—
20 °C	875	—
Viscosity, mPa-s at 20 °C	6.5	—
Solids concentration, wppm	140	—

Figure 5-1. Boiling point distribution of treated light gas oil



used in this study: 0.68 and 5.0 μm (*Table 4-2*). All the reagents were from Fisher Scientific Co. (Toronto, Canada) unless otherwise stated.

The characteristics of three collector materials are tabulated in *Table 5-2*. The method for determining the porosity of a clean packed bed is presented in *Appendix 2*. Glass beads (Sigma-Aldrich Canada, Oakville, Ontario) were washed with chromic acid, rinsed with excess deionized water, and then dried in an oven at 110 °C for 24 h. Fresh and spent commercial hydrotreating catalysts were provided by Syncrude Canada Ltd. The spent catalyst was obtained from a gas oil hydrotreater after approximately 18 months of service, and was used in most experiments in order to minimize chemical alterations of the gas oil during the particle deposition experiments. The spent catalyst was Soxhlet extracted with methylene chloride for 24 h, dried in a vacuum oven at 70 °C for 24 h, and then sieved by a 355 μm mesh (#42). The residual carbon content of the extracted catalyst was 6.84%, due to the deposited carbonaceous matter. Kaolin, glass beads, and catalyst pellets were stored in a desiccator after preparation.

5.2.2 Authentic Solids Derived from Athabasca Oil Sands

Two kinds of authentic TI solids, endcut solids and vacuum residue solids, were prepared in this study. In order to find which fraction of Athabasca vacuum residue is most difficult for processing, the vacuum residue was further separated into nine fractions by supercritical fluid extraction (SCFE) method (Chung et al., 1997). The major finding from SCFE was that asphaltenes only stayed in one of these nine fractions (endcut #9). This asphaltene-rich fraction (asphaltenes, 88.0%) was diluted 40 to 1 by volume with toluene and mixed for 24 h by a magnetic stirrer. The mixture was then centrifuged at 3,100 rpm with an IEC Clinical Centrifuge (IM 174, International Equipment Company,

Table 5-2. Characteristics of collector materials

Glass beads	Density (kg/m ³)	2,487
	Bed porosity	0.37
	Specific physical surface area (mm ² /g)	1,276
	Diameter range (μm)	710 ~ 1,180
	Average diameter (μm)	945
Trilobe spent catalyst	Density (kg/m ³)	1,945
	Bed porosity	0.44
	Specific physical surface area (mm ² /g)	2,915
	Dimension (mm)	average radius: 0.39 average length: 3.6
Trilobe fresh catalyst	Density (kg/m ³)	1,312
	Bed porosity	0.42
	Specific physical surface area (mm ² /g)	3,979
	Dimension (mm)	average radius: 0.41 average length: 4.9

MA, USA) for 1 h to remove the so-called endcut solids. Toluene in the supernatant solution from the centrifuge tube was removed by a rotary evaporator (Buchi Labortechnik AG, Switzerland) under reduced pressure. The residual liquid was then dried in an oven under vacuum at 70 °C for 24 h to evaporate any volatiles. This solids-free asphaltene-rich fraction was Soxhlet extracted with n-pentane for 24 h to remove any residual entrapped pentane-solubles, dried in an oven under vacuum at 70 °C for 24 h, and then stored in a desiccator. The composition of the resulting solids-free asphaltenes is given in *Table 5-1*.

Vacuum residue solid was obtained in a similar way. Athabasca vacuum residue was dispersed in 40 times toluene, and the mixture was filtered through a 0.22- μm filter to separate solids from the remainder of the mixture in toluene.

5.2.3 Treatment of Kaolin with Asphaltenes

A known amount of solids-free asphaltenes (0.05 - 1 g) was mixed with kaolin (2.5 g) in a mixture of 250 mL toluene and 250 mL heptane, using the method in *Section 4.2*. The so-called solids-free asphaltene used here was extracted from the asphaltene-rich fraction of Athabasca bitumen (See also in *Section 5.2.2*). Another difference in preparation of treated kaolin is that the impeller speed of 400 rpm was used.

5.2.4 Analysis of Samples

Kaolin and catalyst pellets were dried in a vacuum oven at 70 °C for 24 h before elemental analysis, which was described in *Section 4.2*. The densities and viscosities of filtered TLGO and liquid products were determined in a 25 mL pycnometer and a Rheomat 115 viscometer (Contraves) at room temperature (ca. 22 °C), respectively.

5.2.5 Amount of Asphaltene Coating on Kaolin

The amount of asphaltene coating on the kaolin was determined indirectly from the carbon content. Assuming that both the adsorbed asphaltenes and asphaltenes in the 1:1 heptane/toluene mixture had the same carbon content, the mass of adsorbed asphaltenes (kg), M_{asp} , was calculated as follows:

$$M_{asp} = \frac{C_{ik} M_k}{C_{asp} - C_{ik}} \quad (5-1)$$

where M_k is the mass of kaolin (kg), C_{asp} is the carbon content of asphaltenes (%), and C_{ik} is the carbon content of asphaltene-treated kaolin (%). The asphaltene concentration remaining in the 500 mL 1:1 heptane/toluene mixture was calculated by subtracting the adsorbed amount M_{asp} from the total asphaltenes added initially. Similar calculations were carried out when the mass of asphaltene-treated kaolin was corrected on a hydrocarbon-free basis with more information given in *Appendix 3*.

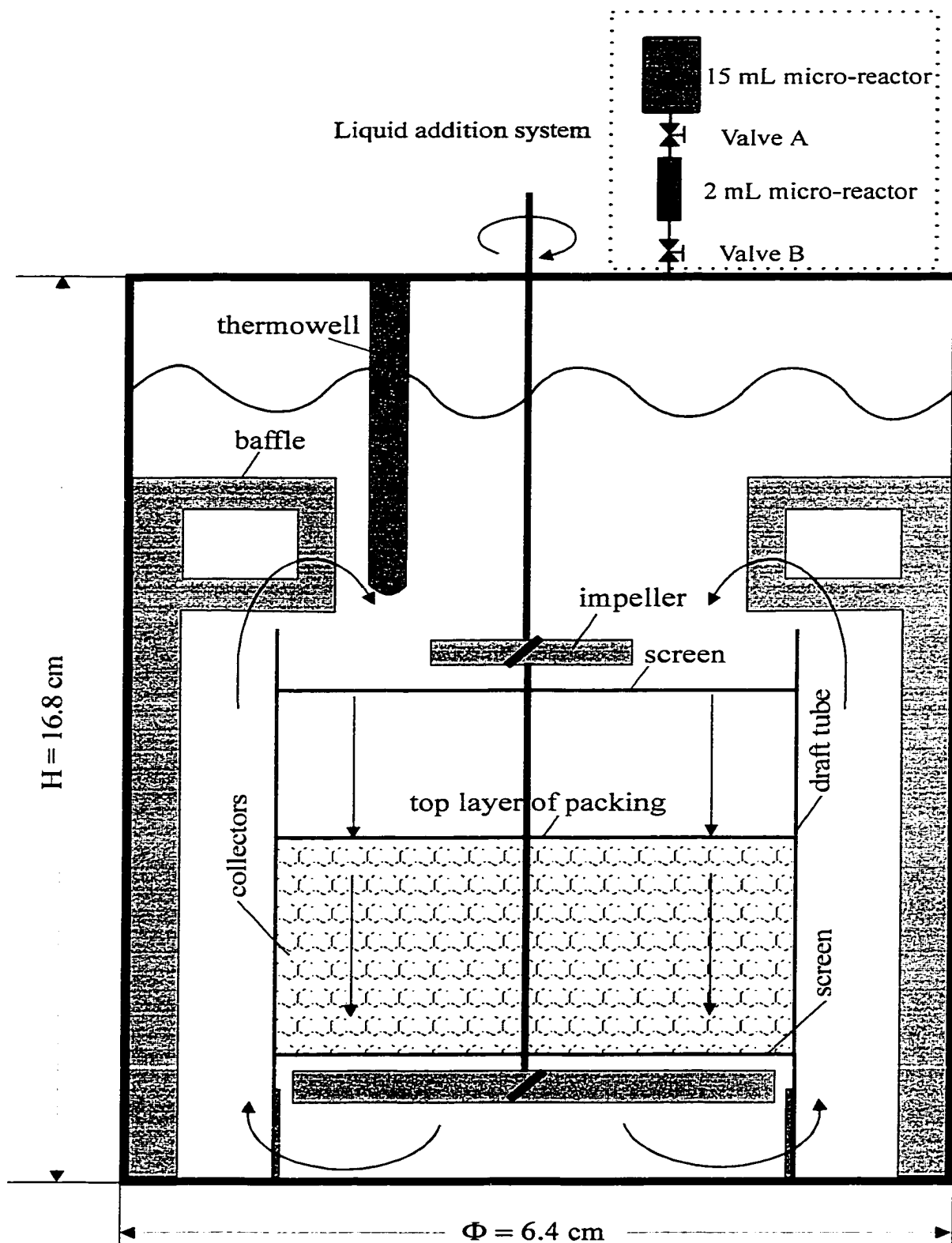
5.2.6 Reactor Apparatus

The hydrodynamics inside an agitated batch reactor are highly undefined. At present, a purely theoretical treatment of the flow within an agitated tank is impossible due to the randomness of turbulence, the three dimensionality of the flow, and the non-linearity of the governing equations of motion. Nagata et al. (1960) extensively investigated the flow conditions in an agitated tank with or without baffles for laminar, transitional and turbulent flow. At low Reynolds numbers the flow is laminar throughout the tank. Around the impeller the liquid velocity is high and decays rapidly away from the impeller blades. With increasing Reynolds number, the flow around the impeller becomes

turbulent while the flow in the bulk of the tank is still laminar. Further increases of Reynolds number result in the propagation of the turbulent state to the bulk away from the neighborhood of the impeller, and finally the flow in the whole tank becomes turbulent. A technique developed in late 1970s – laser doppler anemometry (LDA) – allows non-intrusive measurement of the flow, and records an almost instantaneous response to velocity fluctuations with unambiguous separation of the three directional components of velocity. Ranade et al. (1989) investigated the flow generated by the pitched blade turbine (PBT) extensively using LDA. They found that: (1) the PBT generated strongly accelerated downward flow through the impeller region when impeller diameters are less than the radius of the cylindrical tank; (2) the mean velocities and turbulence intensities were approximately proportional to the impeller speed within the range of Reynolds numbers studied (4×10^4 - 1.4×10^5). The presence of a draft tube has little mitigating effect on the tendency to swirl, and baffles in both the tank and the tube are needed to obtain maximum power consumption (Uhl and Gray, 1967). Draft tubes are usually used as a conduit to control and ensure vertical flow and distribution of solids. An impeller mounted inside the draft tube duplicates the action of the air lift, which provides vertical flow with return by gravity in the annulus between the draft tube and vessel well.

A 500 mL batch stirred reactor (Parr Instrument Company, Model 4575) was used for particle filtration experiments. The reactor, its internals and liquid addition system are illustrated in *Figure 5-2*. Detailed specifications of the reactor and its internals are described in *Appendix A1-1*. The tip of the thermowell was always immersed in the liquid phase during the reaction. The reactor temperature was manipulated by a

Figure 5-2. Schematic diagram of batch reactor, its internals and liquid addition system (All internals are shown to scale with respect to the dimensions of the batch reactor)



temperature controller with its thermocouple inserted inside the thermowell. There was a small tube passing through the draft tube as a passage for the impeller rod. Two pitched blade turbine impellers, each with four blades and a pitch angle of 45°, were employed to suspend kaolin in TLGO and circulate fluid through the packed bed in the draft tube. One impeller was placed above the bed with another one underneath the bed. The impellers were driven by a 2 kW variable speed motor with a speed range of 0 to 800 rpm. The four evenly spaced baffles reduced vortex or swirl in the reactor and provided better circulation through the draft tube. There were three supporting feet for the draft tube, and the middle of each foot was a small lip. The glass beads or spent catalyst pellets were retained by stainless steel mesh (#32) at each end of the draft tube.

5.2.7 Height of Liquid Phase inside Reactor

The top impeller should be completely immersed in the liquid phase in order to create good fluid circulation through the packed bed. The occupied volume of the reactor internals and 20 g of glass beads was determined to be 60 mL by the excluded volume when they were immersed in a vessel with marked volume. Even at room temperature, the height of the liquid phase (10.4 cm) of 240 g TLGO inside the reactor with all internals installed was slightly higher than the top impeller (10.2 cm) but lower than the height of baffles (13.1 cm). All heights are calculated from the inner base of the batch reactor.

The density of TLGO at 375 °C was estimated to be 600 kg/m³ from the O'Donnell correlation (1980):

$$\text{Density at } T \text{ } ^\circ\text{C} = [(\text{Density at } 23 \text{ } ^\circ\text{C})^2 - 0.0011 (T-23)]^{0.5} \quad (5-2)$$

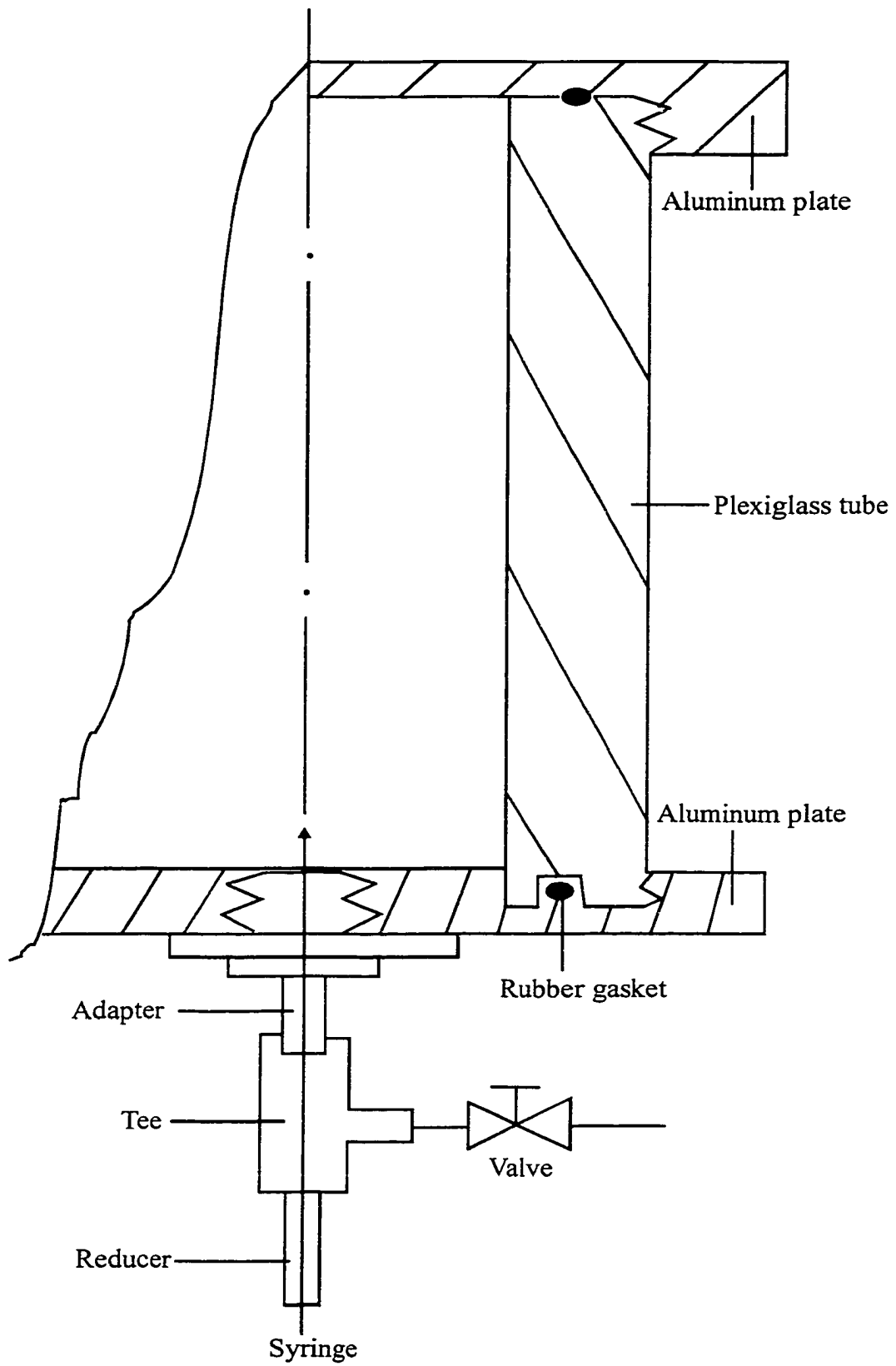
where the density of TLGO at 23 °C was extrapolated to be 865 kg/m³ based on its densities at 15 and 20 °C (*Table 5-1*). This correlation is claimed to be valid for most petroleum products with densities of 930 to 570 kg/m³ and temperatures of 0 to 300 °C. The applicability of this correlation to higher temperature than 300 °C is not known. The dependence of density upon reaction pressure was not considered, and some liquid molecules may evaporate or react at elevated temperatures. However, this correlation was used here anyway to give a rough idea about the liquid height at reaction conditions. The volume of 240 g TLGO at reactor conditions was calculated to be 400 mL based on the estimated density of 600 kg/m³. The sum (ca. 460 mL) of the liquid volume at reaction conditions, the reactor internals, and the packing gave a liquid height of 14.3 cm, which was sufficiently large for the baffles and of course the top impeller to be completely immersed in TLGO.

5.2.8 Observation of Fluid Circulation Pattern

A plexiglass vessel with the identical inner dimensions as the 500 mL reactor was constructed to observe the circulation patterns of fluid at room temperature (*Figure 5-3*). The same reactor internals were installed in the plexiglass reactor during the observation of fluid pattern, but they were not shown in *Figure 5-3* for the simplicity. The vessel was connected to two aluminum plates with good sealing at its ends. The impeller passed through the top aluminum plate that was clapped with the reactor head. The bottom aluminum plate was supported by three aluminum rods which were fixed to the bench.

The fluid (usually water) can be fed into the plexiglass vessel before each run through a one-way valve. The impeller was turned on to a certain speed, and then the dye solution (0.5 g uranine in 100 g water solution) was injected by a 5 cm³ syringe plunger

Figure 5-3. Schematic diagram of plexiglass model of reactor



that passed through the fittings at the bottom of the reactor. The tip surface of the needle was flat and parallel to the bottom of the vessel. The same amount of dye solution was injected each time.

A fluorescent light was used to illuminate the plexiglass tube, and the flow pattern of the dye was recorded by an imaging system, as described in *Section 5.2.10*. The fluid was released from the valve after each recording, and the reactor inside was washed with fresh water a couple of times. The same experiment was repeated five times for the observation of flow patterns with and without the packing of glass beads.

Aluminum powder of 10 μm was also used in conjunction with the fluorescent light to observe the flow pattern. Experiments with and without catalyst packing were both carried out.

5.2.9 Reaction Procedure

A suspension of kaolin or asphaltene-treated kaolin (0.97 ~ 0.98 g) in filtered TLGO (ca. 240 g) was sonicated for 20 min. and then charged into the 500 mL reactor. A predetermined amount of solids-free asphaltenes was added to and sonicated with the feed in some runs to increase the ratio of total asphaltenes to kaolin in the reaction mixture. In order to eliminate any moisture, the draft tube was loaded with a determined amount of cleaned glass beads or catalyst pellets, and dried in an oven at 110 °C for 20 min prior to its addition into the reactor. After the reactor was closed, it was pressure tested with nitrogen at 12 MPa, then pressurized with hydrogen at 12 MPa and purged three times. The initial hydrogen pressure of the reactor was 6.2 MPa at room temperature. When the preset reaction temperature (375 °C) was first reached, the timing of reaction began and the impeller was switched on. The mixture was stirred at 700 rpm

for a measured period of time (10 ~ 60 min) and then the impeller was turned off. At the end of each experiment, the reactor was moved out of the heater to cool in the air without stirring and opened 20 h later. This procedure ensured that particles were only filtered in the packed bed under controlled temperature conditions.

5.2.10 Measurement of Particle Deposition

After the reactor was opened, the draft tube was taken out and allowed to drain for 10 min. The solid in the drained suspension was recovered by filtration and counted as part of the solids deposited in packing. Microscopic images of the top layer of the bed packing were observed and recorded with a microscopy video imaging system consisting of a Stereomicroscope (Stemi 200-C, Carl Zeiss Jena GmbH), a CCD camera (HITACHI, KP-M), a video cassette recorder (Sony EV-S7000) and a video monitor (Hitachi VM-1720). Images were displayed on the monitor and analyzed using a personal computer. The packing of glass beads or spent catalyst was then poured out and sonicated with 250 mL methylene chloride for 20 min. The solids in the supernatant suspension after sonication were recovered by filtration through a 0.22 μm Millipore filter. This process of sonication and then filtration was repeated twice in order to retrieve all the solids that were deposited on the collectors. This method followed Biran et al. (1996) for recovery of fine particles from filters. The filtered solids were dried in vacuum at 70 °C for 24 h and then weighed after cooling for 3 h. The term “solids” was used because some spent catalyst pellets broke during sonication, becoming part of the filter cake. The amount of broken spent catalyst pellets in the filter cake was determined by three blank runs in which no kaolin was added to the feed and spent catalyst went through the same sonication. The broken spent catalyst was deducted from the total filter cake to obtain the

mass of kaolin in all particle trapping experiments involved with spent catalyst. Similar blank experiments and deduction were carried out when fresh catalyst was used as packing material.

Kaolin settled at the bottom of the reactor and suspended in the liquid product was collected, and its amount was determined after filtration. The top mesh of the draft tube and the two impellers were sonicated with methylene chloride for 10 min to remove the trapped kaolin which was also recovered by filtration. The masses of kaolin at the bottom of the reactor, suspended in the liquid phase, and on the top mesh of the draft tube were summed to obtain the overall mass of the kaolin in the liquid phase after the reaction.

The mass of kaolin, either in the feed or in the liquid product or deposited in the bed packing, was corrected to a hydrocarbon-free basis using the measured carbon content of each sample and the carbon content of the asphaltenes or gas oil (*Table 5-1*). The normalized concentration of kaolin in the liquid phase was defined as the mass of kaolin in the liquid phase divided by the mass of kaolin initially added to the feed, assuming that the volume of liquid phase did not change significantly under mild hydrotreating conditions. The specific deposit, σ , was defined as the mass of kaolin deposited per unit volume of the empty bed (kg/m^3). *Appendix 4* gives more details on the calculations of the specific deposit of kaolin. The coverage of kaolin on collector surfaces was the area covered by kaolin particles divided by the total collector surface area, based on the assumption that the kaolin particles were spherical with a mean diameter of $0.68 \mu\text{m}$.

5.3 Results and Discussion

5.3.1. Liquid Phase Circulation at Room Temperature

The pitched blade turbine uses a combination of both axial and radial forces to produce a diagonal flow with an angle dependent on the degree of pitch, number of blades, blade width, rotational speed and vessel shape (Uhl and Gray, 1967). For upwardly directed circulation of a solids suspension, a bottom-mounted turbine in a baffled vessel is one of the most effective types for the difficult suspensions of fast settling, granular solids in a low viscosity fluid such as sand in water. At room temperature the density and viscosity of TLGO were comparable to those of water (*Table 5-1*), and the density of kaolin was $2,580 \text{ kg/m}^3$ (*Table 4-2*). Certainly suspension of kaolin in hydrotreated gas oil fell into the category of difficult suspensions. Employing another pitched blade turbine above the draft tube again promoted the fluid circulation through the draft tube because this turbine generated strongly accelerated downward flow through the impeller region when impeller diameters are less than the radius of the cylindrical tank (Ranade et al., 1989).

The die was dispersed to the top of the liquid phase within 30 seconds after it was injected into the simulated batch reactor. However, this observation cannot give a clear picture about the path of fine particles movement. One g of aluminum powder was mixed with water, and the suspension was added to the simulator. It was observed that the powders moved up along the annulus to the top of the draft tube and then went down into the packed bed. The powders were suspended to such an extent that a negligible amount of powders remained at the bottom.

5.3.2 Adsorption of Asphaltenes on Kaolin

Figure 5-4 shows the adsorption of asphaltenes onto 0.68 μm particles of kaolin at 22 ± 1 $^{\circ}\text{C}$. During the preparation of asphaltene-treated kaolin, a continuous mixing of 24 h ensured that adsorption equilibrium was reached. An equilibration time for the adsorption of asphaltenes on illite was found to be 15 min (Marlow et al., 1987). The equilibrium concentration of asphaltenes on kaolin increased sharply at low asphaltene concentration, followed by a much smaller increase in equilibrium concentration with the subsequent increase in the asphaltene concentration in the liquid phase. The highest concentration of 75 g asphaltenes/kg kaolin corresponded to a surface concentration of 6.3 mg/m^2 , comparable to the data reported by Marlow et al. (1987) for asphaltenes on illite and González et al. (1994) for asphaltenes on kaolin.

5.3.3 Deposition of Kaolin in Packed Beds

5.3.3.1 Material Balance

Kaolin can settle at the bottom of the reactor, remain suspended in the liquid product, or be trapped by the mesh of the draft tube and the bed of packing. The difference between the kaolin in the feed and that distributed inside the reactor is a good indicator for the accuracy of sonication and filtration techniques used to measure particle deposition. Although there was a remarkable difference in kaolin distribution inside the reactor when asphaltene-treated kaolin and untreated kaolin were used in the particle deposition experiment, the mass balance of kaolin was satisfactory (*Table 5-3*). In either case, more than ca. 98% of kaolin was recovered after reaction. The difference in the distribution of untreated kaolin and asphaltene-treated kaolin was explained in later discussion.

Figure 5-4. Adsorption of asphaltenes on kaolin from 1:1 heptane/toluene mixture at 22 °C

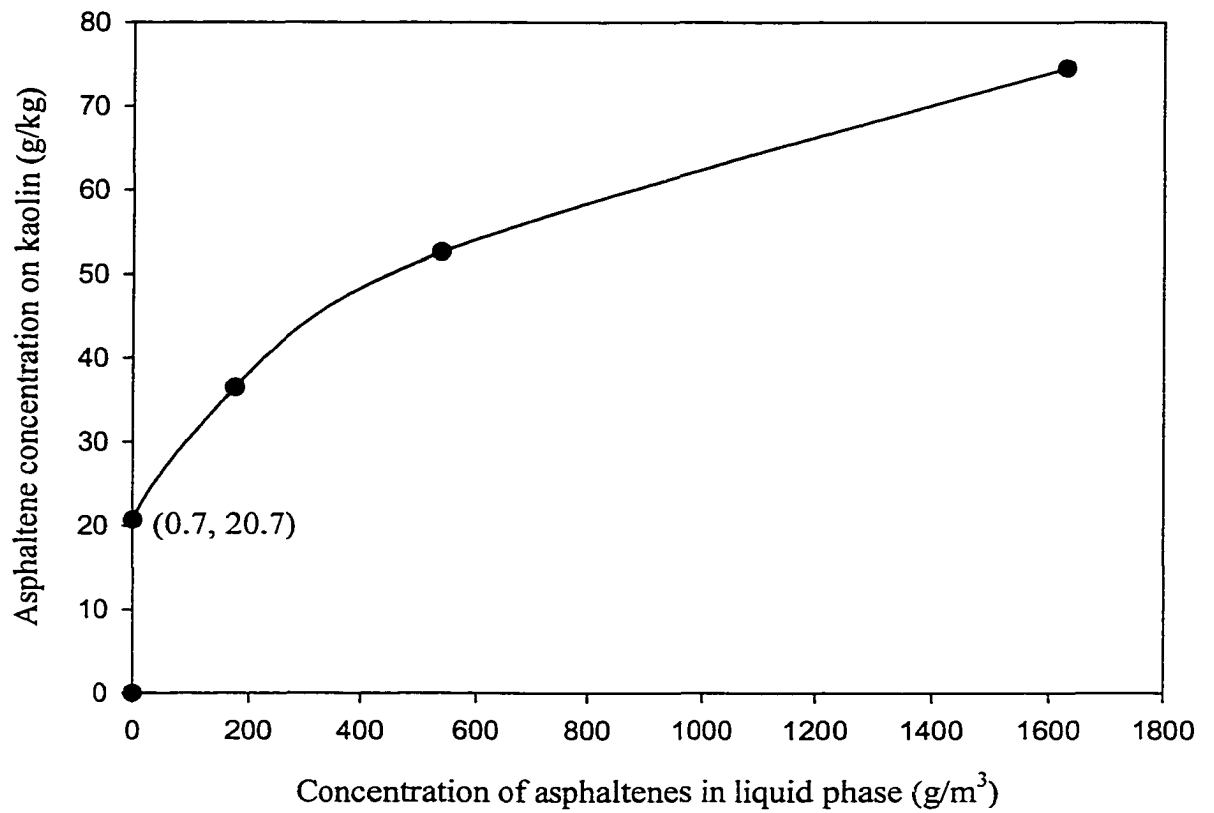


Table 5-3. Distribution of kaolin inside the reactor as the percentage of the total kaolin on a hydrocarbon-free basis (375 °C, 60 min of reaction time, 700 rpm, 20 g of glass beads, 0.98 g kaolin and 240 g TLGO; asphaltene-treated kaolin initially had 75 mg asphaltene/g kaolin)

Particle type	Bottom of reactor (%)	Top mesh of draft tube (%)	Suspended in liquid phase (%)	Bed of packing (%)	Overall recovered kaolin (%)
Asphaltene-treated kaolin	15.1	2.5	58.0	22.3	97.9
Untreated kaolin	4.3	2.1	5.0	87.6	99.0

Based on the three blank runs, about 0.04 g out of 16.8 g of spent catalyst and 0.03 g out of 17.0 g fresh catalyst broke during sonication and were filtered out as deposited particles. One blank experiment was conducted in which no clay was added into the liquid feed, so that the mass change of catalyst pellets after the reaction was determined. It was found that catalyst pellets did not break during experiment to give solids in the liquid product, based on. However, the weight loss of spent catalyst for all experiments was about 2 g out of the input 16.8 g. Carbon content for spent catalyst also dropped from the initial 6.8% to 5.6% after reaction, suggesting the removal of carbonaceous deposit from the spent catalyst. In contrast, 16.8 g of fresh catalyst had a weight increase of about 0.2 g, likely due to sulfidation of fresh catalyst during the particle deposition experiment.

5.3.3.2 Repeatability of Particle Deposition Measurements

The repeatability of the trapping experiments with kaolin was checked under the following reaction conditions: 375 °C, 60 min of reaction time, 700 rpm, 20 g glass beads, 240 g TLGO, and 0.98 g asphaltene-treated kaolin (75 mg asphaltenes/g kaolin). The normalized concentration of kaolin in the liquid product for the five repeated runs with treated kaolin (initial carbon content = 5.9 wt%) was 0.80 ± 0.01 (95% confidence interval). The specific deposit, σ , was $14.3 \pm 0.7 \text{ kg/m}^3$ (95% confidence interval). The normalized concentrations of kaolin in the liquid product for the other two runs with similarly treated kaolin (initial carbon content = 5.6 wt%) were 0.77 and 0.81, respectively. Because experiments with different batches of treated kaolin gave marginally different results, all comparisons of experimental results were within a given batch of treated clay. Each time only 2.5 g asphaltene-treated kaolin was treated, and

treated kaolin from several similar treatments was mixed together to give one batch. More details are described in *Appendix 5* for the reproducibility of particle deposition experiments.

5.3.3.3 Time Course of Particle Deposition

The hydrodynamics and chemistry in hydrotreaters are very complex, so the approach in this study was to control as many variables as possible. Spent catalyst was used to minimize the chemical reactions of TLGO during the particle trapping experiment. The density and viscosity of TLGO after the reaction were 870 kg/m³ and 6.3 mPa-s at 22 °C, respectively, which were equivalent to their initial values (*Table 5-1*). Although the batch reactor had complex hydrodynamics, the selection of TLGO gave constant fluid properties during the particle deposition experiment.

The reactor was approximated as two separate but connected sections (*Figure 5-5*): a packed-bed column and a continuously stirred tank reactor. A mass balance of the kaolin solids on a hydrocarbon-free basis gives the following equation:

$$\sigma(t)V_b = V_L [C_0 - C(t)] \quad (5-3)$$

where $\sigma(t)$ is the specific deposit of kaolin on the bed of packing at time t , V_b is the volume of empty packed-bed in the draft tube, V_L is the volume of liquid phase, C_0 is the initial concentration of kaolin in liquid phase, and $C(t)$ is the concentration of kaolin in

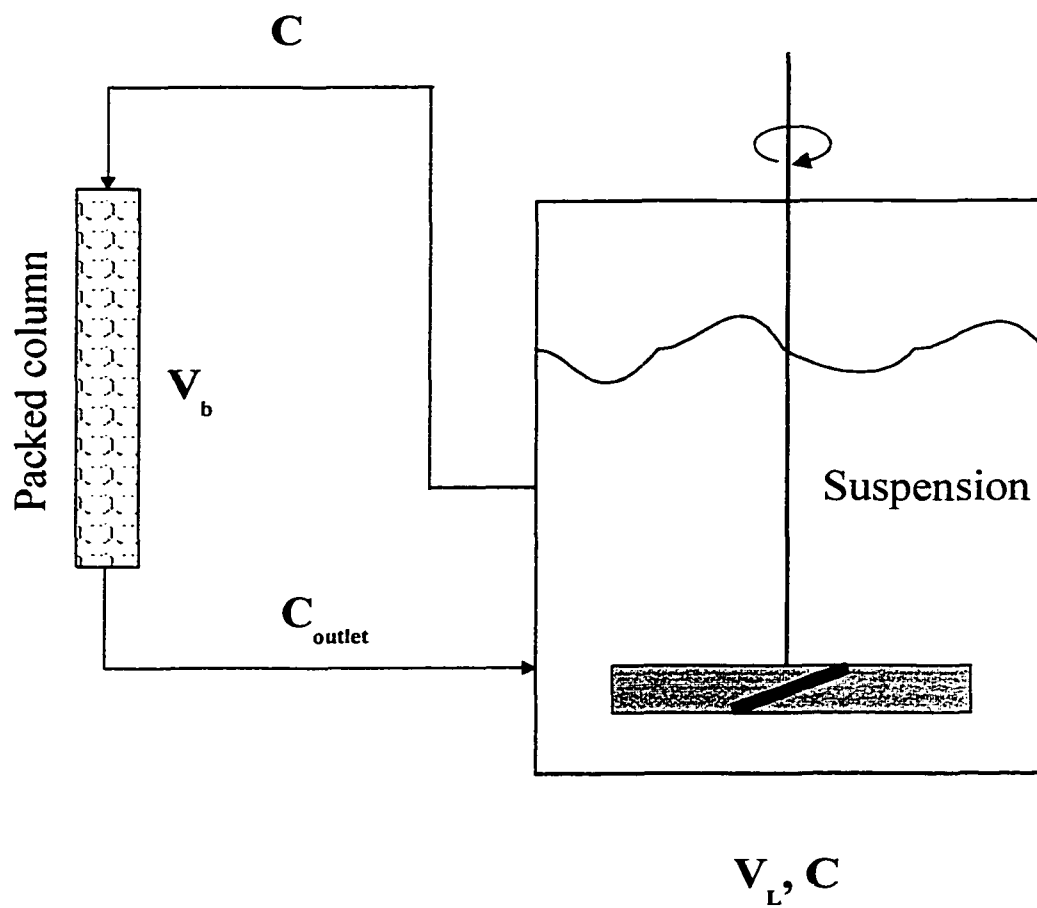
liquid phase at time t . The volume of the packed bed, V_b , is given by $\frac{m}{\rho(1-\varepsilon)}$. At

equilibrium, i.e., at large time,

$$\sigma^* = V_L(1-\varepsilon)\rho \frac{C_0 - C^*}{m} \quad (5-4)$$

where σ^* is the equilibrium specific deposit of kaolin, C^* is the equilibrium concentration

Figure 5-5. Schematic representation of batch reactor as a recycle reactor



of kaolin in the liquid phase, ε is the porosity of the bed packing, ρ is the density of packing materials, and m is the mass of packing material loaded in the draft tube. The concentration of kaolin in the liquid phase was assumed to decrease at a rate proportional to the difference between the kaolin concentration and the equilibrium kaolin concentration as follows:

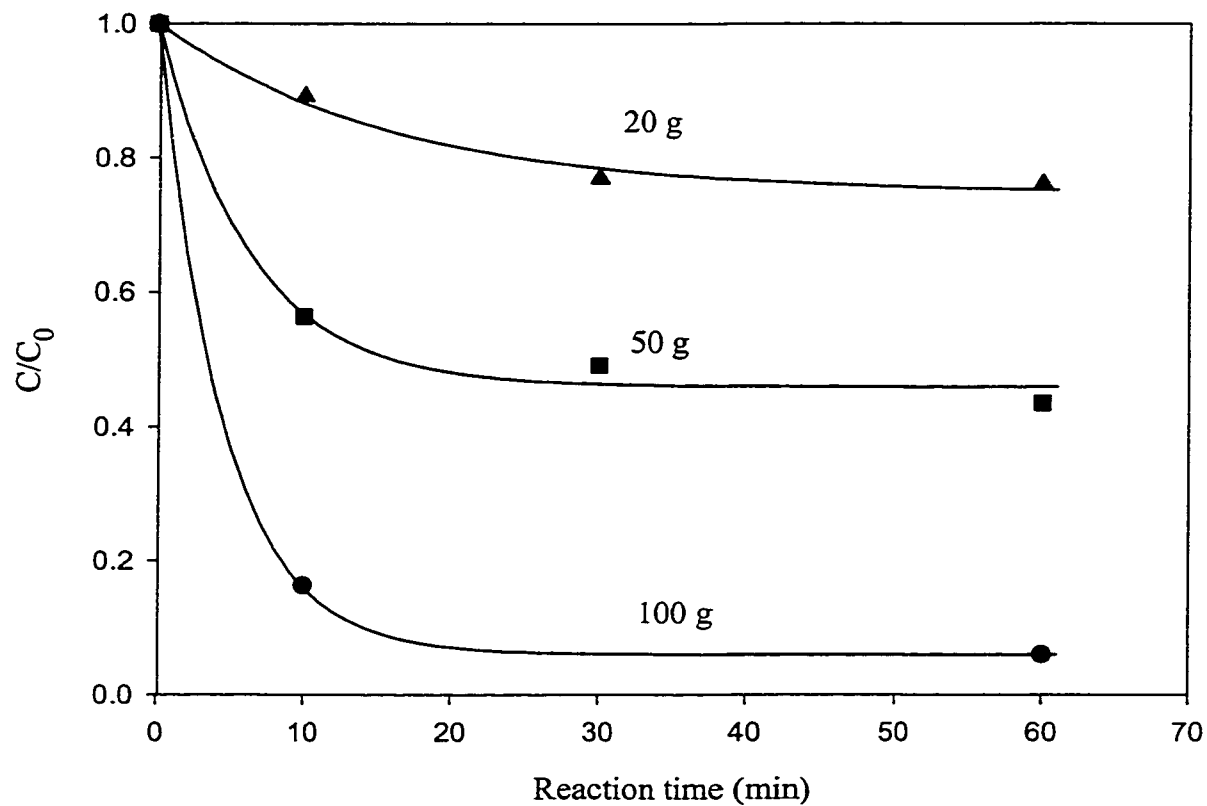
$$\frac{dC(t)}{dt} = -k[C(t) - C^*] \quad (5-5)$$

The parameters k and C^* depend on the stirring speed of the impeller, the liquid and particle properties, the nature of the packing, and so on. Integration of *Equation 5-5* from the initial concentration C_0 gives

$$\frac{C(t)}{C_0} = \frac{C^*}{C_0} + \left(1 - \frac{C^*}{C_0}\right) \exp(-kt) \quad (5-6)$$

When asphaltene-treated kaolin (75 mg asphaltene/g kaolin) was used with different amounts of glass beads, the equilibrium concentration of kaolin in liquid phase depended on the amount of glass beads (*Figure 5-6*). Although a greater amount of glass beads gave a higher rate constant, the rapid progress of particle trapping, as illustrated in *Figure 5-6*, allowed good estimates of C^* but poor approximation of the rate constant k for each set of conditions. The concentration of kaolin in the liquid product decreased as the quantity of glass beads increased, but the equilibrium specific deposit, σ^* , calculated from *Equation 5-4*, was insensitive to the amount of packing. The equilibrium specific deposits on 20, 50, and 100 g of glass beads were 14.3, 15.0, and 14.5 kg/m³. The observation of an equilibrium specific deposit indicated that the experiment reached the stage when the rate of attachment and the rate of detachment of kaolin particles were balanced. Because the power provided by the two stirrers was the same for all these

Figure 5-6. Variations of concentration of kaolin in liquid product with quantity of glass beads at 375 °C and 700 rpm when asphaltene-treated kaolin (75 mg asphaltenes/g kaolin) was used. The data points were fitted to a curve from *Equation 5-6*.



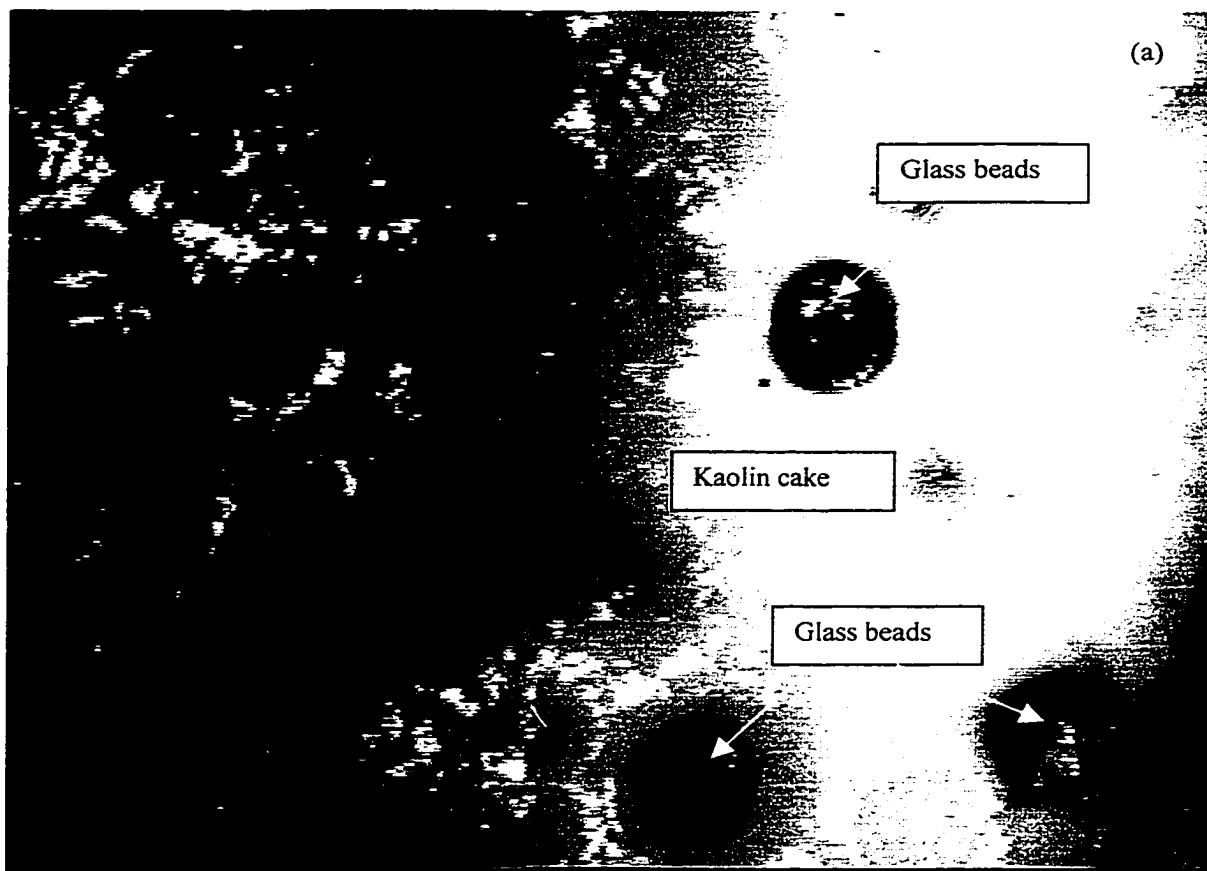
experiments, the liquid velocity through the packed-bed would drop when the amount of packing material was increased. The equilibrium specific deposit was almost the same for all the cases, suggesting that the ultimate particle concentration was insensitive to liquid flow rate. Such a lack of dependence on the liquid flow rate suggested that the deposition mechanism be controlled by interactions between kaolin particles and the collector, and by interactions between kaolin particles, rather than changes in velocity.

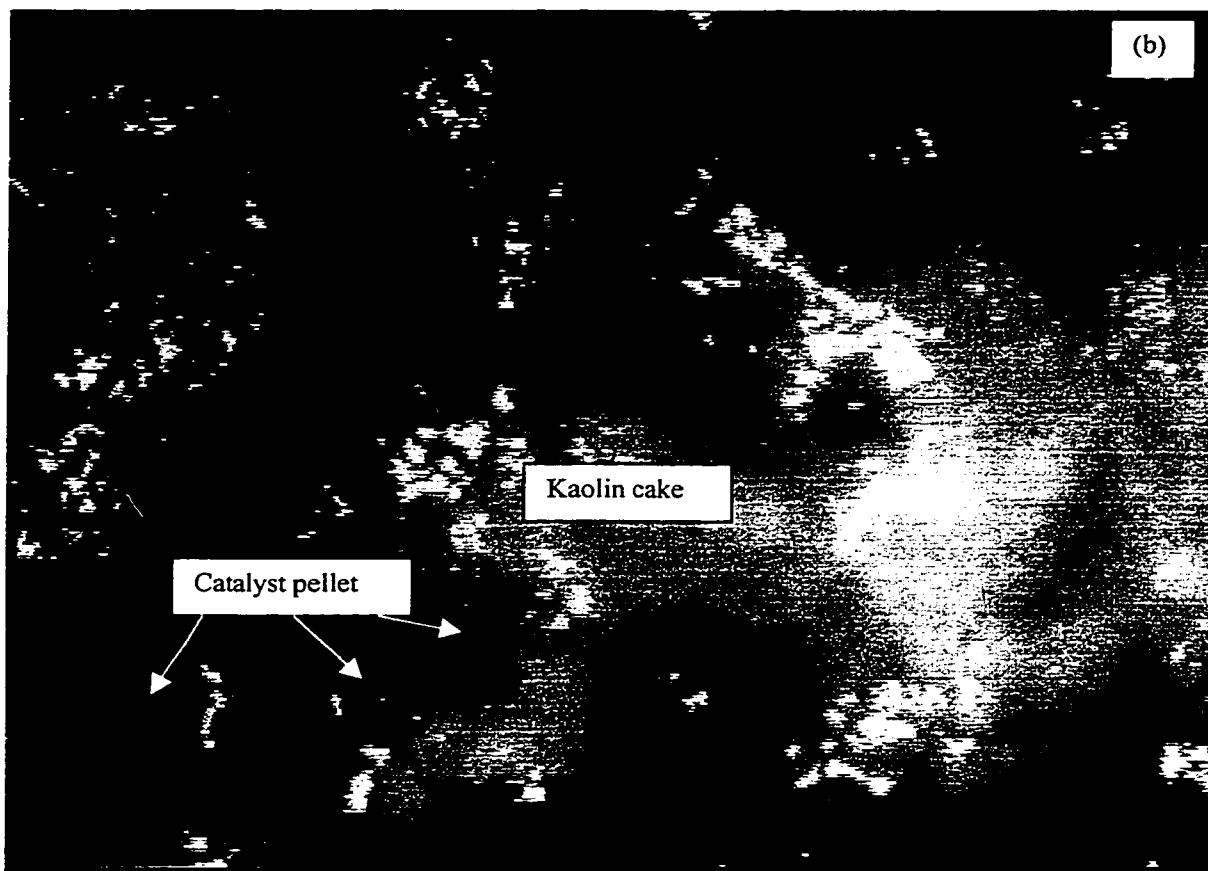
5.3.4 Role of Asphaltene Coating and Free Asphaltenes in Particle Trapping

Microscopic observations of particle deposition on the top layer of packed bed in the draft tube showed that untreated kaolin formed a continuous filter cake for packings of either glass beads or spent catalyst when the reaction time was 60 min (*Figure 5-7*). The average surface coverage by untreated kaolin on both packings was greater than $9 \text{ m}^2/\text{m}^2$, in agreement with the formation of a thick cake of clay on top of the bed. None of the asphaltene-treated kaolins gave a visible filter cake under identical conditions. The filtration mechanism, therefore, switched from cake filtration to deep-bed filtration when the fine particles were changed from untreated kaolin to asphaltene-treated kaolin. The porosities for beds of spent catalyst and glass beads were 0.44 and 0.37, respectively (*Table 5-2*). The flow channels through the packed bed of spent catalyst would be quite irregular compared with those of the glass bead packing. However, both packings showed a distinct change from cake filtration at the top surface of the bed to straining and deposition within the bed when kaolin particles were treated with asphaltenes.

The fine particles from Alberta oil sands naturally adsorb some organic matter. When two particles with adsorbed asphaltene layers approach one another at distance of separation of their surfaces of less than twice the thickness of the adsorbed layer,

Figure 5-7. Photographs of the structure of kaolin deposit on top of the packed bed when untreated kaolin was used: (a) 20 g of glass beads;
(b) 16.8 g of spent catalyst





interaction of the two layers takes place. Two major theories, e.g. entropic stabilization theory and osmotic repulsion stabilization theory, have been proposed to explain the steric stabilization mechanism (Sato and Ruch, 1980). Adsorption of asphaltenes on illite particles can cause surface charge due to the presence of polar groups in asphaltene molecules (Marlow et al., 1987). The presence of charged groups on the surface of mineral particles may be apparent even in a non-aqueous system (Labib, 1988). Besides steric repulsion forces caused by the overlap of hydrocarbon chains of the adsorbed molecules, electrostatic repulsive forces are also important for the stabilization of asphaltene-covered illite particles in hydrocarbon media (Marlow et al., 1987). Although it is prohibitively difficult to verify which stabilization mechanism was dominant for asphaltene-treated particles in TLGO at reaction temperature, this layer of organic matter had a great impact on deposition of the mineral particles once an initial layer of asphaltene-treated particles was deposited. The deposited particles would hinder the further deposition of flowing particles by either steric forces or electrical repulsion. Electrostatic attraction was used to explain the initial high rate of deposition of carbon black from tetralin on a bed of sand (Chowdiah et al., 1982). This high rate of particle deposition also occurred in our study with kaolin, in which deposition and re-entrainment reached equilibrium after 30 min. Continued deposition at a much lower rate may be affected by steric and electrical stabilization.

5.3.4.1 Flocculation of Untreated Kaolin in TLGO

A separate sedimentation experiment demonstrated flocculation of untreated kaolin in TLGO at room temperature. Detailed information of sedimentation experiments was presented in *Appendix 6*. The suspension of untreated kaolin in TLGO was placed in a

1-L volumetric cylinder. The interface between the kaolin-free liquid (the supernatant layer) and the suspension (the lower layer) was monitored. Almost all the kaolin settled after three or four minutes, and flocculation of kaolin was observed. The pore size of the bed of packing was much greater than the mean size of fresh kaolin ($0.68 \mu\text{m}$), therefore, the kaolin must have flocculated before entering the bed of packing in order to give the formation of a filter cake (McDowell-Boyer et al., 1986). Asphaltene-treated kaolin settled much more slowly in TLGO than untreated kaolin, with an average settling time of 20 min. The opaqueness of the suspension prevented direct observations of flocculation, but the reduced rate of sedimentation showed that the clay remained more dispersed after asphaltene treatment. Provided that this stabilization mechanism at room temperature can be extended to reactor temperatures, we would expect good dispersion of asphaltene-treated kaolin in TLGO. Well-dispersed asphaltene-treated kaolin particles would be small enough to enter the bed of packing, where they would be mechanically removed by straining in smaller pore spaces and by deposition on the surfaces of the beads or pellets in the packed bed.

5.3.4.2 Effects of Asphaltene Treatment on the Kinetics of Kaolin Deposition

Three different kinds of kaolin particles (untreated kaolin, asphaltene-treated kaolin with 37 mg asphaltene/g kaolin, and asphaltene-treated kaolin with 75 mg asphaltene/g kaolin) were used to study the effects of asphaltene treatment on the kinetics of kaolin deposition in the bed of 20 g of glass beads. Although untreated kaolin and asphaltene-treated kaolin were deposited by two different filtration mechanisms, all the normalized concentrations of kaolin in the liquid phase were plotted against the reaction time in

Figure 5-8. Due to the filtration of kaolin by the packed bed, the concentration of kaolin decreased rapidly during the first 10 min and reached equilibrium at 1 h. The data of *Figure 5-8* clearly showed that the trapping of kaolin at any given time was significantly reduced when kaolin was pretreated with asphaltene. Untreated kaolin gave the lowest concentration in the liquid due to cake filtration occurring at the top of the bed of glass beads. In aqueous suspensions the steric interactions between humic coatings on particles gave a low deposition rate of particles in a packed bed (Amirbahman and Olson, 1993). A similar mechanism could stabilize the suspensions of asphaltene-treated kaolin. The greater steric resistance against multi-layer deposition provided by asphaltene-treated kaolin with 75 mg asphaltenes/g kaolin would give less deposition at a given time, compared with asphaltene-treated kaolin with 37 mg asphaltenes/g kaolin (*Figure 5-8*).

The deposition of kaolin on spent catalyst and glass beads was studied with varying initial ratios of asphaltenes to kaolin at a given reaction time of 60 min (*Figure 5-9*). A time of 60 min was chosen because an equilibrium between deposition and detachment was reached after 60 min (*Figures 5-6* and *5-8*). The asphaltene treatment had the limit to increase the asphaltene concentration in kaolin sample (*Figure 5-4*). The most heavily treated kaolin in this study was that with 75 g asphaltenes/kg kaolin (*Figure 5-9*). Additional solids-free asphaltenes were added to the liquid feed in some experiments to increase the initial ratio of asphaltenes to kaolin in the reaction system. The x-axis in *Figure 5-9*, therefore, was calculated from the total amount of asphaltenes in the reactor system including the initial asphaltene treatment of the kaolin and the asphaltenes added directly to the liquid feed. The specific deposit, which was proportional to the surface

Figure 5-8. Variations of concentration of kaolin in liquid phase with asphaltene treatment (375 °C, 700 rpm and 20 g glass beads):
(a) asphaltene-coated kaolin with 75 mg asphaltenes/g kaolin;
(b) asphaltene-coated kaolin with 37 mg asphaltenes/g kaolin;
(c) untreated kaolin. The data were fitted to a curve from *Equation 5-6*.

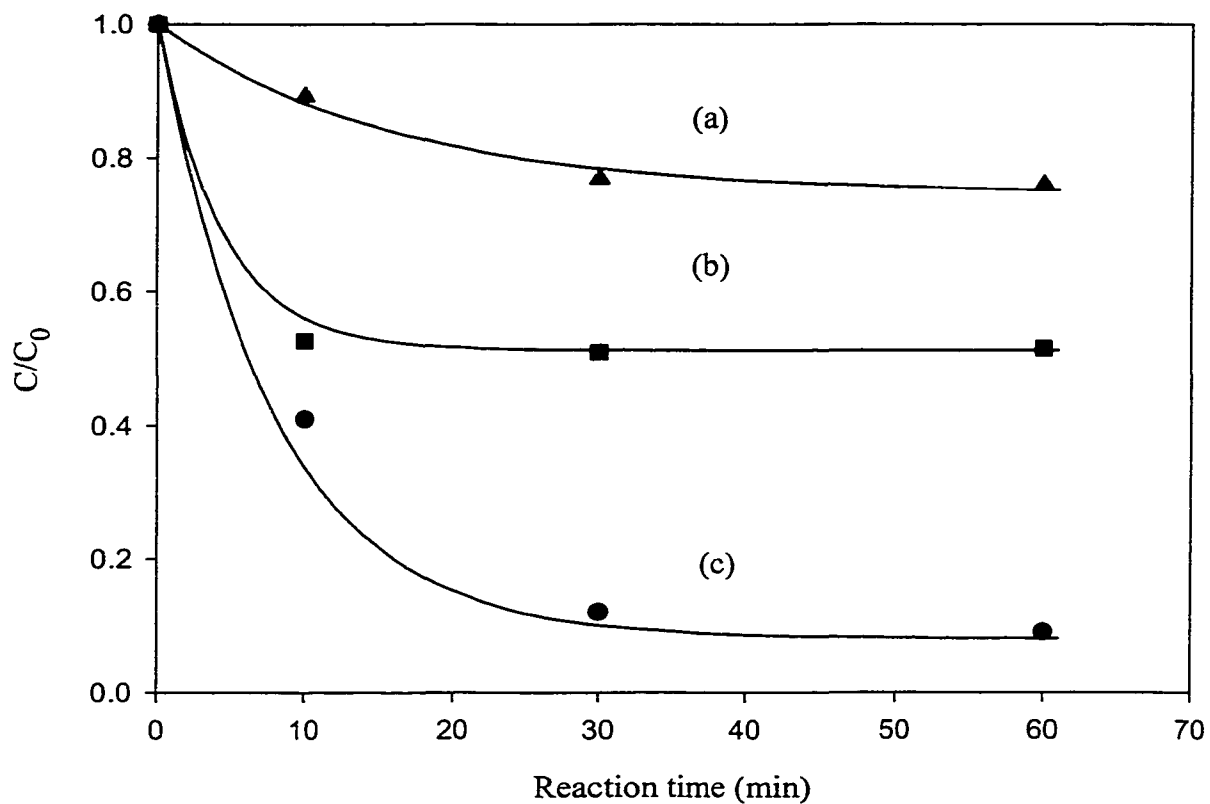
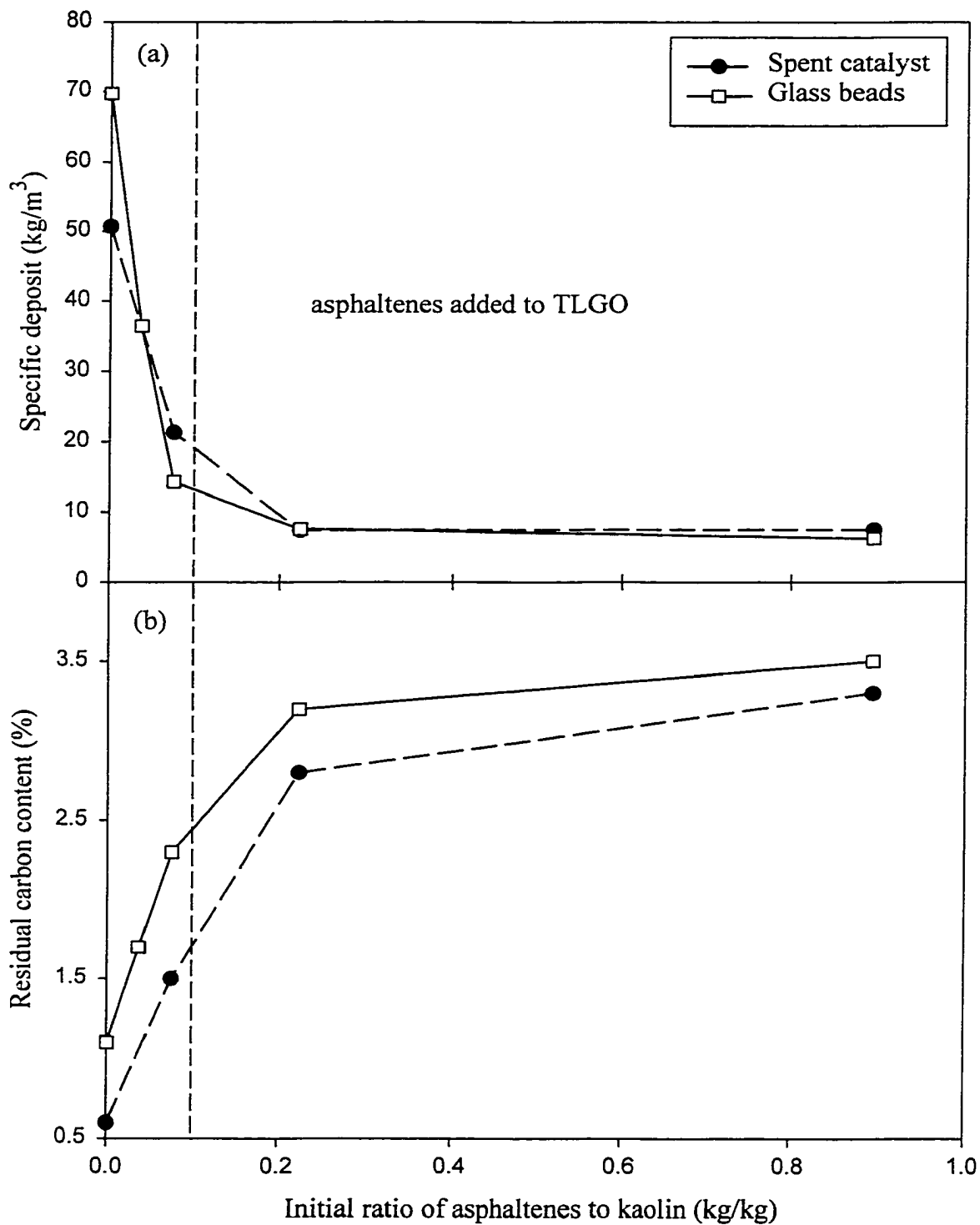


Figure 5-9. Variations of specific deposit and residual carbon content in kaolin from liquid product with the initial ratio of asphaltenes to kaolin (375 °C, 700 rpm, 240 g TLGO, initial 6.2 MPa H₂ and 60 min of reaction time). Asphaltenes were added to TLGO feed in the experiments on the right hand side of the dashed line.



coverage of clay particles on the collectors, decreased appreciably with increasing total concentration of asphaltenes in the reactor (*Figure 5-9(a)*).

The addition of asphaltenes to the liquid feed would decrease the driving force for desorption of asphaltenes from the kaolin surface, thereby producing kaolin particles with residual carbon content greater than 3% at 375 °C (*Figure 5-9(b)*). This kaolin with more residual asphaltenes on its surface would resist deposition due to stronger steric resistance against particle attachment as discussed earlier, giving a lower specific deposit on the collector (*Figure 5-9(a)*). The specific deposit reached a constant value when the initial ratio of asphaltenes to kaolin was above 0.2. It was unknown why the specific deposit was quite similar for the packings of glass beads and spent catalyst, in spite of the marked difference in residual carbon content in kaolin (*Figure 5-9*). The ratio of asphaltenes and filtered solids is about 20 for coker gas oil (*Table 4-1*), suggesting that deep bed filtration mechanism would dominate the deposition of these fine solids.

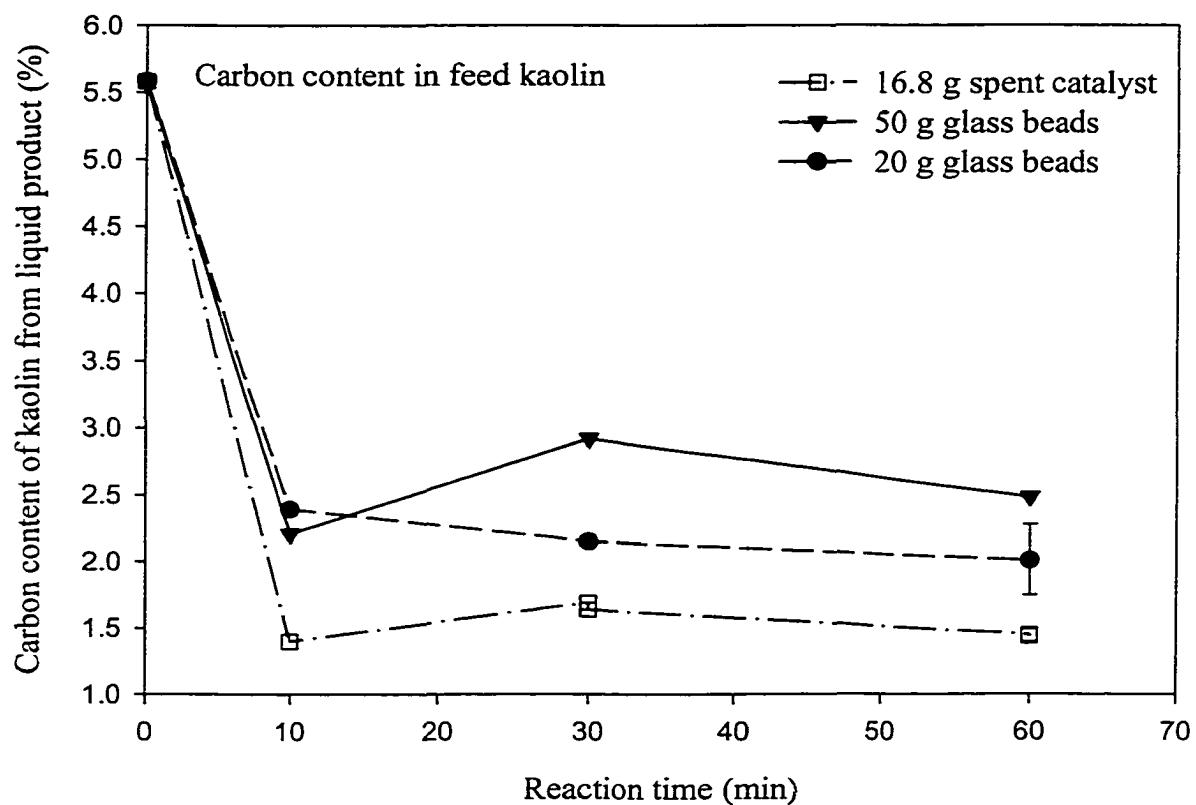
Many deposition processes occurring in aqueous media are restricted to single layer coverage of collector surfaces, because of the prevalence of repulsive interparticle electrostatic forces that prevent contact of particles (Johnson and Elimelech, 1995). Colloidal rather than hydrodynamic interactions between deposited and flowing particles slow down the deposition rate on the collector surface in aqueous systems (Dabros and van de Ven, 1992), such that a single deposited kaolin particle blocked an area that was several times larger than its cross-sectional area. In this study, however, the surface coverage by asphaltene-treated kaolin was always several times larger than $1 \text{ m}^2 / \text{m}^2$ of collector area. For example, deposition of asphaltene-treated kaolin on fresh catalyst was $5.6 - 9.3 \text{ m}^2 / \text{m}^2$. This high coverage was consistent with multi-layer deposition at

particular points in the packed bed, for example, at contact points between the glass beads or catalyst pellets (Narayan et al., 1997).

5.3.5 Thermal Stability of Asphaltenes on Kaolin

Asphaltene-treated kaolin (75 g asphaltenes/kg kaolin) was used to check the thermal stability of the asphaltene coating on kaolin when either glass beads or spent catalyst was present (*Figure 5-10*). The initial carbon content in *Figure 5-10* was the carbon content of kaolin in the feed before heating the reactor. It took ca. 1 h for the reactor to reach its final reaction temperature, so the carbon content would be lower than 5.6% when the timing of the reaction started. In any case, the carbon content decreased dramatically during the 1 h heating period and the first 10-min reaction time. Asphaltene decomposition kinetics were evaluated at 375 °C by Schucker (1983), who found that less than 15 percent of asphaltenes was decomposed after 1 h. Based on the carbon content of the kaolin, the amount of asphaltenes decreased by about 50 % for asphaltene-treated kaolin after ca. 1 h heating and 10-min reaction time. This marked difference from the data of Schucker (1983) suggests that the asphaltene coating mainly desorbed into the oil phase rather than reacting. During the process of asphaltene treatment of kaolin, the filtered kaolin was not further washed with any solvent, leaving some free or weakly adsorbed asphaltenes on the kaolin. After asphaltene-treated kaolin with a carbon content of 4.1% was Soxhlet extracted with methylene chloride for 24 h, its carbon content decreased to 3.6%. This experiment proved the existence of some free or weakly bonded asphaltenes, which could be easily removed in TLGO at 375 °C. The residual carbon content in the kaolin after extraction was comparable to the data of Fendel and Schwochau (1988) for clays from Athabasca oil sands. They found that extraction of oil

Figure 5-10. Thermal stability of asphaltene coating on kaolin (375 °C, 700 rpm and initial hydrogen pressure of 6.2 MPa). The error bar shows the 95% confidence interval for packing of 20 g glass beads at reaction time of 60 min, based on five repeated runs.



sand clays with a series of solvents, ending with methylene chloride, gave a residual carbon content of 3 %. The residual carbon content also depended on the amount of glass beads, as illustrated in *Figure 5-10*. Glass beads should be inactive in desorption of asphaltene coating, but in fact the reduction in carbon content of kaolin from liquid product was greater with the smaller amount of beads. The carbon contents for kaolin particles trapped by glass beads and those remaining in the liquid phase were determined for three experiments. While asphaltene-treated kaolin (75 g asphaltene/kg kaolin) was used in all cases, solids-free asphaltene was added to the liquid feed in two experiments (*Table 5-4*). The trapped kaolin particles had 0.1~0.4% lower carbon content than those remaining in TLGO.

The fractionation of particles according to carbon content could indicate two mechanisms. First, larger kaolin particles with a lower surface:volume ratio and hence lower carbon concentration per unit mass may preferentially deposit in the bed. Second, particles with lower surface coverage of asphaltene may deposit more readily. Thermal decomposition and dissolution of asphaltene from kaolin surface may not occur at the same time for all treated kaolin particles. The kaolin particles, with less asphaltene on their surface, would deposit faster than those particles with more asphaltene on the surface. Both mechanisms for depositional fractionation would leave kaolin particles with a relatively higher level of asphaltene coating in the liquid phase, compared to the deposited material (*Table 5-4*). On the other hand, the mass of deposited kaolin particles with less asphaltene on the surface increased with the amount of glass beads packing. The average asphaltene concentration in kaolin from the liquid phase, therefore, would be higher in the presence of more packing material (*Figure 5-10*).

Table 5-4. Carbon content of kaolin remaining in liquid product and trapped in the bed of glass beads (375 °C, 700 rpm, 60 min of reaction time, 20 g of glass beads, 240 g TLGO, 0.98 g asphaltene-treated kaolin with 75 g asphaltenes/kg kaolin)

Solids-free asphaltene added to the feed (g)	Carbon content (wt %)	
	Kaolin remaining in liquid phase	Kaolin trapped in bed of glass beads
0	2.0	1.9
0.144	3.2	3.1
0.375	3.3	2.9

In order to test the role of particle size in deposition, the experiment was repeated with 5.0 μm kaolin particles coated with asphaltenes. In this treatment 1 g of solids-free asphaltene was dissolved in a 500 mL mixture of heptane and toluene, and 2.5 g of kaolin was added to the mixture (see *Section 5.2.3*). The asphaltene-treated kaolin of 5 μm had about one-eighth of the specific surface area of the asphaltene-treated kaolin of 0.68 μm , so the first kaolin had much lower starting carbon content (2.4 %) than the second (5.9 %), after the identical asphaltene treatment. Accordingly, the treated kaolin of 5 μm had a quite low carbon content (1.3 %) after deposition experiments. If the particles are twice as large, their surface area becomes approximately half for flat platelets, so carbon content should also be half. The specific deposit of 5 μm asphaltene-treated kaolin was 16.5 kg/m^3 , slightly higher than 14.3 kg/m^3 for 0.68 μm asphaltene-treated kaolin. This indicated that specific coverage with asphaltene was important, i.e. g asphaltene/ m^2 kaolin surface, in controlling deposition, but the particle size was not. Multi-layer deposition at particular points in the packed bed, e.g., at contact points between the glass beads or catalyst pellets, was observed by Narayan et al. (1997). When the particle size was smaller than the interstitial space, surface chemistry rather than particle size controlled the deposition rate under a multi-layer deposition mechanism. These results showed that fine particles were fractionated according to the second mechanism. That is, kaolin particles were fractionated depending on their specific coverage with asphaltenes, leaving kaolin with more asphaltene coverage in the liquid phase.

After a given reaction time of 60 min, the residual carbon content of kaolin in the liquid phase was always lower when spent catalyst was used as compared with glass beads (*Figure 5-9(b)*). The carbon content of asphaltene-treated kaolin after a given

reaction time, ranging from 10 to 60 min, was always lower by $0.7 \pm 0.3\%$ in the presence of spent catalyst than in the corresponding runs with glass beads (*Figure 5-10*). This difference was statistically significant, even when comparing the data from 20 g glass beads to those from the catalyst.

The combination of fresh catalyst with hydrogen gave a lower residual carbon content in kaolin than with nitrogen (*Table 5-5*), showing that catalyst was more effective in stripping off asphaltenes in a hydrogen atmosphere than in nitrogen. The total reaction pressure with hydrogen was about 10.3 MPa at 375 °C in the presence of 16.8 g spent catalyst, rather than about 11.7 MPa for 20 g glass beads, indicating hydrogen consumption with the use of spent catalyst. Under the hydrogen atmosphere, the spent catalyst would hydrogenate, desulfurize and denitrogenate asphaltenes or other polar components in the liquid phase, leading to more desorption of polar organics from the kaolin surface. An independent experiment with quinoline added into the feed in the presence of spent catalyst gave 95% conversion of quinoline, demonstrating that the hydrogenation activity of the catalyst is still high. These results show that the hydrotreating reactions may serve to alter the surface composition of suspended solids, and thereby alter the filtration of the solids by a bed of catalyst pellets.

5.3.6. Tests on Authentic TI Solids

Two kinds of authentic TI solids derived from Athabasca oil sands, SCFE residue solid and vacuum residue solid, were used to test their thermal stability and deposition behavior. The carbon content of the solids from the supercritical fluid extraction (SCFE) endcut #9 (See *Section 4.2*) was 30.0 %, which dropped to 27.6 % after Soxhlet extraction with methylene chloride for 24 h. After deposition experiments at 375 °C for

Table 5-5. Residual carbon content in kaolin from liquid product, specific deposit and coverage of kaolin on collectors under hydrogen and nitrogen atmosphere with fresh catalyst (375 °C, 700 rpm, 240 g TLGO, initial 6.2 MPa gas and 60 min of reaction time).

	Untreated kaolin	Asphaltene-treated kaolin	
		H ₂ atmosphere	N ₂ atmosphere
Residual carbon content (%)	0.8	1.5	2.1
Specific deposit (kg/m ³)	39.8	28.7	17.4
Coverage of collector (m ² /m ²)	12.8	9.3	5.6

1 h in the presence of 20-g glass beads, the endcut solid on top of the packing only had a carbon content of 11.5 %. This SCFE end cut solid was highly polymerized and aggregated, so it did not break after the 30-min sonication before reaction, therefore, it was filtered as a cake on top of the packing. The particle size of the vacuum residue solid was more representative of the authentic solids that would enter the hydrotreaters. The range of vacuum residue solid was approximately 0.5-5 μm , based on SEM micrographs.

The carbon content of vacuum residue (VR) solid dropped from 18.5 % to 12.5 %, after reaction at 375 °C for 1 h in TLGO in the absence of any packing. The presence of spent catalyst further reduced the carbon content of VR solid to below 10 %, indicating the catalytic activity of the catalyst in the hydrotreater could remove some organic coating from fine particles. Again the fractionation of this solid depended on its asphaltene coverage. The carbon content of VR solid deposited in the spent catalyst bed was 9.3 %, while the carbon content of VR solid in the liquid product was 9.9 %. This finding supported the deposition mechanism proposed in *Section 5.3.5* that fine particles with less asphaltene coverage would be deposited first.

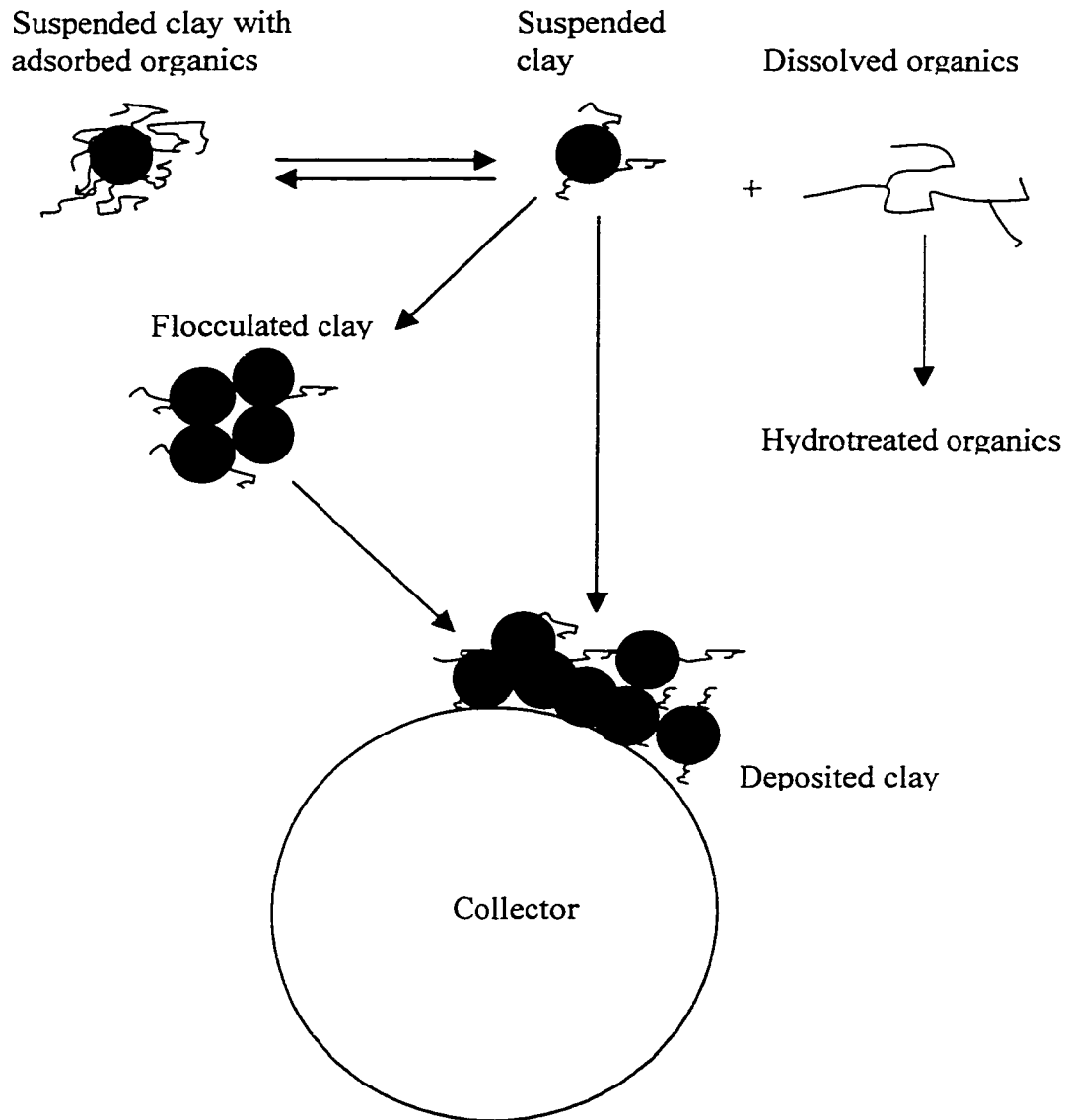
5.3.7 Mechanism of Deposition and Industrial Implications

The present study suggests a mechanism of particle deposition that depends upon the changing surface properties of the particles due to hydrotreating reactions. The presence or absence of adsorbed asphaltenes on the surface of the kaolin particles was crucial to their filtration behavior. In the presence of excess asphaltenes in the liquid phase, only low levels of particle filtration were observed. When asphaltenes were completely absent, the kaolin flocculated so rapidly that a filter cake was formed on top of the bed packing. Asphaltenes were reacted from the gas oil phase due to the catalytic activity of

the catalyst, thereby destabilizing the suspended particles and enhancing deposition. These results can have industrial implications in terms of the changing mechanism of particle deposition at different locations in hydrotreaters. Clays in the gas oil feed to hydrotreaters are hydrophobic, with adsorbed polar organic materials such as asphaltenes or humic matter. As observed in the batch reactor (*Figure 5-10*), part of this coating would desorb at reactor conditions. The dissolved polar organics in the liquid phase are converted by catalytic activity, giving further desorption (*Figure 5-11*). This process would drive more and more desorption of organic coating as the particles travel down the reactor. As the asphaltenes are removed from the clay surface, the clay suspension becomes less stable, and the tendency to flocculate increases, leading to cake filtration (*Figure 5-8 & 5-9*). Consequently, the rate of trapping of particles will increase as they progress down the reactor. Particle deposition was rapid, as indicated in *Figures 5-6 and 5-8*; therefore, the highest rate of particle deposition would occur near the most active zones of the hydrotreating reactors, where the removal of adsorbed organic material would be most active.

This trend is consistent with some industrial observations that more particles are deposited at the lower end of hydrotreaters (Chan et al., 1994). Hydrodynamic changes would also tend to reinforce this trend. As the feed passes down the reactor, the temperature rises and the boiling curve of the liquid shifts to lower temperatures, both due to catalytic reactions (hydrodesulfurization and hydronitrogenation) and saturation of polynuclear aromatics. The resulting reduction in the liquid/gas ratio would also enhance particle deposition.

Figure 5-11. Schematic illustration of the mechanism for deposition of clays. The adsorbed organic components may be asphaltenes, humic material or other polar species.



5.4 Conclusions

When either glass beads or catalyst pellets were used as the packing material, the filtration mechanism depended on the surface properties of the fine kaolin particles. Cake filtration prevailed when untreated kaolin was used, but deep-bed filtration dominated for asphaltene-treated kaolins. Overall, an increase in the concentration of asphaltenes adsorbed on the kaolin surface gave a lower extent of filtration. Asphaltenes desorbed from the kaolin at reactor conditions. More asphaltene was desorbed in the presence of catalyst, consistent with removal of asphaltene from the liquid phase by the action of the catalyst. The addition of asphaltenes to the feed decreased the driving force for desorption of asphaltenes into the liquid phase from kaolin surfaces and gave much higher residual carbon content in kaolin from the liquid phase. This increase in the asphaltene concentration on the kaolin gave a much lower specific deposit of kaolin on the packed bed at these conditions.

References

- Amirbahman, A.; Olson, T. M. Transport of Humic Matter-Coated Hematite in Packed Beds. *Environ. Sci. Technol.* **1993**, 27 (13), 2807-2813.
- Biran, R.; Tang, Y. Z.; Brook, J. R.; Vincent, R.; Keeler, G. J. Aqueous Extraction of Airborne Particulate Matter Collected on Hi-Vol Teflon Filters. *Int. J. Environ. Anal. Chem.* **1996**, 63 (4), 315-322.
- Briggs, D. E.; Cameron, J. R.; Ho, B.; Islip, P. N.; Mckeen, J. A. Filtration of Slurries from Coal Liquefaction Processes. *Separation Sci. Technol.* **1980**, 15 (3), 223-248.
- Chan, E. W.; Chung, K. H.; Veljkovic, M.; Liu, J. K. Hydrodynamics and Fines Capture in Packed-Bed Hydrotreaters. *Int. Petrol. Petrochem. Technol. Symp.*, Beijing, September 15-17, **1994**.
- Chowdiah, P.; Wasan, D. T.; Gidaspow, D. Electrokinetic Phenomena in the Filtration of Colloidal Particles Suspended in Nonaqueous Media. *AIChE J.* **1982**, 27 (6), 975-984.
- Chung, K. H.; Xu, C.; Hu, Y.; Wang, R. Supercritical Fluid Extraction Reveals Resid Properties. *Oil Gas J.* **1997**, 95 (3), 66-69.
- Chung, K. H.; Xu, C.; Gray, M. R.; Zhao, Y.; Kotlyar, L.; Sparks, B. The Chemistry, Reactivity, and Processability of Athabasca Bitumen Pitch. *Rev. Proc. Chemistry Eng* **1998**, 1, 41-79.
- Dabros, T.; van de Ven, T. G. M. Hydrodynamic Interactions between Two Spheres near a Solid Plane. *Int. J. Multiphase Flow* **1992**, 18 (5), 751-764.
- Fendel, A.; Schwochau, K. Heavy Oil Components Sorbed onto Clay Minerals in Canadian Oil Sands. *Prepr. Am. Chem. Soc., Div. Pet. Chem.*, Washington, DC, USA. **1988**, 33(2), p.257.
- González, G.; Moreira, M. B. C. "The Adsorption of Asphaltenes and Resins on Various Minerals." In *Asphaltenes and Asphalts*, I. T. F. Yen and Chilingarian, G. V. (editors), Elsevier Science, **1994**.
- Johnson, Philip R.; Elimelech, M. Dynamics of Colloid Deposition in Porous Media: Blocking Based on Random Sequential Adsorption. *Langmuir* **1995**, 11, 801-812.
- Kotlyar, L. S.; Sparks, B. D.; Chung, K. H. Organic Rich Solids from Oil Sands: Properties and Role in Processing. *Reviews in Process Chemistry and Engineering* **1998**, 1, 81-110.

- Koyama, H.; Nagai, E.; Torri, H.; Kumagai, H. Japanese Refiner Solves Problems in Resid Desulfurization Unit. *Oil Gas J.* **1995**, 93 (46), 82-90.
- Marlow, B. J.; Sresty, G. C.; Hughes, R. D.; Mahahan, O. P. Colloidal Stabilization of Clays by Asphaltenes in Hydrocarbon Media. *Colloids Surf.* **1987**, 24, 283-297.
- McDowell-Boyer, L. M.; Hunt, J. R.; Sitar, N. Particle Transport through Porous Media. *Water Resour. Res.* **1986**, 22 (13), 1901-1921.
- Nagata, S.; Yamamoto, K.; Hashimoto, K. Studies on the Flow Patterns of Liquids in a Cylindrical Mixing Vessel over a Wide Range of Reynolds Number. *Mem. Fac. Eng.*, Kyoto University, **1960**, 22, 68.
- Narayan, R.; Coury, Jose R.; Masliyah, J. H.; Gray, M. R. Particle Capture and Plugging in Packed-Bed Reactors. *Ind. Eng. Chem. Res.* **1997**, 36 (11), 4620 -4627.
- Ng, K. M.; Chu, C. F. Trickle-Bed Reactor. *Chem. Eng. Progress* **1987**, 83 (11), 55-63.
- Ranade, V. V.; Joshi, J. B.; Marathe, A. G. Flow Generated by Pitched Blade Turbines II: Simulation Using k- ϵ Model. *Chem. Eng. Comm.* **1989**, 81, 225-248.
- Rodgers, B. R. "Stability of Coal Derived Particles in Organic Media," Report No. ORNL-5631, Oak Ridge National Laboratory, Oak Ridge, TN, Aug. **1980**.
- Schucker, R. C. Measurement Dependent Variations in Asphaltene Thermal Cracking Kinetics. Symp. on Processing Heavy Oils and Residua, *Am. Chem. Soc. Meet., Div. Pet. Chem.*, Seattle, Wash., March 20-25, **1983**.
- Uhl, V. W.; Gray, J. B. "Mixing: Theory and Practice." Vol. II. Academic press, **1967**.
- Van der Hoeven, PH. C.; Lyklema, J. Electrostatic Stabilization in Non-Aqueous Media. *Adv. Coll. Interface Sci.* **1992**, 42, 205-277.
- Yan, N.; Masliyah, J. H. Effect of pH on Adsorption and Desorption of Clay Particles at Oil-Water Interface. *J. Colloid Interface Sci.* **1996**, 181, 20-27.

Chapter 6: Effects of Hydrotreating Reactions on Deposition of Fine Particles in Reactors

6.1 Introduction

The distilled liquid products from the primary upgrading of residues and bitumens have had their characteristics significantly improved over the raw material, but still fall short of the requirements of a conventional refinery, due to their high contents of undesirable heteroatoms such as nitrogen, oxygen and sulfur. Hydrotreating can selectively remove these heteroatoms to produce ammonia (NH_3), water (H_2O) and hydrogen sulfide (H_2S) by hydrodenitrogenation (HDN), hydrodeoxygenation (HDO) and hydrodesulfurization (HDS) reactions. The heteroatomic compounds in cracked streams are more likely to be present in relatively stable heterocyclic forms such as dibenzothiophene. Some thermal cracking reactions also occur during hydrotreating at ca. 400 °C, because the formation of C1-C3 hydrocarbons is independent of the presence of a catalyst (Khorasheh et al., 1989).

Hydrotreaters usually operate in trickle-flow and pulse-flow regimes, where the liquid feed and hydrogen gas flow downward co-currently through the fixed bed of hydrotreating catalyst. Several flow regimes exist in trickle beds, which govern the hydrodynamic conditions and transport processes. The pulse-flow regime has the advantage of completely wetting the catalyst and fully utilizing its activity due to sufficiently high liquid velocities (Henry and Gilbert, 1973). This flow regime also ensures that the mass transfer between the liquid and vapor phases is rapid enough for products from reactions to equilibrate between the phases.

As discussed in **Chapter 5**, fine particles such as coke, corrosion products, and mineral matter deposit in catalyst beds and limit reactor operation. The data of **Chapter 4** and **5** illustrated the importance of surface chemistry to particle behavior in deposition under hydrotreating conditions. In-situ produced TI organic matter wetted asphaltene-treated kaolin and formed a coating layer around kaolin granules. When either glass beads or catalyst pellets are used as collectors, untreated kaolin forms a filter cake on top of the packed bed, but deep bed filtration prevails for asphaltene-treated kaolin particles. Untreated kaolin flocculates before being filtered by the bed packing, whilst asphaltene-treated kaolin forms a stable suspension in treated light gas oil and is deposited onto the collector grains inside the bed. Kaolin with a lower concentration of adsorbed hydrophobic organics is preferentially deposited, leaving particles with a higher organic content in suspension. In **Chapter 5** it is proposed that asphaltenes sorbed on kaolin surfaces give stronger steric hindrance against particle attachment.

The TI organic material adheres strongly to individual mineral particles as a surface layer, so that it is practically impossible to physically separate the ultra-fine solids from bitumen (Chung et al., 1998). Various TI solids derived from Athabasca oil sands are similar in chemical composition (Chung et al., 1998). In these solids, pyritic sulfur accounts for more than 60% of total sulfur, and iron is present at a relatively large concentration (2.4-8.2 %), compared with such metals as magnesium, calcium and nickel (Kotlyar et al., 1987). The surfaces of some sand particles are stained by iron oxide, a well-known feature of Athabasca oil sands (Ignasiak et al., 1985). Iron oxide and iron salts from corrosion would be entrained into hydrotreaters, where they would be converted to iron sulfide during hydroprocessing of gas oils. The iron compound, for

example, an oxide of iron, an iron salt (a sulfate, chloride, fluoride, nitrate, oxalate or carbonate), or an iron hydroxide, converts to iron sulfide from the action of hydrogen and hydrogen sulfide (Ranganathan et al., 1980). Iron oxide is easily converted to iron sulfide even at low partial pressures of H_2S , so that this reaction can be used to clean gas streams (Goldberg, 1997). Another example is that active transition-metal sulfides are prepared by sulfiding the starting compounds, most often the representative oxides, in the solid state. The sulfide formation is achieved by means of a sulfur compound such as carbon disulfide that forms H_2S upon hydrogenation. Iron sulfide has some activity for hydrogenation of simple aromatic substances, but its activity is inferior to $NiS-WS_2$ or $NiS-MoS_2$ catalysts (Weisser and Landa, 1973). Similarly, iron sulfate supported on coal was a good catalyst for very heavy hydrocarbon oil feed in suppressing coke formation reactions and reducing coke precursors (Ranganathan et al., 1980; Kriz and Ternan, 1984). The same catalyst was found to have very mild activity towards HDS and hydrocracking.

Hydrotreating of heavy oil distillates creates not only iron sulfides from various iron sources, but also H_2O , NH_3 , and H_2S as vapor byproducts. These compounds are present in the hydroprocessing reactors at a background level that depends on feed composition and operating conditions.

One objective of this work was to compare the difference in deposition behavior between iron sulfide and kaolin. Another goal was to understand if the presence of water and ammonia in the vapor phase and unconverted polar compounds in the liquid phase changed the surface properties of fine particles, thus affecting their deposition. The nitrogen compounds are consistently more difficult to remove than the sulfur species.

Two model suspensions were used to study particle deposition in a 500 mL stirred autoclave under hydrogen atmosphere: asphaltene-treated kaolin and iron sulfide (untreated and asphaltene treated) in a hydrotreated light gas oil (TLGO). One g of kaolin (0.68 μm) was used in **Chapter 5** to give a concentration of kaolin of ca. 4,000 parts per million by weight. Based on the density and mean diameter, the initial amount of iron sulfide was determined to be ca. 0.65 g so that it covered the same surface area on collector as one g of kaolin did. Treated light gas oil was used to minimize the change in fluid properties with time. The bed packing of glass beads served as the collector for the fine particles. Water, ammonium hydroxide, and quinoline were introduced into a batch reactor at a temperature representative of hydrotreating. Ammonium hydroxide would give water and ammonia, while in the absence of hydrotreating catalyst quinoline was not reactive. Quinoline was used to represent those unconverted nitrogen compounds in the liquid phase. The deposition of mineral particles in a packed bed within the reactor was measured to identify which compositional variables were significant. In stirred tanks in which turbulent conditions normally prevail, the flow patterns are complex and the shear field is far from uniform. However, all operating parameters (including impeller speed, the amount of packing material, the amount of TLGO, and internals) were the same for all the experiments, which would give the same hydrodynamic conditions in each case, and thereby allow us to identify trends due to composition.

6.2 Materials and Method

6.2.1 Feed and Packing Materials

All the reagents were from Fisher Scientific Co. (Toronto, Canada) unless otherwise stated. Treated light gas oil was filtered before use through a 0.22 μm Millipore

membrane filter to remove solids. The properties of TLGO are tabulated in *Table 5-1*. More information about the kaolin is tabulated in *Table 4-2*.

Corrosion products in oil processing streams would tend to form iron sulfide during hydrotreating, especially iron oxides. Hence, iron sulfide was selected as a model particle. Ferrous sulfide was not used because it was too coarse (ca. 50 μm) for particle deposition experiments. Iron oxide (0.2 μm) was mixed with carbon disulfide (CS_2) in a TLGO suspension under hydrogen atmosphere in a sealed vessel at 375 $^\circ\text{C}$, where CS_2 reacted with hydrogen to produce H_2S which in turn reacted with iron oxide to form iron sulfide. The solid product, which was a mixture of various iron oxides and iron sulfides, was termed iron sulfide thereafter for convenience. Iron sulfide was collected on a 0.22 μm Millipore membrane filter, rinsed with excess methylene chloride, and then dried in an oven under vacuum at 70 $^\circ\text{C}$ for 24 h.

Deionized water, ammonium hydroxide, and quinoline were added as additives, based on the concentrations of oxygen and nitrogen in the feeds for hydrotreaters. The physical properties of these three additives and carbon disulfide were summarized in *Table 6-1*. The typical ranges for nitrogen and oxygen concentration in residues are 0.2~0.7 wt % and ca. 1 wt %, respectively (Gray, 1994). The feeds to hydrotreaters still contained comparable amounts of N and O. For example, the nitrogen contents are ca. 3,380 and 1,300 parts per million in weight in the feed for hydrotreater plants 15 and 18 in Fort McMurray, Alberta, respectively.

Table 6-1. Physical properties of additives (Weast et al., 1983)

	Water	Ammonia	Quinoline	Carbon Disulfide
Formula	H ₂ O	NH ₃	C ₉ H ₇ N	CS ₂
Molecular weight (g/mole)	18.0	17.0	129.2	76.1
Melting point (°C)	0	-77.7	0-15.6	-111.5
Boiling point (°C)	100	-33.35	238	46.2
Critical Temperature (°C)	373.9	132.4	508.8	279
Density (kg/m ³)	1,000	0.771 at 1 atm	1,093	1,263

Glass beads (Sigma-Aldrich Canada, Oakville, Ontario) were used as collectors, with the properties listed in *Table 5-2*. The same glass beads were found to be positively charged with ζ -potential of 16 mV in kerosene (Narayan, 1996). Glass beads were washed with chromic acid cleaning solution, rinsed with excess deionized water, and then dried in an oven at 110 °C for 24 h. Kaolin, iron sulfide, and glass beads were stored in a desiccator after preparation.

6.2.2 Asphaltene Treatment of Kaolin and Iron Sulfide

Hydrophobic mineral materials, such as clays with naturally adsorbed organic matter, usually report in the bitumen stream during extraction. The polar character of this carbonaceous material adsorbed on toluene insoluble inorganic solids is similar to that of n-pentane insoluble, organic matter (Chung et al., 1998). The various toluene insoluble solids derived from Athabasca oil sands contain 2.4-8.2 wt% iron that may originate from pyritic components (Kotlyar et al., 1987). Asphaltenes, humic matter and kerogen give similar chemical compositions, so kaolin and iron sulfide were treated with asphaltenes to simulate mineral solids, corrosion products, or pyritic components that originated from the mining process.

The composition of the solids-free asphaltenes used to treat kaolin and iron sulfide is given in *Table 5-1*. The methods to extract this asphaltene from an asphaltene-rich fraction from Athabasca bitumen and to treat kaolin with asphaltenes were described in *Sections 5.2.2* and *4.2*, respectively. Iron sulfide was treated with solids-free asphaltenes in exactly the same way as kaolin was treated. Asphaltene treatment was intended to produce an organic surface layer that would not be wetted by an aqueous phase. In the oil industry this type of particle or surface is called "oil wet." The properties of

asphaltene-treated kaolin, iron sulfide, and asphaltene-treated iron sulfide are listed in *Table 6-2*.

6.2.3 Reactor Apparatus and Liquid Addition System

The 500 mL batch stirred reactor (Parr Instrument Co., Model 4575) was also used here for particle deposition experiments. The reactor, its internals and the liquid addition system are illustrated in *Figure 5-2*. The reactor and its internals were described in *Section 5.2.6*. The liquid addition system was built in order to introduce liquid additives such as water into the batch reactor under high pressure. The 2 mL micro-reactor connected to the 500 mL batch reactor through valve B. A designated amount of liquid was injected into this micro-reactor with a 2 mL syringe. The 15 mL micro-reactor was pressurized with hydrogen to 17.2 MPa before connecting to the 2 mL micro-reactor through valve A.

6.2.4 Reaction Procedure

A suspension of kaolin (0.98 g) or iron sulfide (0.65 g) in TLGO (ca. 240 g) was sonicated for 20 min and then charged into the 500 mL reactor. The details of setting up the reactor were described in *Section 5.2.7*. The standard reaction conditions were 375 °C, 60 min of reaction time, 700 rpm of impeller speed, 20 g of glass beads, 240 g of TLGO, initial hydrogen pressure of 6.2 MPa. When the reaction temperature first reached the specified value, the liquid was added from the micro-reactor, and then the timing of the reaction began and the impeller was switched on. Valves A and B were successively opened. The pressure difference between the 15 mL micro-reactor and the 500 mL batch reactor gave a temporary but sufficient driving force to push the liquid

Table 6-2. Properties of asphaltene-treated kaolin, iron sulfide, asphaltene-treated iron sulfide

Properties	Asphaltene-treated kaolin		Iron sulfide	Asphaltene-treated iron sulfide
Mass median diameter (μm)	0.68	5	0.2	0.2
Density* (kg/m^3)	2,480	2,539	4,500	4,320
Elements (%)				
C	5.9	2.4	0.7	4.5
H	1.8	1.7	0	0.3
O	-	-	1.4	1.6
N	0.1	0.1	0	0
S	-	-	14.6	17.5

* The density was determined according to the method in *Appendix 3*.

sample in the 2-mL micro-reactor into the autoclave on a time scale of several seconds. The valves A and B were closed after 10 seconds to prevent condensation of the returning vapor phase. The mass change of the 2 mL micro-reactor was determined and deducted from the initial mass of the liquid sample to obtain the approximate amount of liquid entering the reactor.

The reactant mixture was stirred at 700 rpm for 60 min, and then the impeller was turned off. The reactor was moved out of the heater to cool in air without stirring and opened 20 h later. This procedure was used to ensure that particles were trapped in the packed bed only under controlled temperature conditions.

The remaining asphaltenes on kaolin and iron sulfide were represented by carbon contents of the recovered fine solids in the liquid product. With the assumption that residual asphaltenes on surfaces of kaolin or iron sulfide possessed the same carbon content (80.4%) as solids-free asphaltenes (*Table 5-1*), the amount of asphaltene-treated solids was corrected on a hydrocarbon-free basis.

6.2.5 Measurement of Particle Deposition

Section 5.2.10 described the experimental details after reaction, such as the determination of specific deposit of kaolin on collectors. Similar calculations were carried out for iron sulfide except that a particle size of 0.2 μm and a density of 4,500 kg/m^3 were used. More information about the determination of specific deposit was summarized in *Appendix 4*.

6.3 Results and Discussion

6.3.1 Repeatability of Particle Deposition Measurements

The repeatability of particle deposition experiments was checked with 0.98 g asphaltene-treated kaolin (0.68 μm) under the standard reaction conditions (see also *Appendix 5*). The mean specific deposit (σ) for the five repeated runs was 14.3 ± 0.8 kg kaolin/ m^3 packed bed (95% confidence interval). The carbon contents of kaolin from liquid product were determined to be 2.3 ± 0.3 % (95% confidence interval). These results showed that the repeatability of particle deposition experiments was satisfactory.

6.3.2 Effect of Asphaltene Treatment on Particle Deposition

Both iron oxide and iron sulfide exist in various forms with different iron valences. If iron (III) oxide was converted to iron (III) sulfide only, then ca. 26 wt % of iron oxide was converted to iron sulfide, based on the sulfur content of iron sulfide product (*Table 6-2*). The ratio of the number of surface molecules to the total number of molecules in a 0.2- μm iron sulfide particle was much less than 26% (Masliyah, 1994). Only the surfaces of particles contact the collector surfaces and liquid media, so the exact formula and composition of the produced iron sulfide was of little concern after the surface was converted to sulfide. The oxygen contents of iron sulfide and asphaltene-treated iron sulfide were lower than 1.7 %, but they were not determined correctly due to the limitation of the combustion method used for oxygen determination. It was unclear why iron sulfide had a slightly higher sulfur content after asphaltene treatment, considering solids-free asphaltenes had a lower sulfur content than iron sulfide. Iron sulfide had no

significant increase from the initial size (0.2 μm) of iron oxide after sulfidation, based on the optical microscopy observation.

The average specific deposits of iron sulfide and asphaltene-treated iron sulfide on packed beds of glass beads were 30.9 and 33.5 kg/m^3 , respectively, based on two repeated runs for each sample. Consequently, asphaltene pretreatment had no significant influence on the deposition of iron sulfide. This result seemed to contradict the previous finding that a surface layer of asphaltenes could hinder kaolin deposition on a bed packed with either glass beads or catalyst pellets (**Chapter 5**). However, the carbon content of asphaltene-treated iron sulfide dropped dramatically from the initial value of 4.7% to 0.9% after reaction, indicating that most of the asphaltenes were desorbed or thermally decomposed from the iron sulfide surface. The preparation of iron sulfide in TLGO gave a carbon content of ca. 0.7%. After the deposition experiment, this carbon content of untreated iron sulfide in liquid product remained the same. Therefore, the carbon contents of treated and untreated iron sulfide were nearly the same after the reaction at 375 $^{\circ}\text{C}$ for 60 min, which was consistent with the equivalent deposition on the packed bed. The catalytic activity of such a suspended catalyst as iron sulfide may promote the decomposition of asphaltenes from its surfaces. Suspended metal sulfides were employed as the catalyst for destructive hydrogenation of heavy petroleum and tar materials, and the degree of decomposition of asphaltenes was used to judge the activity of the catalyst (Weisser and Landa, 1973).

Although in the feed the amount of asphaltene-treated kaolin (0.68 μm) was 50% more than that of asphaltene-treated iron sulfide, the specific deposit of kaolin was less than half of that of iron sulfide. After reaction, asphaltene-treated kaolin gave a much higher

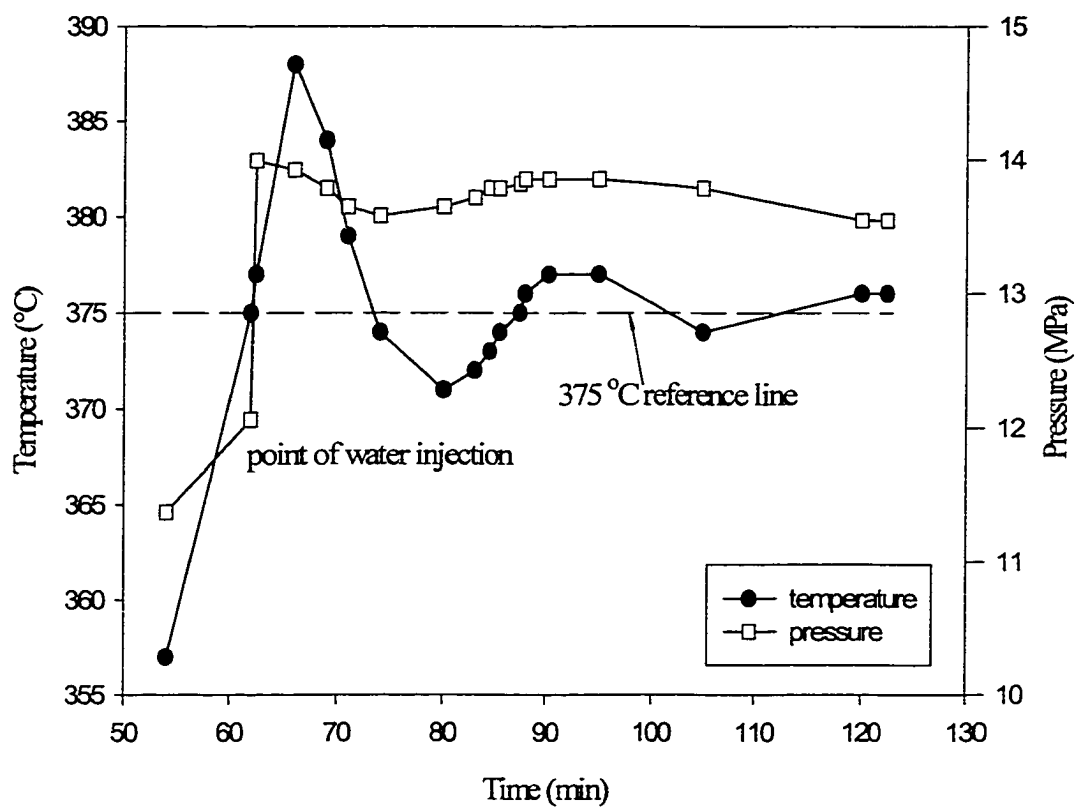
carbon content (2.3 wt%) than the asphaltene-treated iron sulfide (0.9 wt%) in the liquid products. Only the surface layer can contact the collector surface and deposited particles, so the mineral material makes no difference in deposition when it is coated with an organic layer. These results further proved the findings in **Chapter 5** that inorganic particles with a high asphaltene concentration would deposit less than those with a low asphaltene concentration and that particle size was relatively less important.

6.3.3 Effect of Hydrodeoxygenation (HDO) on Kaolin Deposition

6.3.3.1 Pressure Increase and Deposition Behavior

Water is produced at low concentrations in hydrotreaters due to HDO of gas oils. In order to study the effect of water on particle deposition, water was added to the reactor after the final operating temperature was reached. This approach avoided contact between the clay and liquid water during the time required to heat the reactor (ca. 60 min.), which gave a gelled mixture of clay and water in the bottom of the reactor in a preliminary experiment with introduction of water at room temperature. The apparatus allowed injection of 1-2 g of water almost instantaneously at 375 °C, inducing a dramatic pressure increase upon injection (*Figure 6-1*). At least two factors contributed to this pressure increase. The critical temperature of pure water is 373.9 °C, so water would be at its supercritical conditions when the autoclave was operated at 375 °C. The net amount of water entering the autoclave was 1.96 g, measured from the change in weight of the injector apparatus. The increased pressure for an ideal water vapor would be 1.3 MPa in the available volume of the autoclave, which was assumed to be 440 mL (*Section 5.3.1*). A portion of the hydrogen in the 15 mL micro-reactor also entered the autoclave due to the pressure difference between the micro-reactor (19.3 MPa) and the autoclave

Figure 6-1. Temporal variation of temperature and pressure when 2 mL water was added at 375 °C (1 g asphaltene-treated kaolin, 240 g TLGO, and 20 g of glass beads)



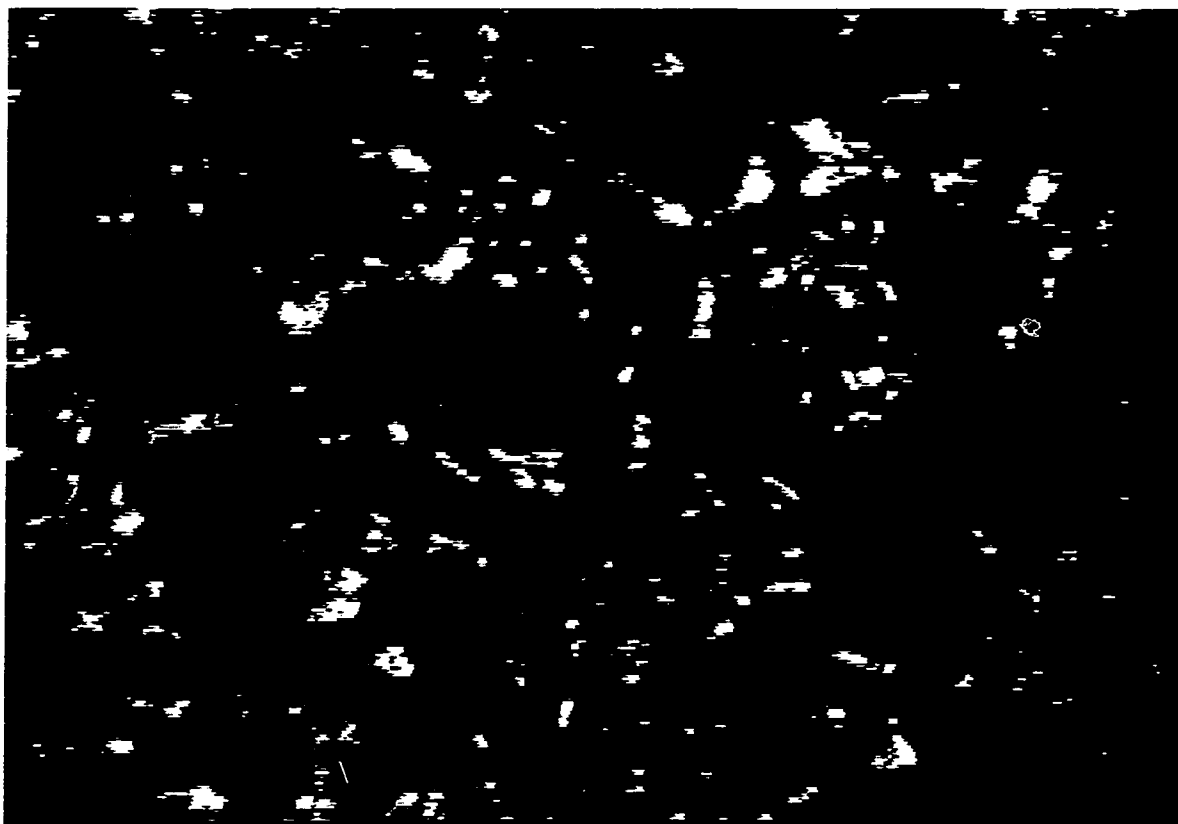
(12.1 MPa), giving a pressure increase of 0.4 MPa. The estimated total pressure increase of 1.7 MPa upon the introduction of 2 g water was very close to the actual value of 1.9 MPa.

Kaolin was deposited throughout the bed of glass beads when no water was added. The addition of water, however, gave a continuous cake of kaolin on top of the bed of glass beads. No agglomerated kaolin was found at the bottom of the reactor. The dark color of asphaltene-coated kaolin and difficulty in adjusting illumination rendered the microscopy picture of poor quality for the top layer of the packed bed (*Figure 6-2*). This cake formation was consistent with the increased specific deposit on glass beads from 14.3 ± 0.8 to a mean value of 47.9 kg kaolin/m³ packed bed (n = 2). When water was introduced into the reaction system, several parameters may become important for the deposition of kaolin. Water evaporated near its critical temperature, giving a dramatic pressure increase. Temperature oscillation may affect the distribution of water in the liquid and vapor phases. Water would condense after the reactor was removed out of the heater at the end of deposition experiment. These factors, including total reaction pressure, temperature oscillations, and condensation of water after the reaction, might have contributed to the increased deposit of kaolin.

6.3.3.2 Effect of Reactor Temperature

Due to the PID settings of the temperature controller, there was an overshoot in reactor temperature after the set point of 375 °C was reached, then the temperature fell below the set point of 375 °C from 75 to 85 min. A portion of water might have existed in the liquid phase during this period because the temperature fell below the critical point of water. The liquid water could agglomerate with the asphaltene-treated kaolin and cause a

Figure 6-2. Cake formation on top of the packed bed of glass beads
(375 °C, 1 h, 2 g of water added before reaction, 700 rpm, and 20 g of glass beads)



greater deposition of kaolin. In order to study the impact of this period of time on particle deposition after water addition, the set point was increased to 380 °C, with other reaction conditions remaining the same, to ensure that the reactor temperature was always above the critical temperature of water. Critical temperature was not likely to be significant under these conditions due to the high mutual solubility of water and oil at elevated temperatures. At room temperature, the hydrocarbon phase and the water phase can be treated as being completely immiscible, but the solubility of water in hydrocarbon liquids increases exponentially with temperature. For example, oils can contain up to 40 mol % of soluble water at 300 °C (Hoot, 1957; Nelson, 1958), far in excess of the < 1 wt % water in this experiment. Furthermore, the mutual solubilities of water and liquid hydrocarbons are only weakly dependent on the total pressure (Nghiem and Aziz, 1983). At high temperature the solubility in water of acid gas components such as hydrogen sulfide or carbon dioxide can be greater than 10 mol %, significantly altering the phase behavior of water, but neither compound was present when hydrotreated light gas oil was used with glass beads.

Nevertheless, it was decided to check the role of temperature. The specific deposit at 380 °C was 36.1 kg kaolin/m³ packed bed, which was still more than 2 times larger than 14.3 kg kaolin/m³ packed bed at 375 °C without water addition. This high specific deposit of kaolin at 380 °C cannot be attributed to the physical interactions between kaolin and liquid water at reaction conditions, due to the high solubility of water in oil under these conditions. However, the specific deposit at 380 °C was lower than that at 375 °C (47.9 kg kaolin/m³).

6.3.3.3 Effect of Reactor Pressure

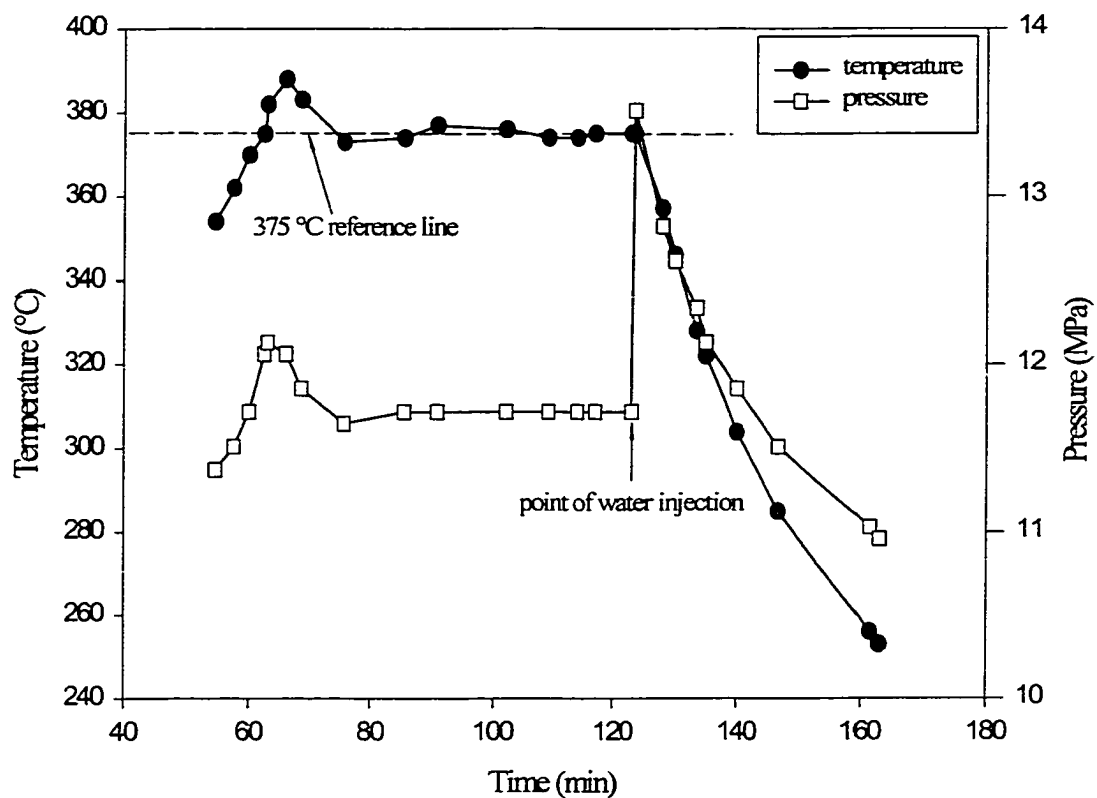
Upon the addition of water at 375 °C, the total reaction pressure increased dramatically from 12.1 to 14.0 MPa. In order to investigate the effect of this pressure increase on particle deposition, the initial hydrogen pressure was increased to be 7.6 MPa. In this case the final reaction pressure was 13.6 MPa, close to the final reactor pressure of ca. 14.0 MPa when 2 g water was introduced. However, higher reaction pressure did not give an increase in specific deposit, but rather a decrease down to 8.8 kg kaolin/m³ packed bed. This result was consistent with the lower specific deposit observed at 380 °C, which produced a final pressure 0.3 MPa higher than at 375 °C. No further study, however, was performed to study the effects of reaction pressure on kaolin deposition.

6.3.3.4 Role of Condensing Water after Reaction

The water would condense after the impeller was switched off and the reactor was removed out of the heater and allowed to cool. In order to test the effect of condensing water on kaolin deposition, 2-mL water was injected after the 60-min reaction time and after the impeller was turned off. *Figure 6-3* highlighted the temporal variations of reactor temperature and pressure after reaction. The changes in temperature and pressure with time were parallel from 120 to 140 min, suggesting little condensation of water during this period.

After the introduction of water after reaction, the specific deposit was 18.8 kg kaolin/m³ packed bed, slightly higher than 14.3 ± 0.8 kg kaolin/m³ packed bed at standard conditions. However, when water of 1 g was introduced before reaction, the specific deposit was 47.9 kg kaolin/m³ packed bed. Therefore, the increase in specific deposit from 14.3 to 18.8 kg kaolin/m³ was not significant. Depending on the position of kaolin

Figure 6-3. Temporal variation of temperature and pressure when 2 mL water was added at 375 °C after reaction (1 g asphaltene-treated kaolin, 240 g TLGO, and 20 g of glass beads)

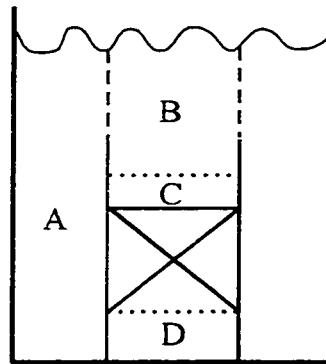


particles, all kaolin particles would have settled after 20 h when the reactor was opened (*Figure 6-4*). Kaolin in the annular space (A) and below the draft tube (D) settled at the bottom of the reactor. Kaolin right above the draft tube (B) settled on the top screen of the draft tube. Kaolin below the top screen and above the packing of glass beads (C) would deposit on the collectors. The deposition on the packed bed of glass beads, therefore, was not affected by the presence of water.

6.3.3.5 Mechanism of Water-Clay Interactions

Our previous work showed that the organic coating on the clay stabilized a suspension in gas oil (**Chapter 5**). Any disruption of this coating by water would destabilize the clay particles and promote flocculation and cake filtration. If water hydrated the clay surface, and displaced the asphaltenes, then the resulting clays would deposit more readily, as illustrated in *Figure 6-5*. The carbon content of asphaltene-treated kaolin decreased after reaction, and it decreased further in proportion to the amount of water added (*Table 6-3*). At room temperature, adsorption of asphaltenes onto kaolin seems to be reversible at low surface coverage, but irreversible when the adsorption density is close to saturation due to the lateral interactions between the adsorbed asphaltene molecules (Pfeiffer, 1950). After water displaced a portion of asphaltene molecules from kaolin surfaces at 375 °C, the lateral interactions between the adsorbed asphaltene molecules decreased, which in turn enhanced the desorption of asphaltene. An alternate explanation was that hydration of asphaltenes with water gave weaker asphaltene adsorption. Kaolin with a lower level of asphaltene coating, due to the displacement of asphaltene molecules with water, would be more easily deposited on the surface of the glass beads (**Chapter 5**). The displacement of the asphaltene layer by water molecules

Figure 6-4. A schematic diagram for the settling of kaolin particles after the impeller was turned off.



A: annular space between reactor inner wall and outer wall of draft tube

B: space right above the top screen of the draft tube

C: space below the top screen and the top layer of packed bed

D: space underneath the bottom screen of the draft tube

Figure 6-5. Mechanism for asphaltene displacement by supercritical water at hydrotreating conditions

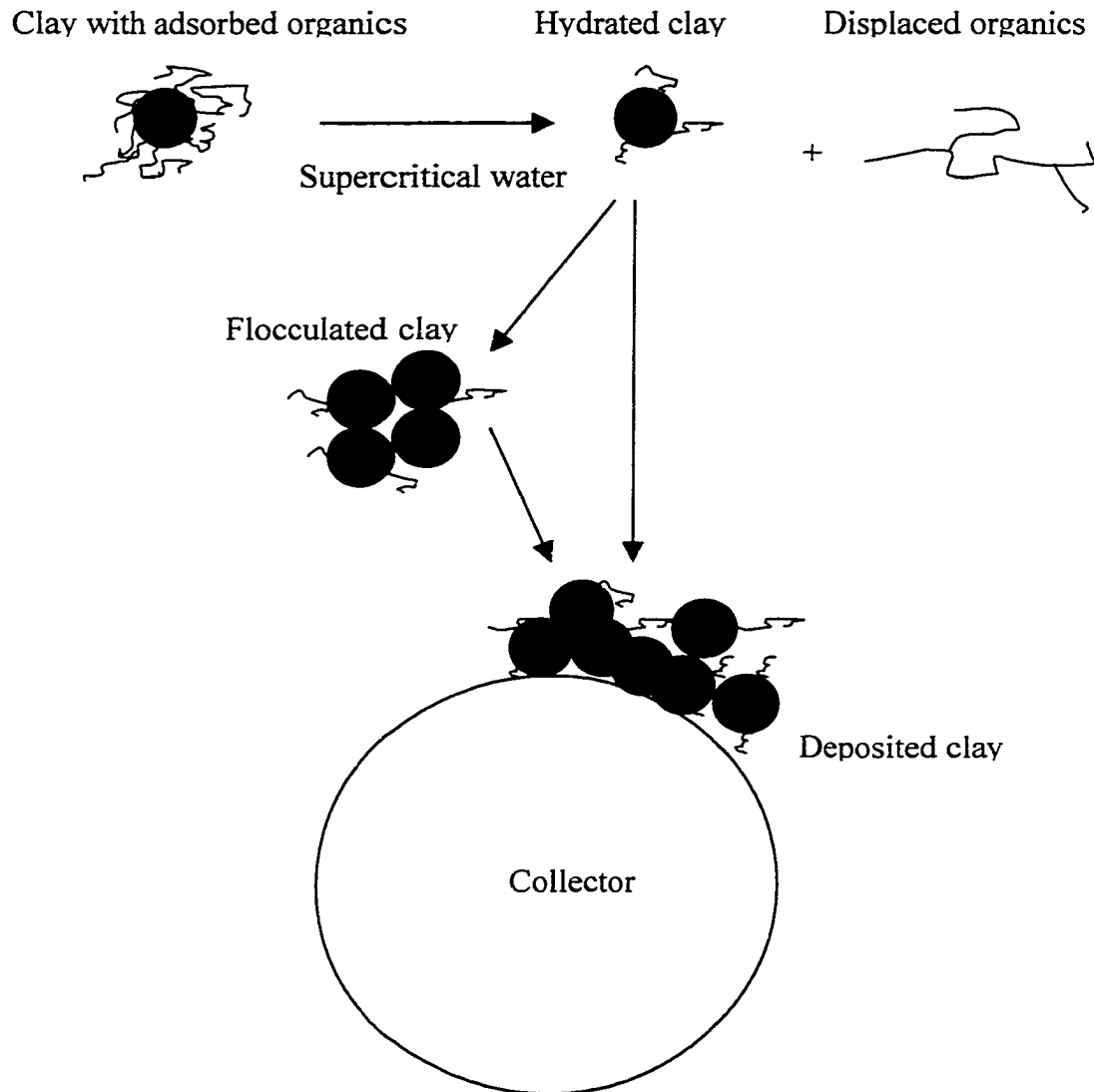


Table 6-3. Role of polar compounds on particle deposition (375 °C, 700 rpm, 20 g of glass beads, 1 h of reaction time, 0.98 g of asphaltene-treated kaolin had a carbon content of 5.9%)

Reaction conditions	C% in kaolin from liquid product	kaolin deposited/initial kaolin (%)	Specific deposit (kg kaolin/m ³ packed bed)
Average data (95% confidence)	2.3 ± 0.3	19.2 ± 1.0	14.3 ± 0.8 (n=5)
0.86 g water	2.1	32.8	24.4
1 g ammonium hydroxide	2.0	34.6	25.8
2 g Water	1.6	64.2	47.8 (n =2)
2 g quinoline	1.9	19.9	14.8

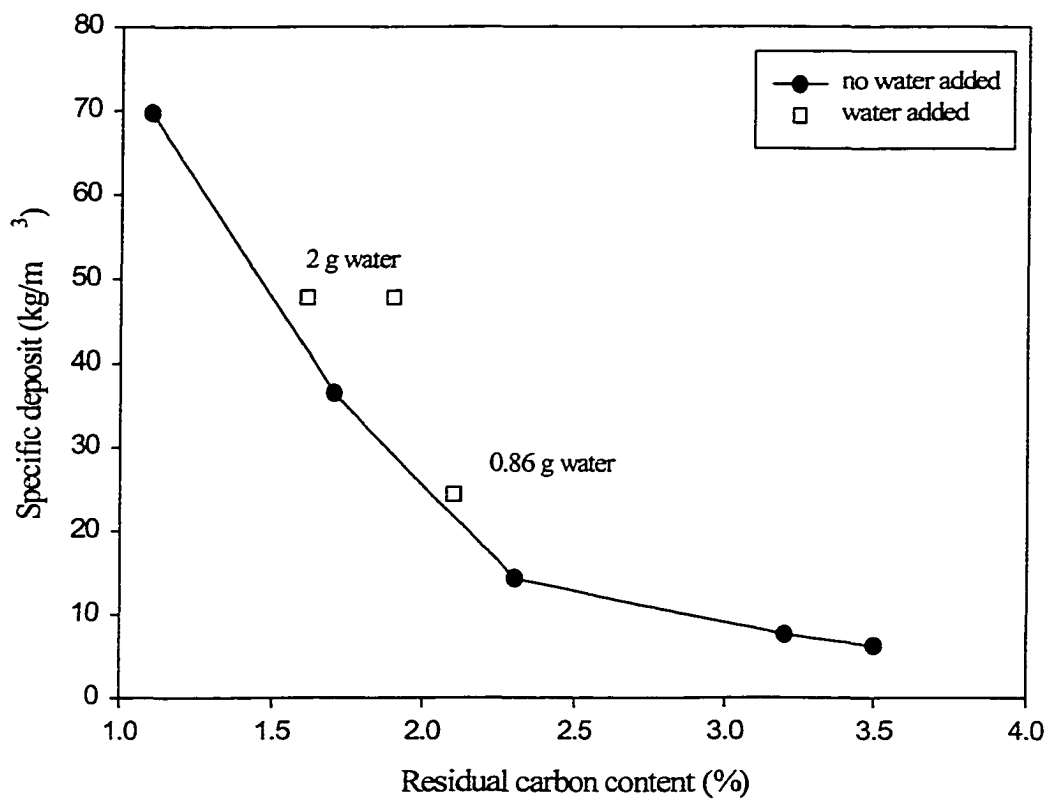
was also checked with the toluene-insoluble solids from Athabasca vacuum residue (525 °C+) under the same reaction conditions. The preparation method for this vacuum residue solid was presented in **Chapter 5**. The carbon content of these solids dropped from 18.5% to 12.5% without water, and decreased further to 11.8% with water addition. Consequently, the model suspension exhibited the same trend as the authentic hydrophobic solids from bitumen.

The reduction in the asphaltene coating was sufficient to explain the increased tendency for deposition, without any need to suggest any additional interactions between water and clay. As illustrated in *Figure 6-6*, the observed deposition of clays in the presence of water was consistent with data for dry clays from **Chapter 5**, once the carbon content of kaolin in liquid product was taken into account.

6.3.4 Effect of Hydrodenitrogenation (HDN) on Kaolin Deposition

Another polar component in the vapor phase liberated during hydrotreating is ammonia due to HDN of nitrogen compounds in oil streams. The role of ammonia in particle deposition was determined by injecting ammonium hydroxide of 1 g into the reactor at reaction conditions. It was found that 34.6 % of asphaltene-treated kaolin (0.98 g) was deposited on 20 g of glass beads. The corresponding specific deposit was 25.8 kg kaolin/m³ packed bed. At 375 °C, the ammonium hydroxide (1 g) would decompose to give 0.86 g water at reaction conditions: $\text{NH}_4\text{OH} \rightarrow \text{NH}_3 + \text{H}_2\text{O}$. The effect of this amount of water on kaolin deposition was determined by injecting 0.86 g of water at reaction temperature. It was found that 32.8 % of asphaltene-treated kaolin (0.98 g) was deposited on 20 g of glass beads with a specific deposit of 24.4 kg kaolin/m³ packed bed.

Figure 6-6. Variation of specific deposit on a packed bed of glass beads with residual carbon content of kaolin that was obtained from liquid product (375 °C, 700 rpm, 60 min of reaction time)



These results suggested no significant effect of ammonia on deposition of asphaltene-treated kaolin.

Nitrogen compounds are consistently more difficult to remove than sulfur compounds. The nitrogen contents of hydrotreated gas oils from gas oil hydrotreaters at Syncrude were 1,030 parts per million by weight. Quinoline (2 mL), in the absence of catalyst, was added at reaction temperature to represent these intractable nitrogen compounds.

Addition of quinoline did not suppress the cake filtration of untreated kaolin (**Chapter 5**), such that more than 82% of 0.98 g kaolin was deposited with a specific deposit of 65.3 kg kaolin/m³ packed bed. At room temperature, quinoline helped to stabilize a suspension of untreated kaolin in TLGO, based on a separate kaolin settling experiment in TLGO (see also *Section 5.3.4*). At elevated temperatures, however, this low molecular weight polar compound did not play the same role as asphaltenes did. Deposition of asphaltene-treated kaolin was also insensitive to the addition of quinoline, giving a specific deposit of 14.8 kg kaolin/m³ packed bed (*Table 6-3*). This value was almost the same as 14.3 kg kaolin/m³ packed bed in the absence of quinoline. Consequently, removal of polar organic species such as quinoline by catalytic reactions in hydrotreaters had no significant impact on kaolin deposition, either for untreated kaolin or for asphaltene-treated kaolin.

6.4 Conclusions

The surface asphaltene layer was reacted off due to the catalytic reactivity of iron sulfide, leading to the same deposition behavior for iron sulfide and asphaltene-treated iron sulfide. The deposition of iron sulfide relative to clays supported the data from **Chapter 5** that surface chemistry dominated over particle size in determining deposition.

Water at supercritical conditions may displace a portion of asphaltene molecules from the surface of asphaltene-treated kaolin particles, exposing more hydrophilic areas on the solid surface, and thereby increased the tendency for particles to deposit on collectors. Polar compounds such as quinoline and ammonia had no significant effect on deposition of fine particles.

References

- Chowdiah, P.; Wasan, D. T.; Gidaspow, D. Electrokinetic Phenomena in the Filtration of Colloidal Particles Suspended in Nonaqueous Media. *AIChE J.* **1982**, 27 (6), 975-984.
- Chung, K. H.; Xu, C.; Hu, Y.; Wang, R. Suspension Fluid Extraction Reveals Resid Properties. *Oil Gas J.* **1997**, 95 (3), 66-69.
- Chung, K. H.; Xu, C.; Gray, M. R.; Zhao, Y.; Kotlyar, L.; Sparks, B. The Chemistry, Reactivity, and Processability of Athabasca Bitumen Pitch. *Rev. Proc. Chem. Eng.* **1998**, 1, 41-79.
- Goldberg, A. S. Economical improvement of the Iron Sponge Gas Sweetening Process. *Proceedings in SPE Annual Technical Conference & Exhibition 1997*, v Omega, n Pt 2, 551-555.
- Gray M. R.; Choi, J. H. K.; Egiebor, N. O.; Kirchen, R. P.; Sanford, E. C. Structural Group Analysis of Residues from Athabasca Bitumen. *Fuel Sci. Technol. Int.* **1989**, 7, 599-610.
- Gray, M. "Upgrading Petroleum Residues and Heavy Oils." Marcel Dekker, Inc. **1994**.
- Henry, H. C.; Gilbert, J. B. Scale-up of Pilot Plant Data for Catalytic Hydroprocessing. *Ind. Eng. Chem. Process Des. Dev.* **1973**, 12, 328-334.
- Hoot, W. F. How to Predict Solubility of Water in Hydrocarbons. *Petroleum Refiner* **1957**, 36(6), 198.
- Ignasiak, T. M.; Zhang, Q.; Kratochvil, B.; Maitra, D. S.; Montgomery, D. S.; Strausz, O. P. Chemical and Mineral Characterization of the Bitumen-free Athabasca Oil Sands Related to the Bitumen Concentration in the Sand Tailings from the Syncrude Batch Extraction Test. *AOSTRA J. Res.* **1985**, 2, 21-35.
- Khorasheh, F.; Rangwala, H.; Gray, M. R.; Dalla Lana, I. G. Interactions between Thermal and Catalytic Reactions in Mild Hydrocracking of Gas Oil. *Energy Fuels* **1989**, 3, 716-722.
- Kotlyar, L. S.; Kodama, H.; Sparks, B. D.; Grattan-Bellew, P. E. Non-Crystalline Inorganic Matter-Humic Complexes in Athabasca Oil Sand and their Relationship to Bitumen Recovery. *Appl. Clay Sci.* **1987**, 2, 253-271.
- Kriz, J. F.; Ternan, M. "Hydrocracking Heavy Hydrocarbon Feedstocks: Aspects of Catalyst Related to Feedstock Coking Tendency," in "Studies in Surface Science and Catalysis," Vol. 19: "*Catalysis on the Energy Scene*," S. Kaliaguine and A. Mahay, Eds., Elsevier Publishing Co., Amsterdam (1984), pp. 545-552.

Labib, M. E. The Origin of the Surface Charge on Particles Suspended in Organic Liquids. *Colloids Surf.* **1988**, 29, 293-304.

Marengo, S.; Iannibello, A.; Tittarelli, P.; Vecchi, C.; Girelli, A. Activity of Iron-Rich Bauxite in the Hydrotreating of a Heavy Petroleum Residue. *Stud. Surf. Sci. Catal.* **1984**, p. 529-536.

Marlow, B. J.; Sresty, G. C.; Hughes, R. D.; Mahahan, O. P. Colloidal Stabilization of Clays by Asphaltenes in Hydrocarbon Media. *Colloids Surf.* **1987**, 24, 283-297.

Masliyah, J. H. "Electrokinetic Transport Phenomena." AOSTRA Technical Publication Series #12, March **1994**.

Narayan, R. "Particle Capture from Non-Aqueous Media on Packed Beds." MSc. Dissertation, University of Alberta, 100 p., **1996**.

Narayan, R.; Coury, Jose R.; Masliyah, J. H.; Gray, M. R. Particle Capture and Plugging in Packed-Bed Reactors. *Ind. Eng. Chem. Res.* **1997**, 36 (11), 4620 -4627.

Nghiem, L. X.; Aziz, K. A Robust Iterative Method for Flash Calculations Using the Soave-Redlich-Kwong or Peng-Robison Equations of State. *Soc. Pet. Eng. J.* **1983**, 521-530.

O'Donnell, R. J. Predict Thermal Expansion of Petroleum. *Hydrocarbon Processing* **1980**, 59(4), 229-231.

Pfeiffer, J. P. "The Properties of Asphaltic Bitumen." Elsevier, New York, N. Y. **1950**, pp. 35-37.

Ranganathan, R.; Denis, Jean-Marie D.; Pruden, B. B. Hydrocracking of Heavy Oils Using Iron Coal Catalyst. US. 4,214,977. July 29, **1980**.

Rankel, L. A. Slurry Hydrocracking of Arab Heavy Vacuum Resid with NiW Bifunctional Catalysts. *Am. Chem. Soc. Div. Petrol. Chem. Prepr.* **1993**, 38(2), 343-345.

Richardson, J. F.; Zaki, W. N. The Sedimentation of a Suspension of Uniform Spheres under Conditions of Viscous Flow. *Chem. Eng. Sci.* **1954**, 3, 65-73.

Sato, T.; Ruch, R. "Stabilization of Colloidal Dispersion by Polymer Adsorption." Marcel Dekker, Inc. New York, **1980**.

Walas, S. M. "Phase Equilibria in Chemical Engineering." Butterworth Publishers, Boston, **1985**.

Weast, R. C.; Astle, M. J.; Beyer, W. H. CRC Handbook of Chemistry and Physics. 64th Edition, 1983-1984.

Weisser, O.; Landa, S. "Sulphide Catalysts, Their Properties and Applications." Pergamon Press, Oxford, New York, 1973, pp. 294.

Chapter 7: Synthesis

This dissertation research had the following objectives:

- (a) To investigate the development of toluene insoluble carbonaceous matter during thermal cracking of untreated gas oil and to investigate the interactions between toluene insoluble carbonaceous matter and solids with different surface chemistry.
- (b) To investigate the effect of adsorbed organic compounds on particle deposition under simulated hydrotreating conditions.
- (c) To investigate the effect of hydrotreating reactions on particle deposition.

Formation of TI coke: an emulsion process

Phase separation of asphaltenes from the rest of the oil is considered an important step during TI coke formation. Wiehe (1993) used the formation of mesophase spheres in a coke product as a direct proof of phase separation, consistent with a kinetic model for coke formation. In this study, TI spheres were observed under SEM within the TI insoluble solids filtered from the liquid product, after coker gas oil was thermally cracked at a range of temperatures from 375 to 420 °C. These spheres were completely soluble in quinoline, indicating they were not mesophase. At elevated temperatures, these TI spheres were coke precursors, which separated from the remainder of the oil and formed spheres due to interfacial tension.

The liquid behavior of the TI matter was further shown by its wetting of solids with non-polar functional groups, such as asphaltene-treated kaolin and carbon black. In the presence of these solids, the TI matter did not exist as spheres, but instead adsorbed on the particle surfaces.

Particle Deposition at Hydrotreater Conditions: Effect of Adsorbed Asphaltenes and Supercritical Water

Iron sulfide and kaolin were treated with an asphaltene solution to give an adsorbed organic surface layer. This asphaltene layer gave strong steric resistance against particle-particle interactions and particle attachment on collector surfaces. The surface coverage with asphaltene rather than the particle size was the dominant variable in determining particle deposition. The extreme case was the cake filtration of untreated kaolin due to the flocculation of the kaolin particles before entering the packed bed. According to their surface properties, asphaltene-treated kaolin was fractionated between the liquid phase and collector surfaces.

Water exerted a significant effect on kaolin deposition. This may be due to water displacing a portion of the asphaltene layer from the particle surfaces. The evidence for this displacement was the comparison of the carbon contents for kaolin from liquid product with and without water addition. After thermal cracking, authentic TI solids from Athabasca vacuum residue also gave a decrease in the carbon content upon the addition of water.

Advances in Knowledge

This work represents the first observation of an emulsion of TI matter in gas oil, which gives further support to the phase-separation kinetic model (Wiehe, 1993). The concentration of the TI matter was at the level of a few hundred parts per million, which is relevant for fouling of process equipment such as furnaces and heat exchangers. This study represents the first effort to characterize the wettability of the TI matter at elevated temperatures on solid surfaces with various chemical properties. Since attachment of

particulates onto hot surfaces is the most important step in fouling, changing the inner surfaces of heat exchangers to minimize their wettability by coke precursors may mitigate fouling problems. These results also suggested that introducing fine particles that were wetted by coke precursors may prevent formation of a bulk phase of toluene-insoluble with undesired properties.

This study also represents the first attempt to investigate particle deposition from a hydrocarbon medium under simulated hydrotreating conditions at elevated temperatures. The adsorbed asphaltenes controlled the deposition mechanism of fine particles. Any factors that affected these adsorbed asphaltenes ultimately influenced the deposition of fine particles. Adding asphaltenes to the feed hindered desorption of the asphaltene layer, thus preventing deposition. Supercritical water displaced a fraction of the asphaltenes, thereby enhancing kaolin deposition. The experiments with authentic vacuum residue solid in this study also showed some of the adsorbed organic compounds were removed.

The results from this study can readily explain the deposition profile in commercial hydrotreaters. As the hydrogenation reactions are exothermic, the reactor temperature increases gradually along the reactor from the inlet of the hydrotreater. Thermal cracking reactions become very active at temperatures over 410-420 °C, and these reactions compete for the available hydrogen (Gray, 1994). The polar organic species such as asphaltenes in the liquid phase are converted to smaller molecules thereby promoting desorption of asphaltenes from the surfaces of fine particles. Therefore, conversion of polar species such as asphaltenes in the liquid phase and removal of adsorbed asphaltenes

gave mineral particles with less asphaltene on their surfaces as they move along the length of the reactor.

Oxygen is present in distillates from bitumen and heavy oils. Furimsky (1978) found that 65 % of the feed oxygen was removed by hydrotreating catalyst at 400 °C. Water is generated along the length of the hydrotreating reactor due to these hydrodeoxygenation reactions. The resulting water would help to displace asphaltene molecules from the mineral surfaces. The hydrocracking of asphaltenes and displacement of asphaltenes by water would combine to give more deposition of mineral particles on the most active zone of the hydrotreaters.

Future Research

Filters at the inlet of hydrotreaters can remove particles greater than 20 μm , but not the smaller particles. Untreated kaolin exhibited cake filtration in the beds packed with either catalyst pellets or glass beads, based on this study. Any treatment that gives such an unstable suspension could be used to give rapid removal of the fines from the oil. For example, a highly reactive catalyst could be loaded inside the first reactor bed, which would remove most of the polar matter from clays. The denuded clay would have a greater tendency to deposit on the catalyst. On the other hand, deposition of the clay could be minimized by preserving the asphaltene coating. In this case, some asphaltenes may be added to the feed of hydrotreaters, which would adsorb on clay and stabilize the clay suspension. Hence, the deposition of clay would be minimized by this asphaltene addition. However, this approach goes against the purpose of hydrotreating, which is to remove such components.

References

Furimsky, E. Catalytic Deoxygenation of Heavy Gas Oil. *Fuel* **1978**, *57*, 494-496.

Gray, M. R. 'Upgrading Petroleum Residues and Heavy Oils' Marcel Dekker, New York, **1994**.

Wiehe, I. A. A Phase-Separation Kinetic Model for Coke Formation. *Ind. Eng. Chem. Res.* **1993**, *32*, 2447-2454.

Appendices

Appendix 1: Use and Maintenance of the 500 mL Autoclave

All the parts for the reactor were obtained from Parr Instrument Co. (211 Fifty-third Street, Moline, IL 61265 USA). The reactor was used extensively in this study, therefore, the details of its operation are covered comprehensively. A labeled schematic of this autoclave is shown in *Figure A1-1*. Some accidents that occurred during its use are also reported, considering that the thesis should also include the unpleasant part of the Ph.D. program.

Some Important Parameters of the Autoclave

The maximum working pressure and temperature in this 4575 high pressure/high temperature reactor must not exceed the limits shown on the identification sticker. The maximum ratings shown in the table below apply to the reactor with the bomb made of T316 stainless steel when equipped with components suitable for the maximum ratings below.

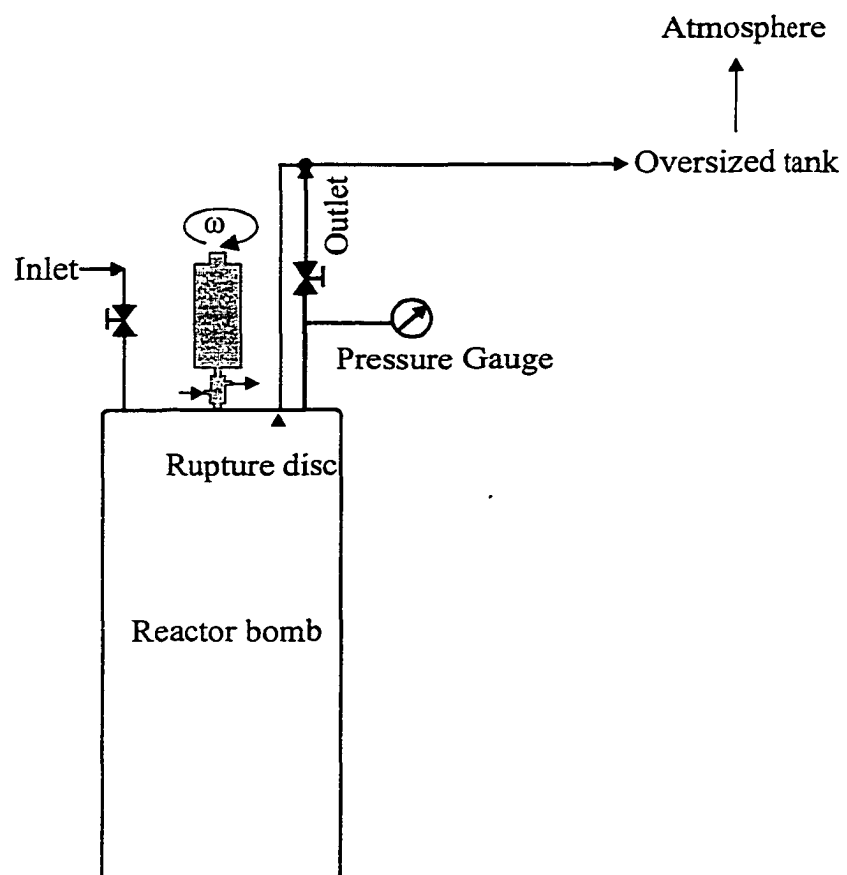
As a general rule, the allowable working pressure in any vessel decreases as the temperature is raised since the strength of all construction materials normally falls off at higher temperature. For example, the maximum working pressure for a T316 SS vessel rated for 34.5 MPa at 350 °C will be reduced to 32.1 MPa at 500 °C. Obviously, the safe operating pressure should be less than that of any attached valves, gauges, and other fittings.

Table A1-1. Specifications of the 500-mL autoclave and dimensions of its internals

Specifications of the autoclave						
Model Number	Nominal Size	Maximum Pressure Rating T316 Stainless Steel	Maximum Working Capacity	Bomb Dimensions		Valve Mounting
				Inside Diameter (cm)	Inside Depth (cm)	
4575	500 mL	34.5 MPa at 500 °C	375 mL	6.4	16.8	On Head

Dimensions of the internals
<p>Impellers</p> <p>Top: width = 0.8 cm; diameter = 3.5 cm; clearance = 10.2 cm</p> <p>Bottom: width = 0.8 cm; diameter = 2.1 cm; clearance = 1.8 cm</p>
<p>Baffles</p> <p>Height = 13.1 cm; width = 0.5 cm</p>
<p>Thermowell</p> <p>Length = 9 cm</p>
<p>Draft tube</p> <p>Outer diameter = 4.9 cm; total height = 11.3 cm; height of its supporting feet = 4.9 cm</p>
<p>Passage tubing</p> <p>Diameter = 0.9 cm</p>

Figure A1-1. A schematic diagram of the 500 mL autoclave



The reactor should never be filled to more than three-fourths of its available free space (i.e. 375 ml). When a liquid is heated in a closed vessel without sufficient free space to accommodate the expanding liquid, excessively pressures can develop quickly. For example, water and water solutions may expand about three times upon heating from ambient temperature to its critical point at ca. 374 °C.

Rupture Disc and Vent System

A safety rupture disc is installed in the reactor to protect the equipment and the operator from unexpected overpressures. The metal tag, identifying the burst rating of the rupture disc at room temperature, must always be retained with the apparatus so that the present and future operators can easily find the disc rating. The operating pressure should never exceed 70 percent of the range covered by the disc. A rupture disc (No. 526HCPG) with a burst pressure of 20.7 MPa was consistently used, because the working pressures in most experiments were less than 15.2 MPa.

Upon the burst of a rupture disc, the instantaneous expulsion of gases and vapors at sonic velocities creates a loud noise that may damage the hearing of any operator or bystander who may be in the neighborhood of the apparatus. Extension tubing will minimize this noise. In our setup, this extension tubing was combined with the gas release tubing, and then connected to an oversized steel tank which in turn was connected to the venting outlet.

Assembly of the Reactor

A dip tube was not installed to connect the gas inlet valve because no continuous gas bubbling is used in the experiments. The gas release valve was connected to a plain opening on the underside of the head. Gas released from this valve was withdrawn from

the top of the reactor. The gas release valve was used to reduce the reactor pressure in case the reactor was accidentally overcharged when filling. Use of this valve can also be made to release any excess pressure during a run and to exhaust the bomb at the end of the run.

Clean all sealing areas and be sure that the flat Grafoil gasket (No. 457HC3KL) fits uniformly in the groove in the bomb head. Examine the gasket carefully to be sure that it is in good condition. Examine the mating surface on the cylinder to be sure that it is clean and free from serious damages; then set the head on the cylinder. Slide the split ring sections into place against the bomb head, positioned so that the cap screws make uniform contact with the lip on the compression ring, then turn each screw down lightly to lock the ring sections into place.

Seal the bomb by tightening each screw with a torque wrench, applying a uniform torque to each screw. The amount of torque to be applied will depend upon the intended maximum pressure to be developed inside the bomb. For a uniform loading, pick a starting screw and tighten it to approximately 10 ft-lbs. Then by-pass the adjacent screws and move around the closure to a screw approximately 180 degrees from the start. Torque the second screw and continue in the same pattern until all screws are snug at approximately 10 ft-lbs. Since bolt-torque of 40 ft-lbs is required for bomb pressure of 41.4 MPa according to the information from Parr Instrument Co., the selected bolt-torque of 24 ft-lbs should be sufficient for all the experiments in which the maximum bomb pressure is 15.2 MPa.

Cooling System

Each magnetic drive has a cooling sleeve that can be used to keep the unit at a safe temperature level even with reactor temperature as high as 500 °C. A steady flow of cold water should be fed to this sleeve during all operations above 100 °C. Hose nipples are provided for water connections to the cooling sleeve. Care must be taken to prevent these components from being heated to temperatures above 130 °C, which would destroy the rubber bonding of the magnetic assemblies.

Temperature Controller

To minimize the heat from the heater, leave a space of at least 12 inches between the controller and the stove. Labeled plug-in sockets are provided on the rear panel for the reactor heater cord and for a Type J (iron-constantan) thermocouple. When the reactor is used only at room temperature for asphaltene treatment of kaolin or iron sulfide, the reactor heater cord was unplugged from the temperature controller to ensure that no heat source is provided for the reactor.

The operating range is 0 to 600 °C, the readout resolution is 1 °C, the set point resolution is 1 °C, and the control action is three term PID control plus limit control. For optimum control performance, tune the settings for the PID parameters that may be somewhat different for different systems. Untreated gas oil of 240 g was placed in the reactor, and the parameters were tuned at the set point of 375 °C.

Examples of Misuse of the Reactor

Case 1:

The reactor was used to treat kaolin with asphaltene in toluene-heptane mixture at room temperature. The thermocouple was not inserted into the thermowell. The reactor

temperature kept rising until the reactor pressure was high enough to burst the rupture disc. In all subsequent operations of this type, the heater was disconnected from the power source.

Case 2:

The cooling water was not switched on. In that reaction the reactor pressure did not reach the expected value, and then the cooling sleeve and the magnetic drive were found to be extremely hot. The magnetic drive showed serious leakage after the reaction, so it was disassembled for the replacement of the inner damaged plastic gasket. More damage could have been done to the magnetic drive if the time without cooling had been longer.

Appendix 2: Porosity of a Clean Bed

Density Determination of Catalyst Pellets

The pellets of spent and fresh catalysts are quite irregular. The dimensions of 50 randomly chosen tri-lobe catalyst pellets were determined with a caliper (with the accuracy of 0.05 mm). The occupied volume of these pellets is given by $\sum_{i=1}^{50} 3\pi r^2 L_i$, where r and L_i were the radius and length of each lobe, respectively. The density of the catalyst pellets was then determined easily with the mass of all the catalyst pellets (*Table 5-2*).

Porosity of the Clean Packed Bed

A measuring cylinder was filled with glass beads up to a volume of 100 cm³. The glass beads were poured out and then weighed. This procedure was repeated five times, and the average mass of glass beads required to fill the 100 cm³ volumetric cylinder was determined to be 156.9 g. The occupied volume of this amount of glass beads with average size of 945 μm was 63.1 cm³ based on its density of 2,487 kg/m³ (*Table 5-2*). The porosity of the clean bed of glass beads (ε) is calculated by

$$\varepsilon = \frac{V_t - V_{gb}}{V_t} = \frac{100 - 63.1}{100} = 0.37$$

where V_t is the volume of the packed bed, and V_{gb} is the occupied volume of glass beads.

The porosities for the packed beds of spent and fresh catalyst were determined in exactly the same way as that for glass beads (*Table 5-2*).

Appendix 3: Correction for the Mass of Asphaltene-treated Kaolin on a Hydrocarbon-Free Basis

The asphaltene-treated kaolin is modeled as shown in *Figure A3-1*. The amount of asphaltene coating on the kaolin was determined indirectly from the carbon content, assuming that the adsorbed asphaltenes had the same carbon content as the solids-free asphaltenes (*Table 5-1*). The following two equations give the mass balance of total asphaltene-treated kaolin and carbon:

$$M_{tk} = M_k + M_{asp} \quad (A3-1)$$

$$M_{tk} C_{tk} = M_{asp} C_{asp} \quad (A3-2)$$

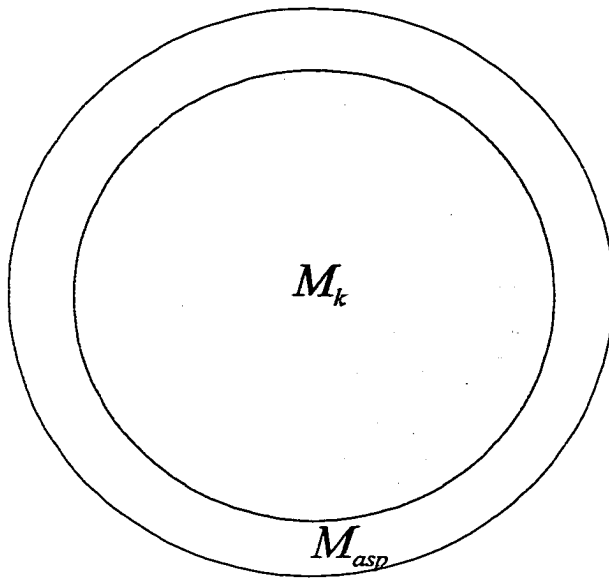
where M_{tk} is the mass of the asphaltene-treated kaolin (kg), M_k is the mass of kaolin (kg), M_{asp} is the mass of adsorbed asphaltene (kg), C_{tk} is the carbon content in asphaltene-treated kaolin (kg/kg asphaltene-treated kaolin), and C_{asp} is the carbon content in asphaltene (kg/kg asphaltene). Hence M_{asp} is given as:

$$M_{asp} = \frac{C_{tk} M_k}{C_{asp} - C_{tk}} \quad (A3-3)$$

Equation A3-3 was mainly used in the adsorption of asphaltenes on kaolin in which the values of M_k and C_{tk} were known or determined. The amount of asphaltenes remaining in the 500 mL 1:1 heptane/toluene mixture was calculated by subtracting the adsorbed amount M_{asp} from the total asphaltenes that were added initially.

Also from *Equations A3-1* and *A3-2*, the following expression was used to correct asphaltene-treated kaolin on a hydrocarbon-free basis, with C_{tk} and M_{tk} being known.

Figure A3-1. A schematic diagram of asphaltene-treated kaolin



M_k : mass of kaolin core

M_{asp} : mass of adsorbed asphaltene shell

C_k : 0 (carbon content of pure kaolin)

C_{asp} : 80.43% (carbon content of
solids-free asphaltenes)

$$M_k = M_{tk} \frac{C_{asp} - C_{tk}}{C_{asp}} \quad (A3-4)$$

Additionally, the density of the asphaltene-treated kaolin (ρ_{tk}) was estimated by the following equation:

$$\rho_{tk} = \frac{M_{asp}}{M_{asp} + M_k} \rho_{asp} + \frac{M_k}{M_k + M_{asp}} \rho_k \quad (A3-5)$$

where ρ_{asp} is the density of dry asphaltenes ($\approx 1,200 \text{ kg/m}^3$), and ρ_k is the density of untreated kaolin ($= 2,580 \text{ kg/m}^3$).

Example 1:

The carbon content of asphaltene-treated kaolin ($0.5 \mu\text{m}$) was 5.9% of the whole sample. This treated kaolin of 0.976 g was added to the feed TLGO. According to *Equations A3-4 and A3-5*, we have $M_k = 0.904 \text{ g}$, $M_{asp} = 0.072 \text{ g}$, and $\rho_{tk} = 2,480 \text{ kg/m}^3$.

Appendix 4: Calculation of Specific Deposit and Surface Coverage

Specific Deposit

In this appendix a packed bed of glass beads was used for explanation. The specific deposit is the mass of particles deposited per unit volume of the packed bed. The specific deposit, therefore, is a function of time and the concentrations of the streams entering and leaving the packed bed. However, the specific deposit at the end of each run (σ^*) was calculated in this study:

$$\sigma^* = V_L(1-\varepsilon)\rho_{gb} \frac{C_0 - C^*}{m_{gb}} \quad (\text{A4-1})$$

or

$$\sigma^* = (1-\varepsilon)\rho_{gb} \frac{m_0 - m^*}{m_{gb}} \quad (\text{A4-2})$$

where V_L is the volume of liquid phase, ε is the porosity of the packed bed, ρ_{gb} is the density of glass beads, C_0 is the initial concentration of kaolin in the feed, C^* is the concentration of kaolin in the liquid product at the end of each experiment, m_{gb} is the mass of glass beads in the draft tube, m_0 is the initial mass of kaolin in the feed, and m^* is the mass of kaolin in the liquid product at the end of each experiment.

Surface Coverage

Kaolin particles are assumed to be spheres with a diameter of 0.68 μm . The excluded area for a kaolin particle was its cross sectional area, πr^2 , where r is 0.34 μm . The total excluded area of x g of kaolin deposited on collector surfaces, therefore, was $\frac{3x}{4r\rho_{kaolin}}$,

where ρ_{kaolin} is the density of kaolin. Similarly, the external surface area of y g of glass beads is $\frac{3y}{r_{gb}\rho_{gb}}$, where r_{gb} is the average radius of glass beads (473 μm). The densities of kaolin and glass beads were 2.58×10^3 and 2.49×10^3 kg/m^3 , respectively.

The dimensions of 50 randomly chosen tri-lobe catalyst pellets were determined with a caliper (with the accuracy of 0.05 mm. The i -th tri-lobe has the length of L_i , and the radius for each lobe is r . The total external surface area of these catalyst pellets was estimated to be $\sum_{i=1}^{50} 6\pi r(r + L_i)$. The total weight of these pellets was determined. For example, when 16.8 g spent catalyst was used, its external surface area would be 0.049 m^2 .

Appendix 5: Repeatability of Particle Deposition Experiments

The repeatability was checked under the following experimental conditions: 375 °C, 700 rpm, 60 min of reaction time, 20 g glass beads, and asphaltene-treated kaolin (carbon content: 5.912 %). *Table A5-1* summarizes the distribution of kaolin in various parts of the reactor.

After each experiment glass beads were poured out from the draft tube and sonicated in 250 mL methylene chloride. The kaolin was recovered from the suspension by filtration, giving the data in the second column. The amount of kaolin draining out from the draft tube was put in the third column. The sum of value in the second and third columns for each run gave the mass of kaolin deposited on glass beads, which was corrected on a hydrocarbon-free basis (*Appendix 3*).

In this study, the repeatability was checked by two parameters, i.e., the normalized concentration of hydrocarbon-free kaolin in the liquid phase and the specific deposit. The normalized concentration of hydrocarbon-free kaolin in the liquid phase was defined as the ratio of the concentration of hydrocarbon-free kaolin in the liquid product to the concentration of the initial hydrocarbon-free kaolin in the feed. The specific deposit on the glass beads was defined as the mass of hydrocarbon-free kaolin per unit volume of packed bed. These two definitions are related by *Equation A4-1* and all the symbols used here were defined in Appendix 4:

$$\sigma^* = V_L(1 - \varepsilon)\rho_{gb} \frac{C_0 - C^*}{m_{gb}} \quad (\text{A4-1})$$

Equation A4-1 was revised to give

Table A5-1. Distribution of kaolin in various parts in the autoclave after particle deposition experiments

Column 1	Column 2	Column 3	Column 4	Column 5	Column 6
Experiment No.	Glass beads	Drainage	Liquid product	Bottom	Top mesh
1	0.132	0.050	0.790	0.008	0.076
2	0.094	0.106	0.643	0.009	0.063
3	0.083	0.107	0.653	0.002	0.082
4	0.113	0.075	0.722	0.009	0.054
5	0.093	0.085	0.701	0.002	0.040

$$\sigma^* = V_L(1-\varepsilon)\rho_{gb}C_0 \frac{1-\frac{C^*}{C_0}}{m_{gb}} \quad (\text{A6-1})$$

Therefore, σ^* and $\frac{C^*}{C_0}$ can be used interchangeably during the discussion of particle deposition and its repeatability. The data on five repeated experiments are summarized in *Table A5-2*.

Table A5-2. Repeatability of particle deposition experiments

Experiment No	Initial kaolin (g)	Deposited kaolin (g)	C% in filtered kaolin	$\frac{C^*}{C_0}$	σ (kg/m ³)
1	0.904	0.177	2.3	0.80	13.9
2	0.906	0.194	2.5	0.79	15.2
3	0.913	0.184	2.6	0.80	14.4
4	0.911	0.183	2.3	0.80	14.3
5	0.909	0.174	1.8	0.81	13.7
Standard deviation within 95% confidence interval			2.3 ± 0.4	0.80 ± 0.01	14.3 ± 0.8

Appendix 6: Settling Experiments for Kaolin Suspension in Gas Oils

Theory

The settling velocity, U_0 , of a particle at infinite dilution is given by Stokes law:

$$U_0 = \frac{V_p(\rho_p - \rho_o)g}{f} \quad (\text{A6-1})$$

where V_p is the particle volume, ρ_p is the particle density, ρ_o is the solvent density, g is the gravitational acceleration, and f is the friction coefficient of the particle. The

settling velocity of a sphere particle of radius a , for which $V_p = \frac{4}{3}\pi a^3$, and Stokes'

law $f = 6\pi\mu_0 a$, in a solvent with viscosity μ_0 is

$$U_0 = \frac{2a^2(\rho_p - \rho_o)g}{9\mu_0} \quad (\text{A6-2})$$

At very low concentrations, particles settle individually. Under these creep flow conditions, Stokes law is valid. At higher concentrations particle-particle interaction occurs, which, on average, should reduce settling rates. The settling rate may also increase with concentration of particles due to cluster formation. The following Richardson-Zaki Equation (1954) can be used to estimate the concentration effect on the settling velocity in the absence of cluster or floc formation.

$$\frac{U_h}{U_0} = (1 - c)^{4.65} \quad (\text{A6-3})$$

and

$$c = \frac{4}{3}\pi \left(\frac{a}{L_0} \right)^3 \quad (\text{A6-4})$$

where U_h is the settling velocity of a particle in the presence of other particles, U_o is the Stokes velocity, and L_o is the interparticle separation.

The suspensions of kaolin (0.68 μm) in TLGO were used to evaluate the effect of concentration on the settling velocity of kaolin particles. It was found that $U_h = 0.99U_o$ for a concentration of 4 g kaolin/kg suspension, and $U_h = 0.72U_o$ for the concentration of 40 g kaolin/kg suspension. Hence the concentration of 4 g kaolin/kg suspension was used in all settling studies in order to minimize the hindered effect.

Experimental Procedure

The untreated kaolin was dried in an oven at 100 °C for 2 h, and asphaltene-treated kaolin was dried at 70 °C under vacuum for 24 h. Then they were kept in a desiccator. Gas oil (1 L), and measured amounts of kaolin and quinoline were well mixed and poured into the 1 L glass cylinder (diameter 6 cm). Quinoline added to the suspension gave an equivalent amount of nitrogen in the range of 0.1 to 0.5 wt %. The asphaltene-treated kaolin contained 37 mg asphaltenes/g kaolin in the sedimentation study. The glass cylinder with the suspension was placed on a heavy vibration-free table. The settling of kaolin was recorded by determining the interface height of the solid free liquid phase and the suspension with time. The absolute value of the settling rate, U , was the slope of the line of the initial stage of the settling curve, in which the interface height was plotted against settling time. However, it should be noted that the settling rate was not considered accurate in this study because it was too high. For example, most of the untreated kaolin settled within the first several minutes. Additional difficulty emerged when asphaltene-treated kaolin was used, because the resulting suspension was quite

opaque. In this case the interface failed to be observed by the naked eyes. The concentration of the top fraction of these opaque suspensions was therefore determined by filtration at a specified interval, e.g. 5 min. The data of the interface height versus settling time for the suspension of 0.04 kg kaolin/treated gas oil was presented in *Table A6-1* to show how the settling velocity was obtained. The density and viscosity of treated gas oil are 925 Kg/m³ and 74.1 mPa×S at 20 °C, respectively. Kaolin settled much faster in TLGO than treated gas oil because TLGO had relatively low viscosity (*Table 5-1*). Hence the settling data was not presented here.

Effect of Polar Compounds on the Stability of TLGO/Kaolin Suspensions

The polar compounds here included quinoline in the TLGO and asphaltenes on the treated kaolin surface. The Stokes settling velocity of the untreated kaolin particles in TLGO was 3.88×10^{-6} m/s according to *Equation A6-2*. The actual settling rate of untreated kaolin in TLGO was 100 times the Stokes velocity so that most of the kaolin was at the bottom of the cylinder upon settling for 4 min. In this case flocculation was observed with the naked eyes. For suspensions with various amounts of quinoline, flocculation still occurred but was delayed. After 4 min, the supernatant suspensions still maintained the initial kaolin concentration when quinoline of various amounts was added. However, flocs started to form after 4-5 min, resulting in fast settling thereafter. The deposit at the bottom showed different packing structures, depending on whether quinoline was added. Without quinoline, the deposit was loose and more porous.

After 24 hours the ultimate kaolin concentration was determined by filtration. It was found that the ultimate kaolin concentration increased from 0.25 to 0.6 g

Table A6-1. Settling Data for 40,000 ppm TGO/Clay Suspension

Time (min.)	0	26	55	67	96	106
Height (m)	0.214	0.211	0.209	0.208	0.207	0.203
Time (min.)	126	151	161	187	205	252
Height (m)	0.196	0.180	0.176	0.165	0.162	0.152
Time (min.)	269	277	290	294	300	307
Height (m)	0.150	0.149	0.148	0.147	0.147	0.146
Time (min.)	320	329	346	370	385	408
Height (m)	0.145	0.144	0.142	0.140	0.140	0.137
Time (min.)	480	649	694	714	1464	1574
Height (m)	0.132	0.122	0.121	0.120	0.098	0.095
Time (min.)	2044	2909	2999	4309	5109	5779
Height (m)	0.086	0.074	0.072	0.054	0.049	0.043

kaolin/kg suspension upon the addition of quinoline which gave the equivalent nitrogen concentration of 0.5 wt %.

Asphaltene-treated kaolin gave an opaque suspension in TLGO, so the interface between the kaolin-free liquid phase and the suspension was not clear. The filtration at each five-min interval was used to determine the stability of the suspensions. About 3.5 g kaolin/g suspension was obtained after 30 minutes of settling. This suggested that most of asphaltene-treated kaolin remained in the liquid phase upon settling for half an hour.

References

Richardson, J. F.; Zaki, W. N. The Sedimentation of a Suspension of Uniform Spheres under Conditions of Viscous Flow. *Chem. Eng. Sci.* **1954**, *3*, 65-73.